

Test of Bell's Inequality and Entanglement Measurement in Collider Experiments

Shion Chen ¹

Department of Physics, Graduate School of Science, The University of Tokyo
7-3-1, Hongo, Bunkyo-ku, 113-0033, Tokyo, Japan
26 February 2014

¹chen@icepp.s.u-tokyo.ac.jp

Contents

1	Introduction	5
1.1	Spin, Entanglement and EPR's argument	6
1.1.1	Description of spin measurement in quantum mechanics	6
1.1.2	Entanglement and non-local action	9
1.1.3	EPR's argument and local hidden variable theories	11
1.2	Bell's Inequality	12
1.3	Review of Previous Experiments	15
1.3.1	Photon pair experiments	16
1.3.2	Loopholes	17
1.3.3	Proton pair experiment	20
1.3.4	$K^0\bar{K}_0, B_0\bar{B}_0$ flavor oscillation	22
1.4	What is still Interesting with testing Bell's inequality?	25
2	Design of the Experiment	29
2.1	Fundamental Idea	29
2.1.1	Source of entanglement	29
2.1.2	Weak decay as polarizer	30
2.1.3	Candidate channels	31
2.2	Weak Decay as Polarization Analyzer	33
2.2.1	Parity violation and ability as a polarizer - in a nut shell	33
2.2.2	Parity violation and ability as a polarizer - a closer look	35
2.2.3	Comparison with the SG type of spin measurement	37
2.3	Phenomenology in terms of Testing LRTs - Possible Loopholes	40
2.3.1	Interpretation of the polarizer decay in LHVTs	40
2.3.2	Passiveness of particle decay and the free will loophole	41
2.3.3	Efficiency loophole in the experiment	41
2.3.4	Space-like separation of decays and the locality loophole	42
2.3.5	Summary of expected loopholes and comparison with other experiments	44
2.4	Description of the measurement and the overview of detector	44
3	Formulation of Bell Inequalities for Our System	49
3.1	Formulation	49
3.2	Axes optimization using the method of C matrix	53

4	QM Analyses and the Violation of the Bell Inequality	57
4.1	$\chi_{c0} \rightarrow \Lambda\bar{\Lambda}$	58
4.2	$\eta_c \rightarrow \Lambda\bar{\Lambda}$	63
4.3	$J/\psi \rightarrow \Lambda\bar{\Lambda}$	64
4.4	$e^+e^- \rightarrow \gamma^* \rightarrow \tau\tau$	74
4.5	$Z \rightarrow \tau\tau$	75
4.6	$H \rightarrow \tau\tau$	77
5	Discussion on Experimental Feasibility	79
5.1	Distribution of C_{11} , C_{33} , Q_{\max} and Sensitivity	79
5.1.1	Shape of $n_i n'_j$ distribution	79
5.1.2	Shape of C_{11} , C_{33} distribution vs number of events	82
5.1.3	Estimator for Q_{\max}	85
5.1.4	Significance and the master formula	90
5.2	Effect from Background	91
5.3	Effect from contamination of the time-like events	96
5.4	Effect from detector resolution	96
5.5	Available sample size with current and future experiment and the feasibility	98
5.5.1	$\chi_{c0}, \eta_c \rightarrow \Lambda\bar{\Lambda}$	98
5.5.2	$Z \rightarrow \tau\tau$	99
5.5.3	$e^+e^- \rightarrow \gamma^* \rightarrow \tau\tau$	100
5.5.4	$H \rightarrow \tau\tau \rightarrow \pi\nu\pi\nu$	100
6	Conclusion	105
	Acknowledgement	108

Abstract

Is the universe can be only described fully by quantum mechanics? Or are we still allowed to have some hope for the regaining of extended classical theories? Bell inequality is known as the experimental distinguisher between them. Though its violation has already been confirmed through a number of photon experiments, from view of the universality and the further understanding toward the mysterious quantum properties, such as the quantum no-locality and entanglement, other type of experiments have been anticipated for a long time, which have still only few examples due to technical complications.

In this sense, the particle decays in high energy collider experiments have been supposed to be the new channels of the test with potential breakthrough, in that unstable particles produced in may serve as the source of entanglement states, the particle spin can be measured without any special apparatus but using its spontaneous decay, and that a variety of systems and interactions can be accessed. From 1970's, it has been approached from both theory and experiment sides however there has not been a successive result yet.

In addition to these precious studies in consideration, this paper presents (i) a comprehensive review of the theoretical background, (ii) a formal establishment of the method, (iii) a formulation of a new Bell inequality, (iv) and a discussion on the feasibility of testing the Bell inequality by this method, with today's high specification collider machines, as a new proposition of the experiment.

In particular, the six decays below are examined:

- $\eta_c \rightarrow \Lambda\bar{\Lambda} \rightarrow p\pi^-\bar{p}\pi^+$
- $\chi_{c0} \rightarrow \Lambda\bar{\Lambda} \rightarrow p\pi^-\bar{p}\pi^+$
- $J/\psi \rightarrow \Lambda\bar{\Lambda} \rightarrow p\pi^-\bar{p}\pi^+$
- $e^+e^- \rightarrow \gamma^* \rightarrow \tau^+\tau^- \rightarrow \pi^-\nu_\tau\pi^+\bar{\nu}_\tau$
- $Z \rightarrow \tau^+\tau^- \rightarrow \pi^-\nu_\tau\pi^+\bar{\nu}_\tau$
- $H \rightarrow \tau^+\tau^- \rightarrow \pi^-\nu_\tau\pi^+\bar{\nu}_\tau$

With analyses, it is demonstrated that all the channels except for the $J/\psi \rightarrow \Lambda\bar{\Lambda} \rightarrow p\pi^-\bar{p}\pi^+$ channel leads to a violation of the Bell inequality, in which the classical theories and the quantum non-locality can be tested. Especially, for the two channels $\eta_c, \chi_{c0} \rightarrow \Lambda\bar{\Lambda} \rightarrow p\pi^-\bar{p}\pi^+$, current experiments already offer sufficient statistics, comparable to 2σ and 3σ of significance for the violation respectively, therefore feasible.

The eye sees only what the mind is prepared to comprehend.

Henri Bergson

Chapter 1

Introduction

From the establishment, with no doubt, the quantum mechanics (QM) has experienced a great success; it explains most of microscopic phenomena that are hardly explained by classical theories, and to an amaze, without having a single counterexample. On the other hand, it roots at a very seemingly artificial and unnatural foundations such as "non-realism" that physics quantities generally do not have definite values until measured but in superposition, or the issues about measurement and so on; these have been provoking wide suspicion even up to today. In addition to it, Einstein-Podolsky-Rosen (EPR) pointed out that QM exhibits even some strange non-locality nature, which decisively illustrated that QM is totally against our intuition.

Something is terribly wrong. It was quite natural that people started to seek the ways to keep the glorious results of QM, but interpret within the picture of intuitive classical physics during the post-EPR years. Though the explicit formalism had not been very successful, people were quite optimistic to it, that "some day, an extended classical theory will overtake QM, and we will retain the peaceful empirical view of physics. QM is probably no more than an effective theory for the scale of atoms. We should take it easy, to use them as an ad hoc tools". It is a quite ironical history that it is such indifferent but decisive attitude towards QM that encouraged people to apply QM in every field of physics as a powerful tool, bringing about a great progress in entire physics, as a result.

The argument on the foundation had been boring during the period. It was kind of theory-must-be-beautiful type of metaphysical discussion. However, J.S. Bell provided a break through that pulls it to active science out of philosophy, with his famous Bell's inequality. It expresses the upper bound that two particle correlation (especially spin correlation) should satisfies in general, providing the realism and the locality which are both basic principles of classical physics. QM is known to predict larger correlation than it in some cases, in particular "entangled states", that it is to say, it can be experimentally testified whether QM or the classical theories are correct through the measurement of the correlation. If the violation is observed, then finally we have to prepare to say good-bye to our intuitive and empirical view of physics.

Many experiments using photon pairs were performed from 1970's and most of them rebutted the classical theories, but upheld QM. Still, the classical theories has managed to survive for a long time, by pointing out the imperfection of experiments, however they are also gradually overcome thus the issue of QM vs the classical seems to be coming to an end with the victory of QM ...

This is the story of the issue regarding to the interpretation of QM. An immediate question should then be casted: is there anything else to do? Yes it is, of course, as you guess by the rest of the 100-page thickness. For example, the vast majority of the tests of Bell's inequality have been done through optical experiments however, there are only few examples of tests in non-optical systems. One interest in the test in non-optical systems is the universality. In particular, since massive particles have less coherence as read in QM, it is attractive to see in such systems if the classical theories are excluded or the quantum non-locality exhibits. The quantum non-locality and entanglement itself arouse more profound interest, in that many of the aspects are not fully understood and still under research today, including the application such as quantum informatics or quantum computation.

To summarize, the proposition of this paper is approaching these themes by means of testing Bell's inequality in a new environment, in collider experiments, with a new method and formalism.

Outline of this thesis

The rest of chapter 1 is spent in more specific introductions, from the definitions of terms, to the review of hidden variable theories, Bell's inequality, overview about the significance of the problems or what is still interesting and so on. In chapter 2, the design of the whole experiments is explained. Starting with introducing the mechanism of spin measurement with particle decays, review of the candidate decay processes available for testing Bell's inequality, and the experimental perfection is described. In chapter 3, a new Bell's inequality is formulated for the experiment, with introducing new mathematical techniques. The chapter 4 shows the result that QM predicts, in which the structure of entanglement are dedicatedly studied and the channels exhibiting the violation of the inequality is specified. In the last chapter 5, the candidate channels are further scrutinized from view of experimental aspects. The expected sensitivity and the feasibility are argued.

1.1 Spin, Entanglement and EPR's argument

Spin is the carter component throughout the paper. In this section, the characteristics are reviewed mainly in terms of the measurement. Then, it is extended to two particle spin states with providing the definition of entangled states and observing the emergence of the quantum non-locality (EPR's argument). Lastly, as solution for the non-locality problem, hidden variable theories are introduced, in comparison with QM.

1.1.1 Description of spin measurement in quantum mechanics

Spin is the intrinsic angular momentum that a particle itself has. In QM, as with angular momentum, it is quantized and hence a discrete quantity. For simplicity, considering the case with spin one-half particles. Also as spin has too wide non-trivial nature, here the argument is confined within the description of spin measurement in QM.

The most striking feature of spin (or angular momentum) in QM is that it has **orientation** which is seems to be a continuous property despite it is discretely valued. Specifying an arbitrary direction \mathbf{n} , the

state of a spin can always be expressed as the superposition of the eigenstates toward the direction; $|\uparrow\rangle, |\downarrow\rangle$

$$|\psi\rangle = c_1 |\uparrow\rangle + c_2 |\downarrow\rangle. \quad (1.1)$$

Here $|\uparrow\rangle$ and $|\downarrow\rangle$ mean the state that the spin orients parallel and anti-parallel to \mathbf{n} respectively.

This expression (1.1) keeps in form even if a different direction \mathbf{n} is chosen. Providing $|c_1|^2 + |c_2|^2 = 1$, the coefficients c_1 and c_2 are uniquely determined with respect to the reference direction \mathbf{n} , which is defined as "quantization axis" (QA).

For single particle spin, a special direction can be defined. There exists such a QA $\mathbf{n} = \mathbf{s}$ that gives

$$|\psi\rangle = |\uparrow\rangle.$$

This is eigenstate where the spin points parallel to \mathbf{s} . This \mathbf{s} is called polarization vector, presenting the direction of spin. Note however that, since the spin operator $\boldsymbol{\sigma}$ does not commuting in each component

$$[\sigma_i, \sigma_j] = i\epsilon_{ijk}\sigma_k \quad (i, j, k = 1, 2, 3),$$

it does not follows that the polarization vector has determined as vector, but fact that it is characterized by a vector is amusing. From now on, the phrase "spin points to the direction of \mathbf{s} " means that the polarization vector is \mathbf{s} . Phenomenologically, this polarization vector corresponds to the classical spin which is proportional to magnetic moment.

Besides the polarization vector \mathbf{n} is related to the spin operator with

$$(\mathbf{n} \cdot \boldsymbol{\sigma}) |\psi\rangle = |\psi\rangle$$

$\boldsymbol{\sigma}$ is Pauli matrices. Solving this, one finds the state in which a spin pointing to direction (θ, ϕ) is expressed as

$$|\psi\rangle = \cos \frac{\theta}{2} |\uparrow\rangle_z + e^{i\phi} \sin \frac{\theta}{2} |\downarrow\rangle_z \quad (1.2)$$

in the representation where the z -axis is chosen as the QA, as indicated by the subscripts.

Next, the description of measurement in QM is introduced. This usually belongs to a framework named "projection measurement", which is roughly as below.

Consider a physical quantity to be measured ("observable") A , and the respective linear operator \hat{A} . The measured system is described generally with a superposition of eigenstates in terms of A value

$$|\psi\rangle = \sum_i c_i |a_i\rangle. \quad (1.3)$$

a_i reads the measurable values of A (eigenvalues of \hat{A}), which can be discrete or continuous either. $|a_i\rangle$ is the eigenstate with respective to $a = a_i$. Assume that an ideal measurement is performed onto the state (1.3) and the outcome turns to $a = a_0$. Then, according to the principle of "projection measurement", the state is projected as

$$|\psi\rangle = \sum_i c_i |a_i\rangle \rightarrow c_0 |a_0\rangle \quad (1.4)$$

through the measurement. This means that only the components that is consistent to the outcome in the state remains, the others are projected out. In another form,

$$|\psi\rangle \rightarrow \langle a_0 | \psi \rangle |a_0\rangle. \quad (1.5)$$

About the mechanism of the projection, QM does not tell anything. This scheme is called the "von Neumann's projection postulate" [1], which is incorporated as an axiom in the usual formalism of QM ¹.

Another interest is that how the outcome $a = a_0$ is determined. Unfortunately, as for this QM provides no hints. Instead, there is an empirical rule called "Born's rule"

$$P(a_i) = |c_i|^2,$$

giving the probability of having $A = a_0, a_1, \dots$ as the outcome [2]. Together with the projection of state above, this consist of the framework of "projection measurement", and the standard QM interpretation which includes this framework is usually referred as "Copenhagen interpretation". There is another "many world interpretation" [3] in contrast, however it is believed that those are equivalent.

Lastly, the two notions are combined and one arrives at the spin and measurement. For later convenience, let me introduce an explicit device; the Stern-Gerlach instrument (SG) [4]. The overview is shown as Fig. 1.1. This is an instrument that generates an non-uniform magnetic field, bending particle trajectories by the interaction between the field applied and the magnetic moment from the particle spins. Specifically, as the interaction potential of the field \mathbf{B} and the magnetic moment $\boldsymbol{\mu}$ is

$$\boldsymbol{\mu} \cdot \mathbf{B}, \tag{1.6}$$

the force the particle experiences F_z is

$$F_z = \boldsymbol{\mu} \cdot \frac{\partial \mathbf{B}}{\partial z} \propto \mathbf{s} \cdot \frac{\partial \mathbf{B}}{\partial z}. \tag{1.7}$$

\mathbf{s} is the polarization vector which is parallel to $\boldsymbol{\mu}$. Thus, it can bend the particles with spin if the gradient of the field toward z direction is non-zero. ² Since the different spin state with respect to \mathbf{B} results in opposite bending, the spin can be measured by the position measured by a screen and a detector ahead. Historically, it is this measurement which discovered that spin is quantized, by observing a two split lines rather than a continuous pattern.

In the language of projection measurement, it process as below. For each incident particle, the spin state can be presented as

$$|\psi\rangle = c_1 |\uparrow\rangle_{\mathbf{B}} + c_2 |\downarrow\rangle_{\mathbf{B}}, \tag{1.8}$$

with \mathbf{B} being the QA. Through the interaction with the B-field, this state $|\psi\rangle$ is projected onto either of

$$|\uparrow\rangle_{\mathbf{B}} \quad \quad \quad |\downarrow\rangle_{\mathbf{B}}. \tag{1.9}$$

One notable thing is that the spin always points parallel or anti-parallel with \mathbf{B} after the measurement. In other words, **spins can be flipped to the direction which the observer intends** (with two-way ambiguity though). This nature of spin measurement causes a big problem when it comes to two particle

¹The projection has many other names such as "reduction of wave packet" or "reduction of state" and so on. Here it is confirmed that the name "projection of state" is consistently used throughout the paper.

²The concept of "trajectory of particles" sounds classical, however it is allowed to treat a particle as such a deterministic object, if the incident particle beam is well collimated that the dispersion of the position is negligible compared with the size of instrument [5].

systems, as observed in the next section.

Note that, from now on, this particular direction is called "measurement axis" and for a while this SG type of measurement is assumed.

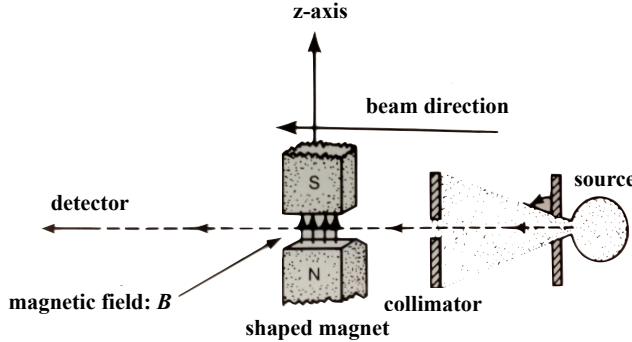


Figure 1.1: The overview of the Stern-Gerlach instrument [5]. The shapely peaked magnet creates gradient in the B-field. The incident particles tell their spins by exposing the which-path information.

1.1.2 Entanglement and non-local action

In QM, two particle composite states are generally described in a form from a direct product of kets

$$|\psi\rangle^1 |\phi\rangle^2, \quad (1.10)$$

where each ket represents its own space of particle state. Let the upper subscripts label particles, which is abbreviated from now on, as long as it is not confusing.

Now consider a case in that a pair of particles with spin one-half forms a spin zero state:

$$|\Psi\rangle = \frac{|\uparrow\rangle |\downarrow\rangle - |\downarrow\rangle |\uparrow\rangle}{\sqrt{2}}, \quad (1.11)$$

referred as spin singlet state. This is interesting in many aspects; it has rotational invariance. The representation (1.11) is held no matter how the QA is chosen; it cannot be factorized in a direct product of single kets. Those unfactorizable states are referred as "entangled state". On the other hand, factorable states, for example, (1.10) are called product states in general.

Then, what does the unfactorability implies? Here let me consider a *gedankenexperiment* as below. Consider a pair of particles 1 and 2 of which spin state in the singlet (1.11) emerges at a point in space, then run back-to-back each other in a free space. Let the two observers Alice and Bob stand ahead of the particle 1 and 2 respectively, and let them measure the spin by the SG instrument. The setup is shown in Fig. 1.2). Suppose that Alice and Bob are spatially distant away. Let Alice first measure the spin of particle 1, with setting the measurement axis (B-field) of the SG instrument to \mathbf{n} , and the outcome is \uparrow . Accordingly, the spin state of the system becomes projected as

$$|\Psi\rangle = \frac{|\uparrow\rangle |\downarrow\rangle - |\downarrow\rangle |\uparrow\rangle}{\sqrt{2}} \rightarrow \frac{|\uparrow\rangle_{\mathbf{n}} |\downarrow\rangle_{\mathbf{n}}}{\sqrt{2}}. \quad (1.12)$$

It is fairly reasonable that the spin state of particle 1 is effected due to the measurement, or the interaction with the B-field applied by the SG instrument of Alice. However, it is terribly strange that the spin state of particle 2 which does not interacted with anything is projected as well. The undetermined spin of particle 2 determined its polarization vector to $-\mathbf{n}$, without being measured. Alice can flip the orientation of the spin 2 to any direction she wants, **with no timing delay after measuring her own spin 1** by tuning the direction of the B-field \mathbf{n} , just like working a puppet. In addition, this unbelievable action can easily be confirmed by the subsequent measurement by Bob. If setting the measurement axis to \mathbf{n} as well, the outcome is, with 100% probability, opposite to that of Alice; \downarrow .

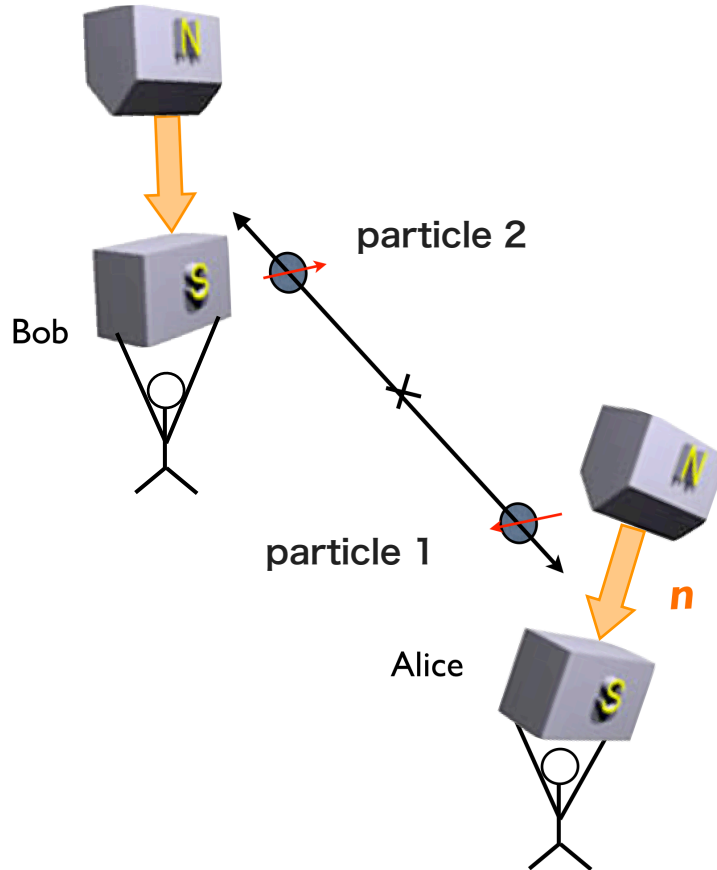


Figure 1.2: The *gedankenexperiment* of measuring spins of two particles. Observers Alice and Bob respectively have a set of SG instrument literally. Alice measure the spin of particle 1, with setting the B-field to \mathbf{n} . (The pictures of SG instrument are referred from [6].)

This "instantaneous" action is devastatingly problematic that the spin state projection on particle 2 takes place with no delay after the Alice's measurement, no matter how they are isolated in distance. How can this "distant" interaction work?

Usually and historically, the description of interaction is done within the framework of "local" interaction with the underlying principle of locality below.

Locality principle

A component in a space-time point is never affected by a change
which occurs in a space-likely isolated point in the space-time coordinates

What it is meant to be is that interaction must take place fairly with the neighbor, and the effect to the distant points in space must be "propagated" continuously but never "jumps". The propagation must forwards at a speed less than the light speed, which means, with finite time. Interestingly, this formalism of interaction is strictly and carefully followed even by QM. The reasons why distant interactions are disfavored are many-fold and profound that here we do not peruse further (please refer [7] [8] [9]). However, the case of the *gedankenexperiment* above clearly shows violation of the locality principle above. This nature of QM is referred as the quantum non-locality.

One remarkable feature about this non-local effect is that it is straightforwardly derived from only the framework of projection measurement and an entangled state. There is no other dynamics can be the cause of it, for example, it takes place all the same even if no interaction is assumed between particle 1 and 2. It solely arises from the formalism of QM using Hilbert space and its interpretation, which is intrinsic to QM.

Unfortunately, as often in literature, the concepts of entanglement and non-locality are confused in many cases. They are actually independent concepts; the entanglement indicates the generic algebraic structure of unfactorability, while non-locality is referred to such physical insight that the the projection takes place on the two particles simultaneously and that the coherently superposed entangled state such as (1.11) lasts forever as long as they are not measured. In the standard QM, the relationship can be summarized as the statement "The entangled states can lead to results that can only be interpreted as non-local effect".

Another interesting point is that the coherency in spin in the entangled state has nothing to do with the superposition of their wave functions. The non-local link ("spooky link") is maintained even if the two particles are localized in space where the wave functions are completely isolated.

1.1.3 EPR's argument and local hidden variable theories

This is the so called EPR argument, proposed by Einstein-Podolski-Rosen (1935) [10], pointing out that QM does not go along with the locality principle. Strictly speaking, they argue over the entanglement of position and momentum instead of spins³, and demonstrated that QM is incomplete if assuming QM and locality together, but the essence of the same as the *gedankenexperiment* in 1.1.2.

Motivated by the result of EPR, many attempts are made to recover the straightforward interpretation of physics instead of the non-realistic and non-local QM, as well as maintaining the result that QM eloquently predicts. The major approach was to extending the conventional classical theories into what perfectly reproduces the prediction of QM.

One of the most poplar approaches is the method the hidden variables in that, physics quantities have deterministic value in any case, and the fluctuation of measurement outcome which is characterized as the superposition of state is regarded as the representation of our ignorance about the state. This is exactly

³Historically, this is the original argument. The *gedankenexperiment* of spins are introduced later by D. Bohm(1952) [11], illustrating the essence of the problem.

same relationship between Newtonian mechanics and statistical mechanics.

Here the measure of the ignorance is introduced with a set of hidden variables λ , and the fluctuating measurement outcome A is considered as the consequence of random distribution of λ , thus ($A = A(\lambda)$). Assuming an ideal measurement, the value of A does not change between before and after the measurement. Therefore, the expectation value of A is denoted as

$$\langle A \rangle = \int d\lambda \rho(\lambda) A(\lambda) \quad (1.13)$$

where $\rho(\lambda)$ is the probability density distribution of λ , characterizing the state of the system.

Reconsidering the *gedankenexperiment* with from the viewpoint of hidden variables, one finds that it can explain the phenomenon without relying on non-locality. That is to say, it does not follow that the particle 2 flips its spin instantaneously after the measurement by Alice on the particle 1 with the measurement axis being \mathbf{n} , but the two spins are pointing to \mathbf{n} and $-\mathbf{n}$ from the beginning, as

$$|\psi\rangle = |\uparrow\rangle_{\mathbf{n}} |\downarrow\rangle_{\mathbf{n}} \quad \text{or} \quad |\psi\rangle = |\downarrow\rangle_{\mathbf{n}} |\uparrow\rangle_{\mathbf{n}}. \quad (1.14)$$

There is no non-locality but just pre-determined; this is the attitude of hidden variable theories towards the EPR problem. In addition, considering a statistical mixture of (1.14) as the initial state, it can perfectly reproduce the outcomes predicted by QM.

Accordingly as demonstrated above, hidden variable theories do have potentiality of recover the classical and empirical view of physics, namely, the realism, and if assuming, the locality, without contradicting to experiment outcome. Those are referred as local hidden variable theories (LHVTs) which may no more than a potentiality, but in principle possible theories.

1.2 Bell's Inequality

Thorough the studies on the EPR *gedankenexperiment*, it is found that there are two possible attitudes as the minimal instrumentalist interpretation of QM: the LHVTs, or the conventional interpretation of QM as represented by the Copenhagen interpretation. The strong point of LHVTs is after all that it completely regains the locality as well as the realism which goes along with our intuition, however they are no more than a potential solution, in that it is even not sure if there exists a specific and explicit LHVT model that can explain all experimental facts as QM does. In contrast, QM goes straightforward only if admitting the weird interpretation of the foundation.

This sort of comparison has long been put in exercise, as a part of philosophical argument, however J. S. Bell discovered that they have a difference in the phenomenology rather than in interpretation, and that there is certainly what can not be reproduced by LHVTs but QM does: the Bell's inequality. In this section, a brief review of the formulation and a quick phenomenological analysis are proposed. Note that for the convenience sake for the later analysis, here the CHSH (Clauser-Horne-Shimony-Holt) type inequality [13] is introduced instead of the original argument by Bell (1964) [12]. The argument in 『量子力学の基礎』 (清水明 著) [15] is extendedly referred.

Back to the *gedankenexperiment*, consider how the correlation of the measured spin is expressed in LHVTs and QM. First of all, let Alice set the measurement axis (B-field of the SG instrument) to \mathbf{a} , and Bob to \mathbf{b} . Then let $A(\mathbf{a}), B(\mathbf{b}) = \pm 1$ denotes the result of the measurement outcome (± 1 corresponds respectively to \uparrow, \downarrow in the argument above). Correlation is the expectation value of the product

$$E(\mathbf{a}, \mathbf{b}) = \langle \psi | A(\mathbf{a})B(\mathbf{b}) | \psi \rangle = \langle \psi | (\boldsymbol{\sigma} \cdot \mathbf{a})^1 \otimes (\boldsymbol{\sigma} \cdot \mathbf{b})^2 | \psi \rangle. \quad (1.15)$$

When the composite spin state $|\psi\rangle$ in the singlet (1.11)

$$\begin{aligned} (\boldsymbol{\sigma} \cdot \mathbf{a}) \otimes (\boldsymbol{\sigma} \cdot \mathbf{b}) | \psi \rangle &= (\boldsymbol{\sigma} \cdot \mathbf{a})^1 \otimes (\boldsymbol{\sigma} \cdot \mathbf{b})^2 \left(|\uparrow\rangle_b^1 |\downarrow\rangle_b^2 - |\downarrow\rangle_b^1 |\uparrow\rangle_b^2 \right) / \sqrt{2} \\ &= (\boldsymbol{\sigma} \cdot \mathbf{a})^1 \left(-|\uparrow\rangle_b^1 |\downarrow\rangle_b^2 - |\downarrow\rangle_b^1 |\uparrow\rangle_b^2 \right) / \sqrt{2} \end{aligned}$$

The upper subscripts label the particles, while the lower indicates the QA direction which \uparrow, \downarrow represents. Multiplying $|\psi\rangle^\dagger = (|\uparrow\rangle_b |\downarrow\rangle_b - |\downarrow\rangle_b |\uparrow\rangle_b)^\dagger / \sqrt{2}$ from the LHS, one has

$$\langle \psi | (\boldsymbol{\sigma} \cdot \mathbf{a}) \otimes (\boldsymbol{\sigma} \cdot \mathbf{b}) | \psi \rangle = -\frac{1}{2} (\langle \uparrow | \boldsymbol{\sigma} \cdot \mathbf{a} | \uparrow \rangle_b + \langle \downarrow | \boldsymbol{\sigma} \cdot \mathbf{a} | \downarrow \rangle_b)$$

Defining the opening angle between \mathbf{a} and \mathbf{b} as θ , according to (1.1),

$$|\uparrow\rangle_b = \cos \frac{\theta}{2} |\uparrow\rangle_a + \sin \frac{\theta}{2} |\downarrow\rangle_a \quad |\downarrow\rangle_b = -\sin \frac{\theta}{2} |\uparrow\rangle_a + \cos \frac{\theta}{2} |\downarrow\rangle_a, \quad (1.16)$$

therefore,

$$\langle \psi | (\boldsymbol{\sigma} \cdot \mathbf{a}) \otimes (\boldsymbol{\sigma} \cdot \mathbf{b}) | \psi \rangle = -\cos \theta = \mathbf{a} \cdot \mathbf{b}. \quad (1.17)$$

On the other hand, $E(\mathbf{a}, \mathbf{b})$ in LHVTs is expressed by hidden variables λ and the probability distribution $\rho(\lambda)$ as follows

$$E(\mathbf{a}, \mathbf{b}) = \int d\lambda \rho(\lambda) A(\mathbf{a}, \mathbf{b}, \lambda) B(\mathbf{a}, \mathbf{b}, \lambda). \quad (1.18)$$

This is the most general form. λ can be both continuous or discrete, singular or multiple, contained by both or either of A, B . Here, it is assumed that Alice and Bob are isolated far apart as described as Fig. 1.3, and that the measurement on the particle 1 and 2 are performed in such a way that those do not effect each other (the locality principle), which said,

$$A = A(\mathbf{a}, \lambda), \quad B = B(\mathbf{b}, \lambda). \quad (1.19)$$

In fact, the QM prediction on the result of $E(\mathbf{a}, \mathbf{b})$ measurement can be managed to reproduced by LHVTs, if with a fixed combination of (\mathbf{a}, \mathbf{b}) , since in the case, the state $\rho(\lambda)$ can be prepared beforehand as illustrated above. However, in the meantime, if Alice change the direction of the axis from \mathbf{a} to \mathbf{c} , as well as Bob changes from \mathbf{b} to \mathbf{d} randomly during the measurement, the correlations $E(\mathbf{a}, \mathbf{d}), E(\mathbf{c}, \mathbf{b}), E(\mathbf{c}, \mathbf{d})$ can be measured as well in the meantime, and the statement from Bell is that, **No LHVTs can reproduce the prediction of QM on the measurement result of $E(\mathbf{a}, \mathbf{b}), E(\mathbf{a}, \mathbf{d}), E(\mathbf{c}, \mathbf{b})$ and $E(\mathbf{c}, \mathbf{d})$ measured at once** (Bell's theorem).

This is mathematically proved by evaluating the range that a quantity

$$S = |E(\mathbf{a}, \mathbf{b}) + E(\mathbf{a}, \mathbf{d}) + E(\mathbf{c}, \mathbf{b}) - E(\mathbf{c}, \mathbf{d})|.$$

takes in LHVTs.

Starting with considering an algebraic relation followed by x, y, x', y' such that $-1 \leq x, y, x', y' \leq 1$

$$-2 \leq x(x' + y') + y(x' - y') \leq 2, \quad (1.20)$$

which is derived easily as

$$\begin{aligned}
|x(x' + y') + y(x' - y')| &= \leq |x(x' + y')| + |y(x' - y')| \\
&= |x||x' + y'| + |y||x' - y'| \\
&\leq |x'| + |y'| + |x' - y'| \\
&= \pm 2x' \quad \text{or} \quad \pm 2y'. \\
&\leq 2
\end{aligned} \tag{1.21}$$

Note that $-1 \leq x = A(\mathbf{a}, \lambda), A(\mathbf{c}, \lambda), B(\mathbf{b}, \lambda), B(\mathbf{d}, \lambda) \leq 1$, substituting $x = A(\mathbf{a}, \lambda)$, $y = A(\mathbf{c}, \lambda)$, $x' = A(\mathbf{b}, \lambda)$ and $y' = B(\mathbf{d}, \lambda)$ into (1.20) and integrating over $\int d\lambda \rho(\lambda)$ immediately leads to

$$-2 \leq E(\mathbf{a}, \mathbf{b}) + E(\mathbf{a}, \mathbf{d}) + E(\mathbf{c}, \mathbf{b}) - E(\mathbf{c}, \mathbf{d}) \leq 2,$$

which is say,

$$S = |E(\mathbf{a}, \mathbf{b}) + E(\mathbf{a}, \mathbf{d}) + E(\mathbf{c}, \mathbf{b}) - E(\mathbf{c}, \mathbf{d})| \leq 2. \tag{1.22}$$

This is one of the most popular form of Bell's inequality, the CHSH inequality. While S is restricted under 2 in LHVTs, which is usually quoted as the classical limit, QM generally breaks the limit. For example, if in the singlet state, plugging (1.17) into respective terms, one has

$$S = |-\mathbf{a} \cdot \mathbf{b} - \mathbf{a} \cdot \mathbf{d} - \mathbf{c} \cdot \mathbf{b} + \mathbf{c} \cdot \mathbf{d}|. \tag{1.23}$$

Here, with specifying \mathbf{b}, \mathbf{c} and \mathbf{d} with $\mathbf{a} \cdot \mathbf{c} = 0$, $\mathbf{b} = (\mathbf{a} + \mathbf{c})/\sqrt{2}$ and $\mathbf{d} = (\mathbf{a} - \mathbf{c})/\sqrt{2}$ (examples are shown in Fig. 1.4), the S value becomes

$$S = 2\sqrt{2} \tag{1.24}$$

beyond the limit as described by the inequality (1.22). It is easily shown that (1.24) is the maximum value that QM can reach, which is referred as the quantum limit.

One of the biggest reason why the Bell's inequality is appreciated is that it only requires two factors: the realism, and the locality, thus greatly general. In other words, a single observation of the violation can mean exclusion of all possible LHVTs. This is amazing that such a powerful inequality can be derived in the brief discussion.

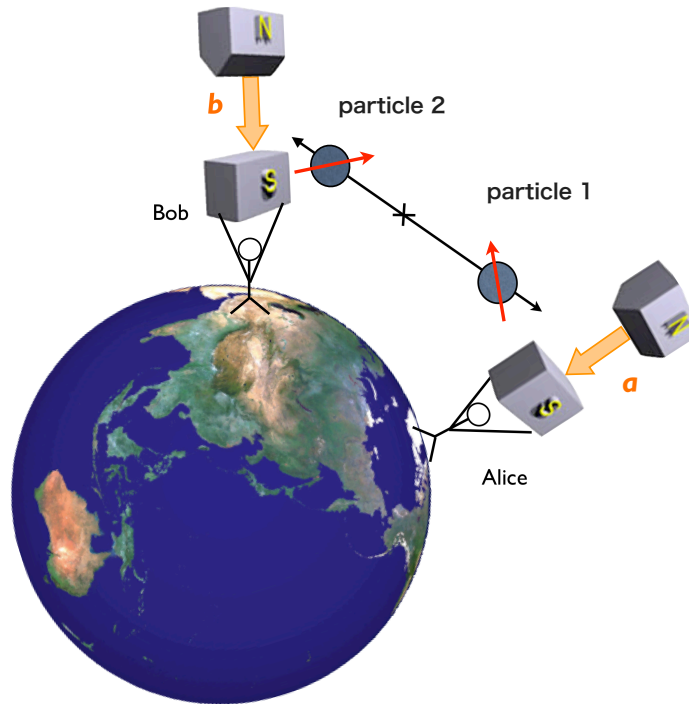


Figure 1.3: An example of setup of the *gedankenexperiment* supposed in Bell's theorem. In order to guarantee the locality condition, the both observers are placed far apart. In the figure, Alice stands at Greenland, Bob settles around Afghanistan, waiting for the spins flying from the space. The geographical condition and choice of places can be arbitrary, as long as the two spin measurements take place in a space-likely separated timing, however it is better to have the Internet otherwise they would be bored during the experiment (the picture of earth and SG instruments are referred from [6] and [14] respectively).

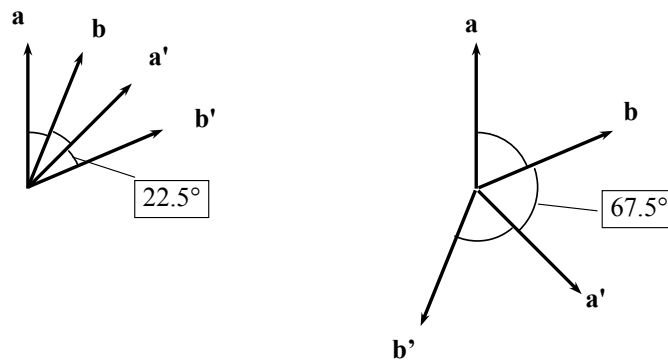


Figure 1.4: Examples of axes configurations maximizing S in eq. (1.22).

1.3 Review of Previous Experiments

The final judgement is left to experiment. In the section, some noble precedent experiments are introduced in short, such as one measuring the polarization of photon pairs, one observing spin one-half proton pairs, as an example of test using particles, and one using the meson oscillation as a sole example of test in collider

experiment. A more dedicated review and summary is given by [16] [17].

1.3.1 Photon pair experiments

The most convenient source of spin is the polarization of photon which can be easily measured by very simple equipment for example birefringent plates which is a type of crystal giving different reflection indices respective to the polarization of photon passing through. The experiment design was first established by Crauser, Horne, Shimony and Holt (1969) [13], from then on, there have been bunch of experiments done up to today, in which some of the milestone experiments are Freedman and Clauser (1972) [19], A. Aspect *et. al.* (1981) [20] (1982) [21][22], Y. H. Shih and C. O. Alley (1988) [23]. Here A. Aspect *et. al.* (1982) [21] is illustrated as an example. The review paper [24] is widely referred.

The two photon singlet state is prepare here again. In Aspect's experiment, those photon pairs are produced from the cascade decay of Calcium atoms as Fig. 1.5. This is a good source of singlet states where the emitted two photons are entangled with a high purity. Fig. 1.6 exhibits the setup of the experiment. A source is placed at the center and two birefringent plates are settled at the both sides, of which orientations are respectively \mathbf{a} , \mathbf{c} for ones at the left side (polarizer 1 and 1') and \mathbf{b} , \mathbf{d} for ones at right side of the source (polarizer 2 and 2'). Before the plates, there are optical switches (C_1 , C_2) that determine way the photon to be guided. Photo-multiplier tubes (PMTs) are set at the both ends, detecting the transmitting photons through the polarizers.

As the transmission ($A, B = +1$) and reflection ($A, B = -1$) at the polarizers in orientation of \mathbf{a} corresponds to the outcome of \uparrow, \downarrow in the SG type spin measurement with the measurement axes pointing to \mathbf{a} , the coincidence rate of the PMT signals $N(\mathbf{a}, \mathbf{b})$ is, considering in analogy, proportional to the correlation amplitude $E(\mathbf{a}, \mathbf{b})$ defined above (1.18), therefore the inequality (1.22)

$$S = |E(\mathbf{a}, \mathbf{b}) + E(\mathbf{a}, \mathbf{d}) + E(\mathbf{c}, \mathbf{b}) - E(\mathbf{c}, \mathbf{d})| \leq 2$$

can be tested experimentally. Technically, as this inequality has the upper limit of 2, the proportional coefficient between $N(\mathbf{a}, \mathbf{b})$ and $E(\mathbf{a}, \mathbf{b})$ needs to be specified in precision, in this type of experiments using coincidence rate, it is preferred to using another extend form (CH74 type inequality [18]):

$$\begin{aligned} S &:= E(\mathbf{a}, \mathbf{b}) - E(\mathbf{a}, \mathbf{d}) + E(\mathbf{c}, \mathbf{b}) + E(\mathbf{c}, \mathbf{d}) - E(\mathbf{c}) - E(\mathbf{b}) \\ -1 &\leq S \leq 0 \end{aligned} \tag{1.25}$$

where $E(\mathbf{c})$ and $E(\mathbf{b})$ are transmission rate of polarizer 1' and 2 irrespective to the other hand. Now (1.25) has 0 for the upper limit, hence written in observable $N(\mathbf{a}, \mathbf{b})$,

$$S := \frac{N(\mathbf{a}, \mathbf{b}) - N(\mathbf{a}, \mathbf{d}) + N(\mathbf{c}, \mathbf{b}) + N(\mathbf{c}, \mathbf{d}) - N(\mathbf{c}, \infty) - N(\infty, \mathbf{b})}{N(\infty, \infty)}. \tag{1.26}$$

∞ labels the case that the corresponding polarizers are absent, whose coincidence count rate are given in the auxiliary runs.

The measurement gave

$$S = 0.101 \pm 0.020,$$

violating the inequality (1.26) by 5σ standard deviation.

As seen above, optical experiments generally boast of their huge statistics, leading to an extremely high significance. On the other hand, the detection efficiency for these kind of soft photons from atomic cascades is substantially low. For example the efficiency for the PMTs are less than 20%, thus for the coincidence events far below 4%. Beside the limited solid angle acceptance of detectors, the detected photons count only on very tiny fraction of the sample. This is the major imperfection of the experiment, so called "efficiency loophole", as discussed below.

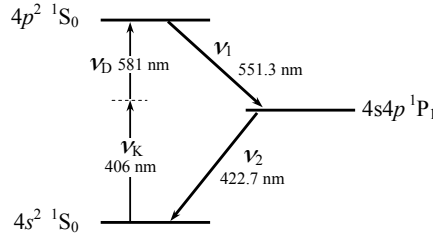


Figure 1.5: Diagram for the calcium cascade decays. Two entangled photons ν_1 and ν_2 are emitted through the atomic de-excitation.

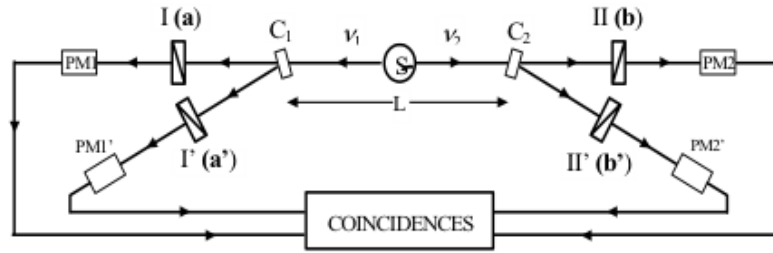


Figure 1.6: A typical setup for the photon pair experiments [24]. The two photons ν_1 and ν_2 emitted from the source (S, center) are guided to the polarizers (1 and 1' for ν_1 , 2 and 2' for ν_2) by the optical switches (C_1 and C_2 respectively). PMTs are set further behind, of which coincidence signals are collected.

1.3.2 Loopholes

Up to today, there have been astonishingly huge statistics of announcements reporting the violation of Bell inequalities. However, they are never ever perfect experiment which rigorously satisfies the conditions required in the Bell's theorem. The experimental incompletenesses are often called "loopholes". Under such a setup, the possibility of a LHVT model which reproduce everything QM predicts about measurement results can not be excluded. Therefore, the experiments so far only negate a subgroup of LHVT models. Largely, there are two types of loopholes (i) the efficiency loophole, and (ii) the locality loophole, which are individually explained in detail in the following.

The efficiency loophole

Since in experiments, it is in effect impossible to detect all the photons punching through the polarizers, usually it is forced to make an assumption for the detected sample that the sampled sub-ensemble statistically represents the nature of the entire ensemble, which is to say, the sample is not biased. This is referred to

the "homogeneous assumption" or "no enhancement assumption [18]).

For most of the case it is a very plausible and reasonable assumption, and the correction to bias can be nevertheless applied, however it can never be justified in a mathematically rigorous sense. There is no difficulty in constructing a LHVT model as rebuttal to the assumption, where the detected events exhibits large correlation than the undetected events, and the S value calculated from the detected sample surpasses the classical limit of the inequality (1.22) but never if using the sample of both events [25] [26].

Admittedly, those model are bastard as physics since they assume, for example, unknown and untestable interactions that are by far even more strange than quantum non-locality, what they meant are no more than demonstration of the counterexamples.

Without the homogeneous assumption, by considering the worst scenario that the detected sample are maximally biased, the CHSH inequality (1.22) is modified with the detection efficiency ϵ as:

$$S = |E(\mathbf{a}, \mathbf{b}) + E(\mathbf{a}, \mathbf{d}) + E(\mathbf{c}, \mathbf{b}) - E(\mathbf{c}, \mathbf{d})| \leq \frac{4}{\epsilon} - 2. \quad (1.27)$$

As the quantum limit is $2\sqrt{2}$, $\epsilon > 2/(\sqrt{2} + 1) = 0.83$ is at least required to observe the violation of (1.27). By further technical extension of the inequality, the lower bound for the decent necessary efficiency can be dragged down. For example, in the case of the Eberhard inequality (1993) [27], it is $\epsilon > 0.67$, if the background level is sufficiently low.

Since the photon energy is low due to the production mechanism of entangled states, the efficiency loophole has been the weak point for the photon pair experiments for a long time. However, according to the long-term development of devices and experimental techniques, it has been gradually overcome that nowadays there is even an experiment that confirms the violation of the Eberhard inequality, with 75% efficiency [28], which closes the efficiency loophole.

On the other hand, the experiments using charged particles tends to less serious on the loophole. For example, the proton pair experiments which is described below or one using ions pair (Rowe (2001) [29]) reaches almost 100% efficiency.

The locality loophole

In proving the Bell's theorem, the most important fact used is the locality condition (1.19):

$$A = A(\mathbf{a}, \lambda) \quad B = B(\mathbf{b}, \lambda)$$

There are mainly two types of situations in experiments that fail to maintain the locality condition (for simplicity, here we go back to the example of the EPR *gedankenexperiment*).

- (i) The space-like separation of the two measurements (on spins,) are not strictly guaranteed.

In such a case, it is allowed to explain the correlation in a way that, the measurement result of Alice propagates to the opposite particle, and then the particle changes its spin according to it, before measured by Bob. This is nothing but the description of "local physics" and it does not conflict against the reality as well. Thus the result can be totally explained by LHVTs, even though the violation of Bell's inequality is measured.

- (ii) The particles (or photons) can in principle know direction of measurement axes \mathbf{a} and \mathbf{b} .

In other words, the ideal setup is that those spin or polarization are measured before the information that the axes are set to certain directions arrives at them ("delayed choice"). This is essentially related to the concept of LHVTs during the EPR argument that if the state can be "prepared" beforehand, it does not have to ascribe the result of measurement to non-locality.

Recall that LHVTs can make an identical prediction on the correlation amplitude $E(\mathbf{a}, \mathbf{b})$, with that QM predicts on for the singlet state, by considering the case where the spin 2 points along or against \mathbf{a} in the initial state, if Alice measures first. But this initial state can not give the concise prediction on $E(\mathbf{c}, \mathbf{b})$ with QM. Hence, the only possible way for LHVTs to make "correct" prediction on both $E(\mathbf{a}, \mathbf{b})$ and $E(\mathbf{c}, \mathbf{b})$ is to prepare different initial states according to the axes setting, such that the spin 2 points along or against \mathbf{a} if the measurement axis of Alice's machine is \mathbf{a} , and vice versa. The reason why the decayed choice is needed and (ii) should be prohibited, is to exclude this last possibility, otherwise there will be still a slight hope for LHVTs to reproduce the prediction of QM on $E(\mathbf{a}, \mathbf{b})$, $E(\mathbf{a}, \mathbf{d})$, $E(\mathbf{c}, \mathbf{b})$ and $E(\mathbf{c}, \mathbf{d})$, and to violates Bell inequalities.

Associated with it, the free will of observers' choice have to be assured as well. If the choices of \mathbf{a} and \mathbf{b} are not independent but in a function relation through a parameter ϕ

$$\begin{aligned} \mathbf{a} &= \mathbf{a}(\phi), \quad \mathbf{b} = \mathbf{b}(\phi) \\ \mathbf{a} &= \mathbf{a}(\phi(\mathbf{b})), \end{aligned} \tag{1.28}$$

it is easily shown that Bell inequalities is not satisfied even by LHVTs [15]. This is in essence because the information of axes is eventually sheared with the particles.

If categorizing further, the loophole arising from the situation (i) is usually referred as "locality loophole" and (ii) as "free will" loophole since it is common to the experiments without free will of observers to choose the axes.

As for the photon pair experiments, those loopholes have been also the challenges. However, the locality loophole (i) is closed by some experiments. Weihs *et al.* (1998) [30] and Tittel *et al.* (1998) [31] are some of the examples, where the two detection points are isolated respectively 400m and more than 10km distant, with extended optical fiber cables. In recent years, there is even an similar experiments with 144km long base-line (Uesin *et al.* (2007) [32]).

To the contrary, particle experiments suffer from the locality issue more than efficiency loopholes in general, since it is not easy to extend the whole setup. In addition, in the experiments measuring spins through scattering or particles decays, the lack of active and controllable measurement axes will cause the free will loophole as seen below.

The issues regarding to the free will loophole are basically two-fold; practical possibility of achieving an ideal decayed choice. It is mostly considered to be solved by randomly reorienting the polarizer during the measurement, just as done in Aspect's third experiment (1982) [22] or Weihs *et al.* (1998) [30] and so on. The other, more serious problem is about the free will itself. Though in most cases in physics argument,

observer's free will is taken for granted, it is highly non-trivial when it comes to the criteria of who/which has it. Frankly, there is no good reason to allow only human to be "free" while the other "objects" are considered to be ruled by physical principles.

An interesting observation is given by J. Conway and S. Kochen with the "The Free Will Theorem" [33]. It is **derived** that if the free will of observer is guaranteed, it has to be extended to "objects", and even ultimately to elementary particles. Therefore, randomly distributed outcome of measurements, such as spin measurements, may have to be interpreted as the representation of those particles' free will. What this implies to our Bell's inequality experiments is thus significant, since it can never be ensure that the two measurements are independent in a true sense. However, since the issue of intrinsic free will is a too much generic problem and needs by far more general insight outside the scope of the thesis, here as is often the case, we would not go any further, and only the former issue on the delayed choice is considered as the free will loophole argument.

1.3.3 Proton pair experiment

The experiments of massive particles basically belong to two families: ones using spin entangled proton pairs reviewed here, and the other is ones using the flavor oscillation of neutral mesons such as $K^0\bar{K}^0$ or $B^0\bar{B}^0$ as referred in the next section. For the proton experiments so far, there are M. M. Lamahi-Rachti and W. Mitting (1972) [34], and H. Sakai (2006) [35] etc. but here we confine the discussion in reviewing H. Sakai (2006) for simplicity.

A proton pair from the decay of short-lived ^2He spin-singlet state, populated in the nuclear reaction $d+H \rightarrow ^2\text{He} + n$ is in a purity spin singlet state. As shown in Fig. 1.7, these pairs are guided through the event-ready instruments first, and scatters in the graphite target. Since there is anisotropy in the scattering distribution according to the incident proton spin, the scattered angle has information of the proton spin before scattered, which measured by the multi-layered hodoscopes settle at the down-stream.

The inequality tested in the experiment is the CHSH type (1.22)

$$S = |E(\mathbf{a}, \mathbf{b}) + E(\mathbf{a}, \mathbf{d}) + E(\mathbf{c}, \mathbf{b}) - E(\mathbf{c}, \mathbf{d})| \leq 2. \quad (1.29)$$

\mathbf{a} , \mathbf{b} , \mathbf{c} and \mathbf{d} are the measurement axes however here the comparable components do not exist. Instead, a set of virtual axes is considered. Suppose that there are two virtual axes \mathbf{a} and \mathbf{b} standing in front of the path of proton 1 and 2 respectively (see Fig. 1.8). Then, think of a set of quantities $A(\mathbf{a})$, $B(\mathbf{b})$ which is measured as +1 if the proton passes the left-side of the axis, and -1 if it passes the right-side. Considering that the proton direction is related to the spin before scattered, $A(\mathbf{a})$, $B(\mathbf{b})$ can be straightforwardly regarded as the outcomes of spin measurement, just as in the EPR *gedankenexperiment*, and $E(\mathbf{a}, \mathbf{b})$ can be defined as above (1.18).

Note that these axes are virtual thus they can even be chosen after the data taking. This is because the proton trajectory can be acquired in three dimensions, and it is thus uniquely determined if the proton passes left or right, for any arbitrary setting of the axis. Therefore, with a series of data taking, the dependency of $E(\mathbf{a}, \mathbf{b})$ on \mathbf{a} and \mathbf{b} is completely reconstructed (tomography), where all events can be applied to each setting of (\mathbf{a}, \mathbf{b}) .

Experimentally, $E(\mathbf{a}, \mathbf{b})$ is obtained by

$$E(\mathbf{a}, \mathbf{b}) = \frac{1}{P^2} \frac{N_{++}(\mathbf{a}, \mathbf{b}) - N_{+-}(\mathbf{a}, \mathbf{b}) - N_{-+}(\mathbf{a}, \mathbf{b}) + N_{--}(\mathbf{a}, \mathbf{b})}{N_{++}(\mathbf{a}, \mathbf{b}) + N_{+-}(\mathbf{a}, \mathbf{b}) + N_{-+}(\mathbf{a}, \mathbf{b}) + N_{--}(\mathbf{a}, \mathbf{b})}. \quad (1.30)$$

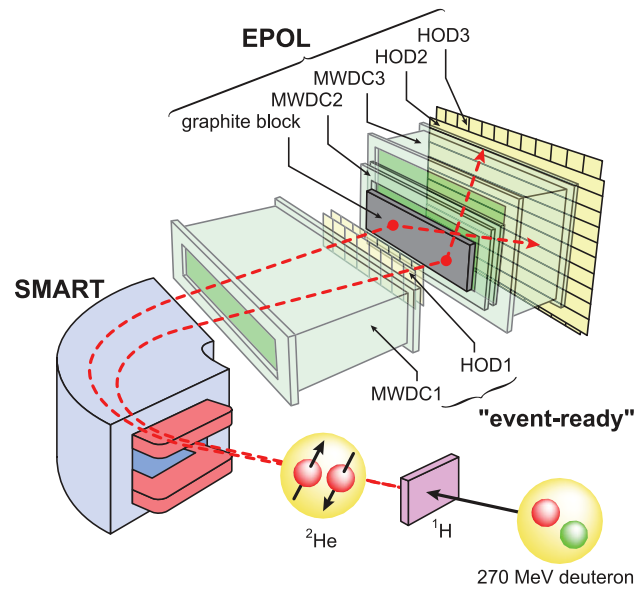


Figure 1.7: The overview of the setup in H. Sakai (2006) [35]. A helium ${}^2\text{He}$ atom is generated through the ($d, {}^2\text{He}$) reaction, from which a pair of protons emerge. The proton momentum is selected by the spectrometer (SMART) in the event ready in order to extract pure entangled pair sample. The protons eventually scatter with the graphite target, and the hodoscope in the rear measure the trajectories 3 dimensionally.

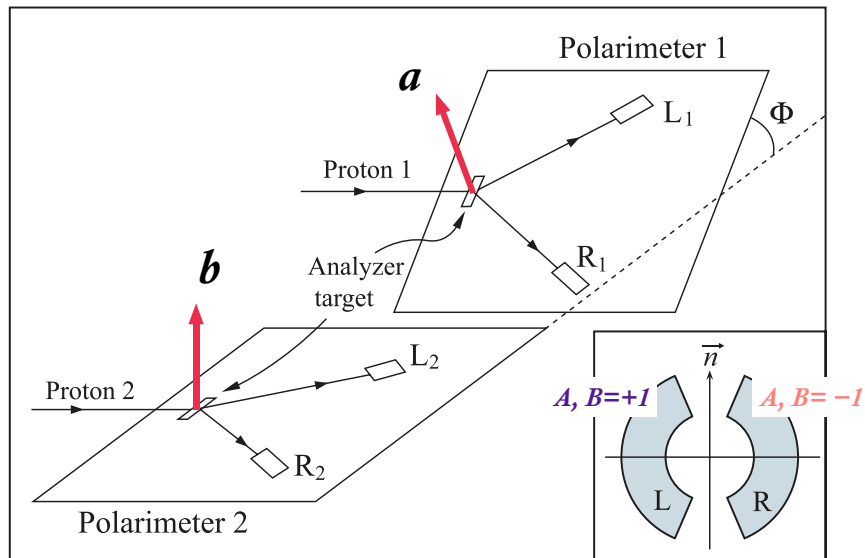


Figure 1.8: Definition of the quantity A and B respective to the virtual axes \mathbf{a} and \mathbf{b} , which are measured as $+1$ if the proton passes the left-side of the axes, and -1 if it passes the right-side, Φ is defined as the angle between the planes.

$N_{ij}(\mathbf{a}, \mathbf{b})$ is the frequency of having events where $A(\mathbf{a}) = i, B(\mathbf{b}) = j$ ($i, j = \pm 1$).

P is the polarization efficiency of scattered single proton, defined as

$$P_+(\mathbf{a}) = 1 + P\mathbf{s} \cdot \mathbf{a} \quad (1.31)$$

with $P_{\pm}(\mathbf{a})$ being the probability of having the outcome of $A(\mathbf{a}) = \pm 1$, thus P represents how much information of the spin is translated into the asymmetry of the distribution. The form (1.31) can be derived from QM calculation, however it is used as the measured result since here the aim is to testing LHVTs. With the calibration runs, $P = 0.16 \sim 0.24$ is obtained. Using (1.31), $E(\mathbf{a}, \mathbf{b})$ is derived for the spin singlet proton pairs, assuming the locality condition,

$$E(\mathbf{a}, \mathbf{b}) = -P^2 \mathbf{a} \cdot \mathbf{b}. \quad (1.32)$$

Renormalizing this by dividing into P^2 so that the upper limit becomes to unity, the inequality (1.29) can be derived in the same manner as described in section 1.2.

The result is $S = 2.83 \pm 0.24(stat.) \pm 0.07(syst.)$ violating the inequality (1.29) by 99.93% confidence level, and the tomographed function shape of $S(\Phi)$ is also in perfect agreement with the QM (Fig. 1.9) (Φ is an angle defined in Fig. 1.7).

On the virtual axes, it has to be pointed out that, these can not realize the delayed choice condition, though they can be chosen well after the data taking because it has nothing to do with the physical result of protons scattering, while the magnetic field of the SG instrument plays an more active role that it can change the direction of spins if in QM, which makes the difference from all kinds of LHVTs. In this setup here, a LHVT model in which the direction of a scattered proton is determined before it is scattered can reproduces the prediction of QM, which creates therefore the free will loophole.

Another weak point of the massive particle experiments are the statistics. In contrast to photons, it is difficult to generate huge number of particles in a definite state. On the other hand, it tends to be easier to detect particularly for charged particles thus robust against the efficiency loophole. For example, the experiment by Sakai (2006) attains more than 96% efficiency.

1.3.4 $K^0\bar{K}^0, B^0\bar{B}^0$ flavor oscillation

The experiment proposed in this paper is not actually the first attempt of testing Bell's inequality in colliders. The notable meson oscillation of $K^0\bar{K}^0$ and $B^0\bar{B}^0$ observed in colliders has been put in application for testing LHVTs and QM. The analysis by CPLEAR (1999) [36] for $K^0\bar{K}^0$ and Belle (2004, 2007) [37] [38] for $B^0\bar{B}^0$ are famous. Here Belle (2007) is reviewed.

The flavor number has the identical $SU(2)$ structure called quasi-spin, which represents quite analogous properties as spin. A $B^0\bar{B}^0$ pair from decay $\Upsilon(4S) \rightarrow B^0\bar{B}^0$ is in the flavor singlet as follows:

$$|\psi\rangle = \frac{|B^0\bar{B}^0\rangle - |\bar{B}^0B^0\rangle}{\sqrt{2}} \quad (1.33)$$

The "measurement" on flavor number is performed when either of the B^0 decays, for example, through $B^0 \rightarrow D^*l\nu$. As it follows

$$B^0 \rightarrow D^{*+}l^-\bar{\nu} \quad \bar{B}^0 \rightarrow D^{*-}l^+\nu, \quad (1.34)$$

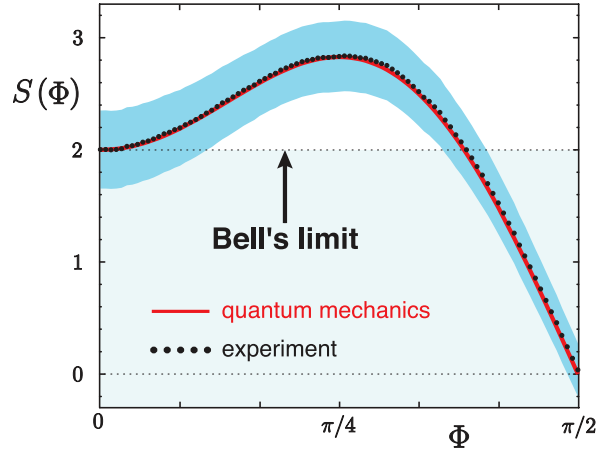


Figure 1.9: The result of H. Sakai (2006) [35]. \mathbf{c} and \mathbf{d} are fixed so that S is maximized, and Φ is defined as the angle between \mathbf{a} and \mathbf{b} . The red line is theoretical prediction by QM, not a fit to the experiment.

by identifying the charge of the lepton, one can find the flavor of the decayed b-meson; B^0 or \bar{B}^0 , **as well as that of the living b-meson** as the projection on (1.34) occurs

$$\frac{|B^0\bar{B}^0\rangle - |\bar{B}^0B^0\rangle}{\sqrt{2}} \rightarrow \frac{|B^0\bar{B}^0\rangle}{\sqrt{2}} \text{ or } -\frac{|\bar{B}^0B^0\rangle}{\sqrt{2}}, \quad (1.35)$$

in which the dynamics of state projection is the identical to the case with spin measurements. Thus, defining the quantities $A, B = \pm 1$ as the charge of the leptons in the final state (1.34), the rest of the argument in the Bell's theorem seems to work in the same way.

However, one problem peculiar to this case is that, the measurement outcome (A, B) is always $(+, -)$, $(-, +)$, which corresponds to a spin measurement with setting the both measurement axes in the same orientation. This is apparently boring and of course no difference is manifested between QM and LHVTs. Yet, here comes the flavor oscillation saving the situation.

The flavor oscillation is a phenomenon that a neutral meson, here B^0 , exchanges the flavor due to the intermediate box diagrams as Fig. 1.10. If the prompt meson decay at $t = t_1$ reveals it is B^0 , the flavor of the rest meson is determined as \bar{B}^0 at the moment. However the time evolution is written as:

$$\begin{aligned} |\psi(t')\rangle &= g_+(t) |B^0\rangle + g_-(t) |\bar{B}^0\rangle \\ g_+(t) &= (-e^{-\lambda_S t'} + e^{-\lambda_L t'})/2 \\ g_-(t) &= (e^{-\lambda_S t'} + e^{-\lambda_L t'})/2 \end{aligned} \quad (1.36)$$

where the contribution from CP violation is ignored. t' is defined the time lapse $t' := t - t_1$. It is analogous to the precession of spins, except the damping factor λ which represents the decay rate into the channels other than (1.34) in interest.

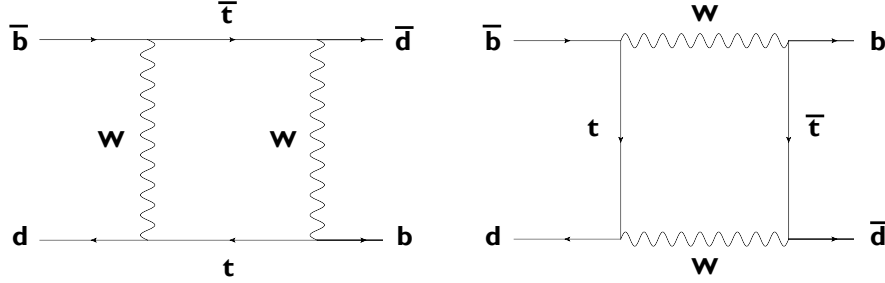


Figure 1.10: Processes responsible for flavor oscillation. The valence quarks inside B^0 and \bar{B}^0 exchange their flavor spontaneously driven by this inner dynamics of weak interaction.

Therefore, though the situation that only the lepton charge \pm can be measured, the state itself evolves instead, analogous to that the measurement axes are still fixed but the spin itself rotates. In fact in QM, the measurements are equivalent between rotated spin with fixed axes and fixed spin with the axes rotated, if the relative configuration is the same. Thus, selecting a measurement time in the cases of meson oscillation, corresponds to setting a measurement axis to a direction.

In this sense, the correlation amplitude $E(t_1, t_2)$ is analogously defined as

$$E(t_1, t_2) = \frac{N_{++}(t_1, t_2) - N_{+-}(t_1, t_2) - N_{-+}(t_1, t_2) + N_{--}(t_1, t_2)}{N_{++}(t_1, t_2) + N_{+-}(t_1, t_2) + N_{-+}(t_1, t_2) + N_{--}(t_1, t_2)}, \quad (1.37)$$

where $N_{ij}(t_1, t_2)$ represents the rate of observed events where the two meson decays at $t = t_1, t_2$ yielding $A(t_1, t_2) = i, B(t_1, t_2) = j$ ($i, j = \pm 1$).

With this $E(t_1, t_2)$ and the locality assumption, one can construct an inequality like (1.22) and test it in experiment. However, as the test of LHVTs, there are bunches of problems, for example the free will loophole since the decay time can not controlled by observers; The assumed locality are also suspicious since the decays occur one after the other; the efficiency is low enough to induce the efficiency loophole; finally, there is also the "unitarity problem" typical to this meson experiments, which is in short: here events to the decay branches other than (1.34) are ignored, and effectively the flavor correlation (1.37) is reconstructed with the sampled small fraction of events. Thus, the observed violation can be attributed to the potential biasing due to the sampling. Comprehensive discussion is provided in R. A. Bertlmann *et al.* (2004) [39] and T. Ichikawa (2008) [40].

For those complications, this kind of experiments usually aims for observing the quantum coherence of (1.33) by comparing the modulating correlation $E(t_1, t_2)$ (1.37) between data and the prediction of QM or some other models, rather than excluding the entire class of LHVTs by testing Bell's inequality. For example, the standard QM, which interprets (1.33) a coherent superposition, predicts

$$A(t_1, t_2) = \cos(\Delta m_d \Delta t), \quad (1.38)$$

showing a modulation against Δt but not respective t_1 and t_2 , representing the inseparability of the state (1.33). On the other hand, if the two mesons are not coherently superposed but in a statistical mixture $\rho = |B^0 \bar{B}^0\rangle \langle B^0 \bar{B}^0| + |\bar{B}^0 B^0\rangle \langle \bar{B}^0 B^0|$,

$$A(t_1, t_2) = \cos(\Delta m_d t_1) \cos(\Delta m_d t_2) \quad (1.39)$$

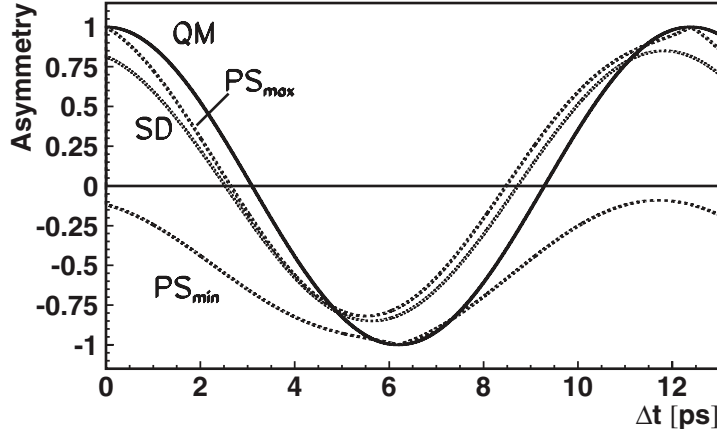


Figure 1.11: Theoretical prediction for of the function $E(t_1, t_2)$ against Δt between the models; the standard QM (1.38); SD (simultaneous decoherence; (1.39)) and PS (Pompili-Slleri) which is a class of LHVT model describing meson oscillation [41]. Since the PS provides a range of models with different prediction on $E(t_1, t_2)$, it is expressed with a band sandwiched by the dotted lines.

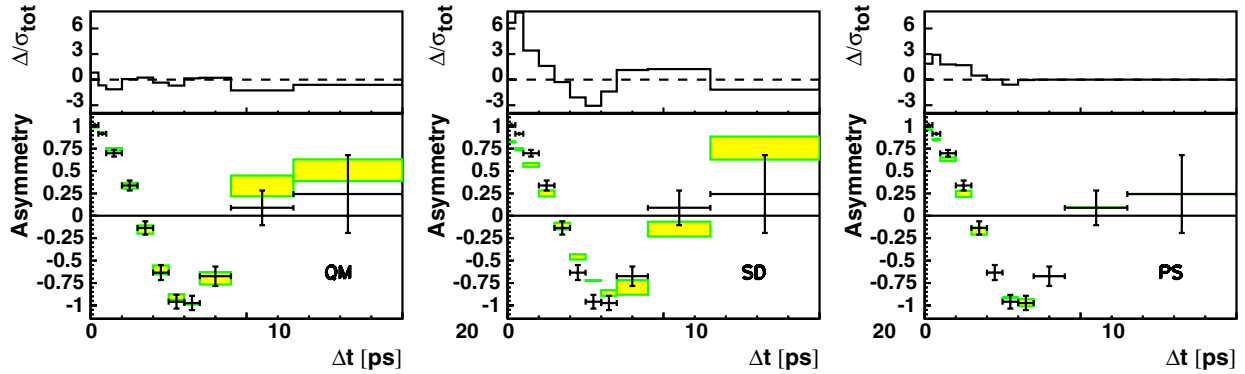


Figure 1.12: The result of Belle (2007) analysis [38]. The respective plots indicate the comparison between measurement and the models. The boxes show theoretical value with uncertainty on Δm_d . While QM shows a nice consistency with $\chi^2 = 5.2$, SD and PS give large deviations respectively $\chi^2 = 174, 31.3$.

(see Fig. 1.11). The result of Belle (2007) is presented in Fig. 1.12. The modulation quite agrees with the standard QM curve.

The case of $K^0\bar{K}^0$ is essentially similar, though there are some phenomenological differences (larger mass discrepancy between K_S^0 and K_L^0 etc.) which is important to other physics.

1.4 What is still Interesting with testing Bell's inequality?

As mentioned above, the photon experiments evolve day-by-day, and it seems matter of times that the efficiency and the locality loophole at once. The triumph of QM is close. Then what should we do in the "post-war" days. Apart from the main theme of thesis, in the section, a review of recent activities relevant to Bell inequalities is provided from a general viewpoint first, and then the motivation of the study done in the paper is presented.

Test of non-local realistic theories

It is shown by the violation of Bell's inequality that the realism and the locality do not coexist in the nature, then which is wrong after all, or they are both wrong as in QM is next interest. As for this, it has been great works from both theory and experiment sides: the Leggett inequality.

It is formulated by A. Leggett (2003) [43] by extending a Bell's inequality that expresses the bound of correlation where any realistic theories, including non-local ones, have to follow. As done in Bell inequalities, it has been also tested through experiments. With some auxiliary assumption though, the violation is demonstrated [44]. Thus, the concept of reality is also endangered. It is utterly astonishing that the seemingly trivial statement that physical quantities have determined value provokes this much rebuttal, and that it is demonstrated through the method of positive science rather than philosophy.

Test of local QM models

On the other hand, what if a combination of the local non-realistic theories? As there has been almost no necessity to consider such group of theories so far, there is no great motivation for perform a general test of them. However, testing a specific sub-group, local-QM is interested. For example, the Bohm-Aharonov postulate [45], a simple model of QM where the many-body coherence is described to dissolve when they are far apart. This idea itself is truly reasonable since naively thinking, it is weird that the coherence is conserved forever.

This local-QM model, or inversely quantum non-locality, can be tested by ordinary Bell's inequalities without any extension. It is even easy to test, since the it is free from the loopholes affair thus most of the experiments which are regarded as imperfect tests of LHVT could be good tests of quantum non-locality.

Test of universality of the violation

Aside from non-locality, another interest is casted on if the Bell's inequality violation is a general nature of the world or only the case in a specific system. To answer the question, similar tests in various type of systems are desirable, especially in massive particles system since the violation is less trivial. This is because of shorter coherence length of massive particles, leading to a more localized wave function (more like a particle) compared with massless particles with broaden wave-packet in position.

In addition, tests in massive particles system can lay more emphasis on testing non-locality since the particles are more localized. In contrast, the violation in photon systems may be able to be explained by the overlapped wave function rather than the non-locality.

Motivation on the study

The primary aim of the experiment described in the thesis is testing universal validity of QM, by observing the violation of Bell's inequality in various systems. At least in terms of the variety of systems, current collider experiments provide a preferable environment: wildly ranged energy scales $1\text{GeV} \sim 1000\text{GeV}$ are

available, including particles in variations (bosons and fermions, leptons and hadrons, massive and light etc.) with 3 interactions (strong, weak and electro-magnetic) involved.

The $K^0\bar{K}^0$ and $B^0\bar{B}^0$ experiments above are the examples, however the method is hardly extendable to tests in other systems, since it has to exploit highly specific properties of the flavor oscillation. On the other hand, this thesis focuses again on spin entanglement, which is a quite ubiquitous phenomenon in collider experiments, trying to extend the horizon of testability of Bell's inequality in general systems.

Chapter 2

Design of the Experiment

The paper presents an experiment in colliders, using the spin entanglement of two particles from a decay instead of quasi-spin, which is more close to the Bell's original argument (section 1.2). This section illustrates the detail.

2.1 Fundamental Idea

To carry out a Bell's type experiment, there are two components at least to be maintained.

- Production of entangled states with high purity
- Accurate measurement on spin polarization

Though these are in fact the bottleneck in the particle experiment in terms of technology and statistics, in the following, it is shown that these two can be managed in collider experiments. Note that these are the decent minimum requirement and there are more other conditions to be satisfied to perform a "better experiment" for example with fewer loopholes. These details are argued in the later section 2.3.

2.1.1 Source of entanglement

Collider experiments are the experiments that studies the physics in high energy scale, by hitting parcels face-to-face each other creating a high-energy state. Through the collision process, many unstable particles are created as intermediate states which decay into other particles usually after a certain short while within the detector. The entanglement often emerges between the secondary decay particles, just as the meson pairs $K^0\bar{K}^0$ from $\phi \rightarrow K^0\bar{K}^0$ in which their flavor number (strangeness) are entangled (see section 1.3.4). The spin entanglement is in fact more ubiquitous phenomenon in colliders. For example, when a pseudo-scalar charmonium ($c\bar{c}$, bound state of a c quark and an anti-c quark) η_c decays into spin one-half fermions pair $\Lambda\bar{\Lambda}$, they realizes the spin singlet state

$$|\psi_{\Lambda\bar{\Lambda}}\rangle = \frac{|\uparrow\rangle|\downarrow\rangle - |\downarrow\rangle|\uparrow\rangle}{\sqrt{2}}. \quad (2.1)$$

This is a maximally entangled state in spin, and a faithful realization of Bohm's type of *gedankenexperiment* 1.1.2. There are enormous example such as $\pi_0 \rightarrow \gamma\gamma$ that demonstrates the entanglement of spin or polarization between the daughter particles, therefore particle decays can serve as the source of entangled state.

The purity is another problem. The key factor is the performance of selecting particular events where the target decay process takes place ("signal"), out of the huge mess with other types of events which is not interested in. ("background"; BG). Fortunately, this is also the important subject for most of the other physics programs in collider experiments (such as new physics search and so on), the detector technology or know-how in analysis etc. have been developed to a substantially high level that, in a low BG environment such as the e^+e^- collision, with appropriate selection procedures, the BG fraction in the acquired final samples can be suppressed under $2 \sim 3\%$, for the channels interested in the paper. In contrast, in a high BG environment, proton-proton collider for example, it is very difficult even with current technologies.

2.1.2 Weak decay as polarizer

Direct measurement on spins of unstable particles in colliders are not feasible in any current colliders, however instead, the nature endows us the parity-violating weak interaction somehow, particles decaying through the weak interaction emit their daughters to (against) the direction of their spins; the particles tell their polarization by themselves. For instance, in the process $\Lambda \rightarrow p\pi$, the π tends to emerge against the Λ spin direction; π from $\tau \rightarrow \pi\nu$ prefers the direction of the τ spin and so on. Therefore the spin of parent particles can be inferred by the direction to which the daughter particles orient in the final state. This kind of decays are referred to "polarimeter decays" in the rest of the contents. Generally, the distribution of a daughter particle C coming from a certain 2-body weak decay $B \rightarrow CD$ is expressed as:

$$\frac{d\Gamma}{d\Omega} \propto 1 + \alpha \mathbf{s} \cdot \mathbf{n} \quad (2.2)$$

where the \mathbf{s} and \mathbf{n} are respectively the spin of the parent B and the direction of motion of the daughter C. The parameter α indicates the strength between their correlation, characterized only by the decay process, valuing over -1 to 1 . Larger α^2 enables \mathbf{s} to be measured more precisely since \mathbf{n} and \mathbf{s} are more correlated, thus α^2 is the measure of the "performance" of the decay. The sign of α represents the sign of the correlation, that is to say, \mathbf{s} and \mathbf{n} tends to be parallel when $\alpha > 0$ and verse visa. The decay $\Lambda \rightarrow p\pi$ has a large α value with $\alpha = -0.642 \pm 0.013$ (PDG 2012) [48] so we let it serve as the "polarimeter" of Λ . The mechanism of this "self-polarimeter" [46] that the spin is estimated from the direction of the final state particles is basically the same as that of proton-graphite scattering in the proton pair experiment 1.3.3, but this mechanism is amazing and profound in that the nature prepare such a scheme by itself.

As a matter of course, large α^2 is preferred. Tab. 2.1 is the list of $B \rightarrow CD$ type 2-body weak decay with large α^2 value. $\tau \rightarrow \pi\nu$ boasts of the largest α value with almost 1. In general, leptonic decays channel tend to have large α , while the number is quite limited. The variety of hadronic decay channels is in contrast huge however, as generally they have the contribution from the parity conserving strong or electro-magnetic (EM) interaction and with some reasons regarding to kinematics, it is difficult to have α unless it is hyper lucky. The physics determining the α and its quantitative formulation is given in the next section. Considering practical utility (statistics, easy to measure etc.), the useful channels in Tab.2.1 are $\Lambda \rightarrow p\pi^-$, $\tau^- \rightarrow \pi^- \nu$ and their charge conjugation $\bar{\Lambda} \rightarrow \bar{p}\pi^+$, $\tau^+ \rightarrow \pi^+ \bar{\nu}$.

Table 2.1: The list of "polarimeter decay". The upper stacks are hadronic, the lower are leptonic decay channels. For the hadronic channels, α are referred as the measured value [48], while for the leptonic channels they show theoretical values (Standard Model) [49]. Ignoring the tiny effect from the CP violation, the charge conjugate processes exhibit the identical properties except the sign of α is opposite.

B \rightarrow CD	α	Branching of B \rightarrow CD
$\Lambda \rightarrow p\pi^-$	-0.642 ± 0.013	$(63.9 \pm 0.5)\%$
$\Lambda \rightarrow n\pi_0$	-0.648 ± 0.045	$(35.8 \pm 0.5)\%$
$\Sigma^+ \rightarrow p\pi_0$	$-0.98^{+0.017}_{-0.015}$	$(51.57 \pm 0.3)\%$
$\Lambda_c^+ \rightarrow \Lambda\pi^+$	-0.91 ± 0.015	$(1.07 \pm 0.28)\%$
$\Lambda_c^+ \rightarrow \Sigma^+\pi_0$	-0.45 ± 0.34	$(1.00 \pm 0.34)\%$
$\tau^- \rightarrow e^- \nu_\tau \bar{\nu}_e$	0.33	$(17.83 \pm 0.04)\%$
$\tau^- \rightarrow \mu \nu_\tau \bar{\nu}_\mu$	0.33	$(17.41 \pm 0.04)\%$
$\tau^- \rightarrow \pi^- \nu_\tau$	1.00	$(10.83 \pm 0.06)\%$
$\tau^- \rightarrow \rho^- \nu_\tau$	0.46	$(25.52 \pm 0.09)\%$
$W^- \rightarrow l^- \bar{\nu}$	1.00	$(32.6 \pm 0.03)\%$

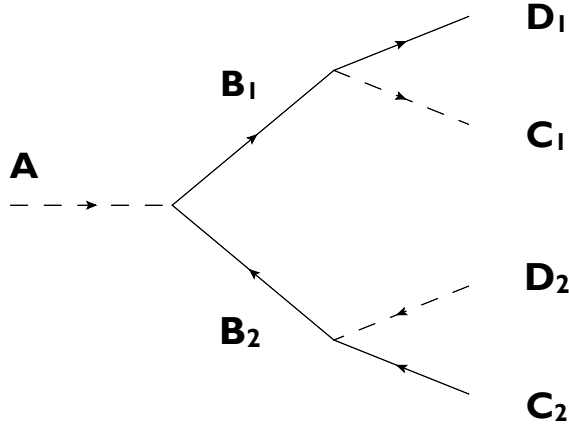


Figure 2.1: The cascade decays $A \rightarrow B_1 B_2$; $B_1 \rightarrow C_1 D_1$; $B_2 \rightarrow C_2 D_2$. Find initial states A such that the subsequent B_1 and B_2 are entangled in their spin. The spin of B_1 and B_2 are measured respectively through the direction of motion of C_1 and C_2 .

2.1.3 Candidate channels

To summarize the result of the two section above, here a cascade decays $A \rightarrow B_1 B_2$; $B_1 \rightarrow C_1 D_1$; $B_2 \rightarrow C_2 D_2$ is in consideration in which the spin entanglement is given through $A \rightarrow B_1 B_2$, and the subsequent decays $B_1 \rightarrow C_1 D_1$, $B_2 \rightarrow C_2 D_2$ have be a certain type of weak decays so as to measure the B_1, B_2 spins (Fig. 2.1). Practically, $(B_1, B_2) = (\Lambda, \bar{\Lambda}), (\tau^-, \tau^+)$, $(C_1, C_2) = (\pi^-, \pi^+)$ seem to be promising. The last thing to be discussed is then the first decay $A \rightarrow B_1 B_2$, the source of $\Lambda\bar{\Lambda}$ or $\tau^-\tau^+$ ¹.

The main production channels of $\Lambda\bar{\Lambda}$ are the charmonium decays $c\bar{c} \rightarrow \Lambda\bar{\Lambda}$ such as η_c, χ_{c0} and J/ψ . The $\tau\tau$ pairs are mainly generated in the e^+e^- colliders via $e^+e^- \rightarrow \gamma^* \rightarrow \tau\tau$ or $e^+e^- \rightarrow Z^* \rightarrow \tau\tau$.

From view of the strength of spin entanglement, the spin 0 initial states are desirable since they lead to maximally entangled states. As for charmoniums, η_c and χ_{c0} are scalar thus the candidates. Those are

¹In the following, $\tau^+\tau^-$ is abbreviated as $\tau\tau$ if no confusion.

massively produced in the recent "charm factory" experiments such as BES3 [51] or CLEO [52] therefore the statistics is abundant even though the branching fractions to $\Lambda\bar{\Lambda}$ are small (typically $\sim 1\%$). Decays from scalar to $\tau\tau$ are not easily accessible. Heavy meson decays $\eta_b \rightarrow \tau\tau$ or $\chi_{b0} \rightarrow \tau\tau$ etc. can be supposed as the candidate however they have even not confirmed yet [48]. The other candidate is the Higgs boson decay $H \rightarrow \tau\tau$ ². Although, it does include problems in every aspect to test LHVTs and so on with the Higgs decay (statistics, sample purity, the character of Higgs is not trivial as well etc.), it is interesting to think how much they can be solved in the future Higgs factory project in the ILC (International Collider) [53]. This is the first application of the Higgs boson, as well as the BI test in the most exotic system.

Vector initial states are the second choices from the viewpoint of spin entanglement but still potentially available. In particular, since the J/ψ has been the primary target of charm physics for a long time, J/ψ has incredibly high statistics produced in the charm factories, so does the $J/\psi \rightarrow \Lambda\bar{\Lambda}$ channel accordingly ($\sim 10^9$). This is the most promising channel in terms of experimental sensitivity if $\Lambda\bar{\Lambda}$ has enough strong entanglement. As for the $\tau\tau$ channel, the $Z \rightarrow \tau\tau$ event samples are available, collected in the Z factory experiment LEP [54] with a large sample size about 10^6 . This channel is important in that the energy scale is at the weak scale ($\sim 100\text{GeV}$), which is by far higher than that of other BI experiments done ever.

The initial state A is not necessarily to be at a particle resonance. The direct production via beam collision such as $e^+e^- \rightarrow \gamma^* \rightarrow \tau\tau$ is also available as long as the τ spins are entangled. This reaction is very common which massively occurs in many experiments as continuum background. For example, at the Belle experiment [55], the e^+e^- beam energy is tuned to create b-mesons such as $\Upsilon(4S)$, however the $e^+e^- \rightarrow \gamma^* \rightarrow \tau\tau$ has a huge cross-section of 7.8nb which is comparable to $\sim 10^9$ events, assuming the integrated luminosity 771fb^{-1} , which is the most promising candidate if considering only statistics.

This type of test of BI, using the spin entanglement of unstable particles generated in colliders, was first proposed by N. A. Törnqvist with $c\bar{c} \rightarrow \Lambda\bar{\Lambda} \rightarrow p\pi\bar{p}\pi$ [46][56]. The DM2 experiment responded to it and carried out the measurement in the $J/\psi \rightarrow \Lambda\bar{\Lambda}$ channel [57], however observing no inconsistency to the BI due to the ineffective entanglement of $\Lambda\bar{\Lambda}$ pairs, which will be shown in detail in chapter 4. Recently, the same test is planned, with the samples of the different channel $\eta_c \rightarrow \Lambda\bar{\Lambda}$ collected in the BES [58]. From theoretical side as well, J. P. Baranov provided a new formalism regarding to the test [59]. In the paper, the author deals with these with different formulation of the inequality to test and analysis as illustrated in chapter 3 and 4. The $\tau\tau \rightarrow \pi\nu\pi\nu$ channel used to be intensively studied from both theory and experiment side, in the context of electro-weak theory such as the test of the V-A interaction in CLEO (1999) [62]. A proposal has been made by P. Privitera (1992) [63] that the result of the LEP analysis can be used to test LHVT and quantum non-locality, as this paper suggests. However, it has been controversial on the conditions of the formulation [64], [65], and the final result has not pushed yet. The argument will be reviewed in section 2.3. The $H \rightarrow \tau\tau \rightarrow \pi\nu\pi\nu$ channel is first studied in the paper.

To sum up, this paper discusses the channels of two groups: the Λ series channels $c\bar{c}(\eta_c, \chi_{c0}, J/\psi) \rightarrow \Lambda\bar{\Lambda} \rightarrow p\pi^-\bar{p}\pi^+$; the τ series channels $Z, H \rightarrow \tau\tau \rightarrow \pi\nu\pi\nu, e^+e^- \rightarrow \gamma^* \rightarrow \tau\tau \rightarrow \pi\nu\pi\nu$. The corresponding diagrams are shown as Fig. 2.2. The channels of both series have the common event topology, as a result highly analogous. Therefore for simplicity, here the case of the Λ series is basically described. The difference from the τ series is mentioned if it becomes significant.

²The decay $H \rightarrow \tau\tau$ has been verified in LHC. [50]

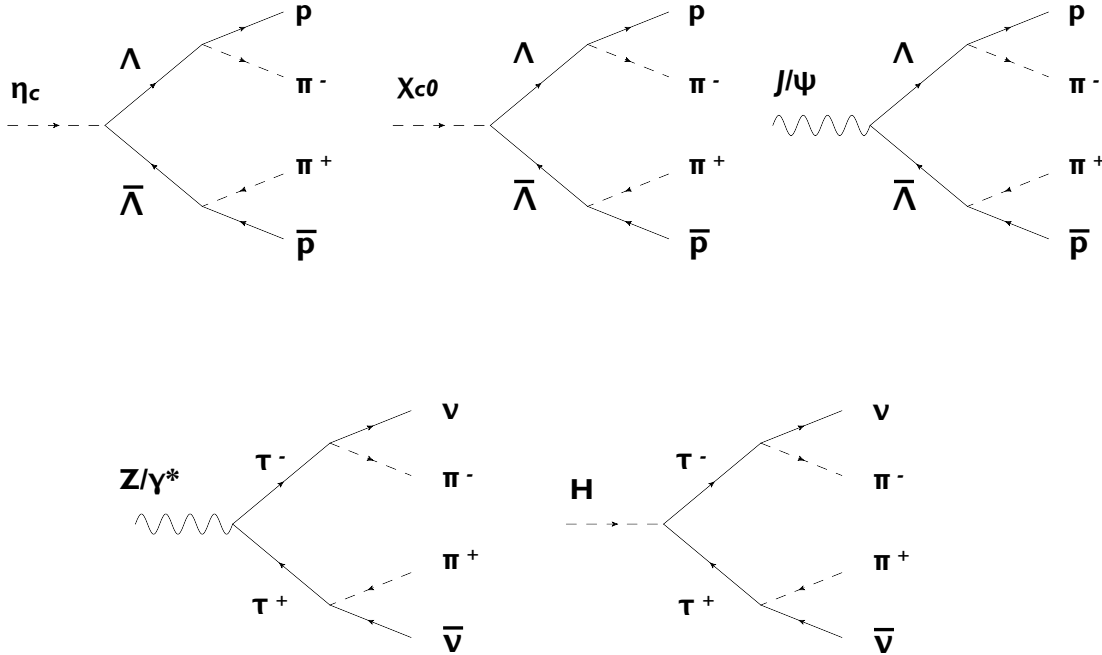


Figure 2.2: The candidate channels analyzed in the paper. $\eta_c \rightarrow \Lambda\bar{\Lambda} \rightarrow p\pi^-\bar{p}\pi^+$ (upper left), $\chi_{c0} \rightarrow \Lambda\bar{\Lambda} \rightarrow p\pi^-\bar{p}\pi^+$ (upper center), $J/\psi \rightarrow \Lambda\bar{\Lambda} \rightarrow p\pi^-\bar{p}\pi^+$ (upper right), $Z/\gamma^* \rightarrow \tau\tau \rightarrow \pi\nu\pi\nu$ (down left), $H \rightarrow \tau\tau \rightarrow \pi\nu\pi\nu$ (down right)

2.2 Weak Decay as Polarization Analyzer

The polarimeter decay is interesting by itself, aside from the context of testing Bell's inequality. In section, the phenomenology is dedicatedly studied, namely, how the parity violation is associated with the asymmetry in the decay distribution in the polarimeter decays, how much precision the spin measurement offers, comparisons with the measurement by the SG instrument.

2.2.1 Parity violation and ability as a polarizer - in a nut shell

With a brief relation between the intrinsic parity of particles and the orbital angular momentum, the asymmetry in decay distribution can be derived (here chapter 9 of [47] is partially referred).

We start with intrinsic parity, which is the parity number associated to the particle itself. For elementary particles, +1 is allocated for bosons. Fermions dose not have unique intrinsic parity³ but the relative intrinsic parity to anti-fermions are always -1 according to a simple inspection on Dirac equation. Composite particles are therefore have the opposite intrinsic parity to that of their anti-partners, providing that parity is multiplicative quantum number. Here we choose a notation that lets baryons and anti-baryons have +1, -1 for their intrinsic parity respectively. For mesons, whose anti-partner are themselves, the intrinsic parities are defined without ambiguity of notation, when the intrinsic angular momentum (spin) is taken into account. They earn another factor $(-1)^S$ (S : spin) as a result, thus scalar mesons (spin 0) have -1 , vector mesons have +1 etc.

³This is caused by the fact that fermion field ψ is not observable [66].

In the example of $\Lambda \rightarrow p\pi^-$, intrinsic parity +1 is attached to proton and Λ baryons while -1 is to π . Assuming the process conserves parity, there must be the contribution $(-1)^l$ from the relative orbital angular momentum l in the final state, since the intrinsic parity is not conserved by itself. Considering that Λ is at rest initially ($l = 0$) and total angular momentum conservation (initial state: $J=1/2$, the total spin in the final state $S=1/2$), l is uniquely determined to $l = 1$ (P-wave). On the other hand, if parity is not conserved during the decay, $l = 0$ (S-wave) mode is also allowed, which is the case here.

Total transition amplitude is the superposition of both. With S and P being the amplitude for each mode, the final state is written as

$$|\psi\rangle = S |0, \rangle |1/2, \rangle + P |1, \rangle |1/2, \rangle. \quad (2.3)$$

The indices in kets label $|l, m\rangle |S, S_z\rangle$; the relative angular momentum between p and π , and the composite spin. Assume Λ spin points to z -axis initially where $J = 1/2$, $M = 1/2$. According to the Clebsh-Gordan table, (2.3) is specified to be

$$|\psi\rangle = S |0, 0\rangle |1/2, 1/2\rangle + P \left[\sqrt{\frac{2}{3}} |1, 0\rangle |1/2, 1/2\rangle - \sqrt{\frac{1}{3}} |1, 1\rangle |1/2, -1/2\rangle \right]. \quad (2.4)$$

Note that the latter two terms of P-wave mode can be characterized by a common amplitude P . This is of representative that the physics is independent of the spatial rotation (Wigner-Eckart's theorem).

The amplitude that a proton is found to the direction (θ^*, ϕ^*) with spin state $|S = 1/2, S_z \pm 1/2\rangle$ is then

$$\langle 1/2, 1/2 | \langle \theta^*, \phi | \psi \rangle = S Y_0^0 - P \sqrt{\frac{1}{3}} Y_0^1 \quad (2.5)$$

$$\langle 1/2, -1/2 | \langle \theta^*, \phi | \psi \rangle = P \sqrt{\frac{2}{3}} Y_1^1, \quad (2.6)$$

using the spheric harmonics function $Y_l^m = \langle \theta^*, \phi^* | l, m \rangle$. The angular distribution for the proton is therefore derived as

$$\begin{aligned} \frac{d\Gamma_\Lambda}{d\Omega_p} &\propto |\langle 1/2, 1/2 | \langle \theta, \phi | \psi \rangle|^2 + |\langle 1/2, -1/2 | \langle \theta^*, \phi | \psi \rangle|^2 \\ &= \left| S \frac{1}{\sqrt{4\pi}} + \sqrt{\frac{1}{3}} P \sqrt{\frac{3}{4\pi}} \cos \theta^* \right|^2 + \left| \sqrt{\frac{2}{3}} P \sqrt{\frac{3}{8\pi}} \sin \theta^* e^{i\phi^*} \right|^2 \\ &= \frac{1}{4\pi} |S|^2 + |P|^2 - 2\text{Re}(SP^*) \cos \theta^* \\ &\propto 1 + \frac{-2\text{Re}(SP^*)}{|S|^2 + |P|^2} \cos \theta^*. \end{aligned} \quad (2.7)$$

Note that the spin sum is taken after squaring. This is because the proton is supposed to experience decoherence through the interaction with matter in the detector, in other word, the interference with the other spin state $|1/2, \pm 1/2\rangle$ dissolves.

The asymmetry $\cos \theta$ arises from the parity violating S-wave, more strictly, the interference between the S-wave and the P-wave, and it becomes maximized when the contribution from the S-wave and the P-wave are equal ($|P/S| = 1$). The distribution for π^- is similarly as

$$\frac{d\Gamma}{d\Omega_\pi} \propto 1 + \frac{2\text{Re}(SP^*)}{|S|^2 + |P|^2} \cos \theta^*. \quad (2.8)$$

$$=: 1 + \alpha \cos \theta. \quad (2.9)$$

where θ is the helicity angle; the angle between the π^- direction and the Λ spin polarization vector in the

Λ rest frame.

Since this argument only exploit general relation of parity and orbital angular momentum, it holds for the other decays such as $\tau \rightarrow \pi\nu$ as well.

2.2.2 Parity violation and ability as a polarizer - a closer look

To understand how the parameters S , P (and α) are related to physics, the method of S-matrix of QFT provides a good insight. Using the effective Lagrangian approach in the lowest level, the matrix element for $\Lambda \rightarrow p\pi^-$ is built as

$$\mathcal{M} \propto \bar{u}_p(c_V + c_A\gamma^5)u_\Lambda. \quad (2.10)$$

u_p , u_Λ are the 4-spinors of the proton and the Λ respectively. Coefficients c_V , c_A represent the fraction of Yukawa and pseudo-Yukawa coupling contributing the process, which here we call V-type and A-type interaction for the sake of convenience here, analogously to the vector / axial current interaction in the electro-weak theory. As π is pseudo-scalar, if parity is conserved during the decay, it has to couple only to the pseudo-Yukawa component (A) of the vertex (2.10), and of course this is not the case again since it is weak.

Moving to the components of matrix for $\Lambda \rightarrow p\pi$. Supposing that the Λ is at rest, the corresponding 4-spinor is

$$u_\Lambda^i = \sqrt{m_\Lambda} \begin{pmatrix} \xi \\ \xi \end{pmatrix} \quad (i = \pm). \quad (2.11)$$

Here m_Λ is the mass of Λ , ξ is 2-spinor, which describes the spin state $c_1|\uparrow\rangle + c_2|\downarrow\rangle$ in the two component expression ${}^T(c_1, c_2)$. Taking the QA and z -axis to the direction of the Λ spin, one finds $\xi = {}^T(1, 0)$.

The 4-spinor for a proton with the momentum \mathbf{p} is a bit more complicated:

$$\begin{aligned} u_p^j(\mathbf{p}) &= \begin{pmatrix} \sqrt{p \cdot \sigma} \xi_p^j \\ \sqrt{p \cdot \bar{\sigma}} \xi_p^j \end{pmatrix} \\ &= \frac{1}{\sqrt{2(E+m)}} \begin{pmatrix} (E+m - \mathbf{p} \cdot \boldsymbol{\sigma}) \xi_p^j \\ (E+m + \mathbf{p} \cdot \boldsymbol{\sigma}) \xi_p^j \end{pmatrix} \\ &= \frac{1}{\sqrt{2(E+m)}} \begin{pmatrix} (E+m \mp p) \xi_p^j \\ (E+m \pm p) \xi_p^j \end{pmatrix} \\ &=: \sqrt{\frac{E+m}{2}} \begin{pmatrix} (1 \pm \eta) \xi_p^j \\ -(1 \mp \eta) \xi_p^j \end{pmatrix} \quad (\eta := p/(E+m)) \end{aligned} \quad (2.12)$$

From the top line to the second line, one uses

$$\begin{aligned} \sqrt{p \cdot \sigma} &:= \sqrt{E - \mathbf{p} \cdot \boldsymbol{\sigma}} = \frac{E+m - \mathbf{p} \cdot \boldsymbol{\sigma}}{\sqrt{E+m}} \\ \sqrt{p \cdot \bar{\sigma}} &:= \sqrt{E + \mathbf{p} \cdot \boldsymbol{\sigma}} = \frac{E+m + \mathbf{p} \cdot \boldsymbol{\sigma}}{\sqrt{E+m}} \end{aligned}$$

with p , E and m being respectively the energy, momentum and mass of the proton. j labels the helicity, which is the spin component with respect to the particle's direction of motion $\hat{\mathbf{p}} := \mathbf{p}/|\mathbf{p}|$, and a helicity eigen-spinor $u_p^\pm(\mathbf{p})$ is defined so as to satisfy the eigen-function of helicity operator

$$\boldsymbol{\Sigma} := \begin{pmatrix} \boldsymbol{\sigma} \\ \boldsymbol{\sigma} \end{pmatrix}$$

thus,

$$(\hat{\mathbf{p}} \cdot \boldsymbol{\Sigma}) u_p^\pm(\mathbf{p}) = \pm u_p^\pm(\mathbf{p}). \quad (2.13)$$

If $\hat{\mathbf{p}}$ is set to the QA, as $(\hat{\mathbf{p}} \cdot \boldsymbol{\sigma}) \xi_{\mathbf{p}}^{\pm} = \xi_{\mathbf{p}}^{\pm}$, ξ is represented as

$$\xi_{\mathbf{p}}^{+} = \begin{pmatrix} 1 \\ 0 \end{pmatrix}_{\mathbf{p}}, \quad \xi_{\mathbf{p}}^{-} = \begin{pmatrix} 0 \\ 1 \end{pmatrix}_{\mathbf{p}},$$

or if setting the QA to the z -axis,

$$\xi_{\mathbf{p}}^{+} = \begin{pmatrix} \cos \frac{\theta^*}{2} \\ e^{i\phi^*} \sin \frac{\theta^*}{2} \end{pmatrix}_z, \quad \xi_{\mathbf{p}}^{-} = \begin{pmatrix} -e^{-i\phi^*} \sin \frac{\theta^*}{2} \\ \cos \frac{\theta^*}{2} \end{pmatrix}_z. \quad (2.14)$$

with the polar coordinates of $\hat{\mathbf{p}}$ being (θ^*, ϕ^*) .

\bar{u} is given as $\bar{u} := u^{\dagger} \gamma^0$. Here I promise that all gamma matrices are expressed in the Weyl representation throughout the paper therefore

$$\gamma^0 = \begin{pmatrix} & 1 \\ 1 & \end{pmatrix}, \quad \gamma^i = \begin{pmatrix} & \boldsymbol{\sigma} \\ -\boldsymbol{\sigma} & \end{pmatrix} \quad (i = 1, 2, 3), \quad \gamma^5 = \begin{pmatrix} -1 & \\ & 1 \end{pmatrix}.$$

The vertex component $c_V + c_A \gamma^5$ is then

$$\begin{pmatrix} c_V - c_A & \\ & c_V + c_A \end{pmatrix}. \quad (2.15)$$

Substituting (2.11), (2.12), (2.15) into (2.10), one arrives at

$$\begin{aligned} \mathcal{M} &\propto ((1 \pm \eta) \xi_{\mathbf{p}}^{\dagger j}, (1 \mp \eta) \xi_{\mathbf{p}}^{\dagger j}) \begin{pmatrix} & c_V - c_A \\ c_V + c_A & \end{pmatrix} \begin{pmatrix} \xi \\ \xi \end{pmatrix} \quad (j = \pm) \\ &= [(1 \pm \eta)(c_V - c_A) + (1 \mp \eta)(c_V + c_A)] \xi_{\mathbf{p}}^{\dagger j} \xi \\ &= 2(c_V \mp \eta c_A) \xi_{\mathbf{p}}^{\dagger j} \xi. \end{aligned}$$

Using $\xi = (1, 0)$ and (2.14), it follows for respective j as

$$\mathcal{M} \propto \begin{cases} (c_V - \eta c_A) \cos \frac{\theta^*}{2} & (j = +) \\ -(c_V + \eta c_A) \sin \frac{\theta^*}{2} e^{i\phi^*} & (j = -) \end{cases} \quad (2.16)$$

The angular distribution of the proton is obtained by squaring and summing over the spin,

$$\begin{aligned} \frac{d\Gamma}{d\Omega_p} &\propto \sum_{j=\pm} |\mathcal{M}|^2 \\ &\propto |c_V - \eta c_A|^2 \cos^2 \frac{\theta}{2} + |c_V + \eta c_A|^2 \sin^2 \frac{\theta}{2} \\ &= (|c_V|^2 + \eta^2 |c_A|^2) - 2\eta \operatorname{Re}(c_V c_A^*) \cos \theta^* \end{aligned}$$

The π distribution is given, in the polar coordinates representation (θ, ϕ)

$$\begin{aligned} \frac{d\Gamma}{d\Omega_{\pi}} &\propto 1 + \alpha \cos \theta \\ \alpha &= \frac{2\eta \operatorname{Re}(c_V c_A^*)}{|c_V|^2 + \eta^2 |c_A|^2} \end{aligned} \quad (2.17)$$

Comparing (2.7) with (2.17), one has

$$\frac{S}{P} = \frac{1}{\eta} \frac{c_V}{c_A} = \frac{E + m}{p} \frac{c_V}{c_A}$$

It is demonstrated that the mixing of the S-wave and P-wave, which is the source of the asymmetry, depends

on the ratio of the V and A coupling strength (c_V/c_A) and a kinematical factor ($1/\eta$) with respect to the outgoing particles. In the ultra-relativistic limit ($\eta \rightarrow 1$), $|S/P| = 1$ or the maximized asymmetry α^2 is achieved when $|c_V/c_A| = 1$, referred to the $V \pm A$ type interaction. Also in this limit, the extent of parity violation and the phenomenological distribution asymmetry have a direct correspondence. It does not true however, when the kinematical factor $1/\eta$ falls apart from 1. In this case, the point giving $|S/P| = 1$ deviates from $|c_V/c_A| = 1$, reflecting the emerging disagreement between chirality and helicity.

In fact, in $\Lambda \rightarrow p\pi^-$, the ratio of coupling strength is found to be far away from 1; $c_V/c_A = -0.147 \pm 0.004$ or $c_V/c_A = -0.0194 \pm 0.0005$ providing the measured value of α , (Fig. 2.3). Since the final state particles are soft ($1/\eta = 18.7$), it can still have a relatively large α value in spite of a small mixing of V and A coupling. On the other hand, $\tau \rightarrow \pi\nu$ gives $\eta = 1$, $S/P = 1$ and $\alpha_\tau = 1$, which are the straightforward consequence of that the neutrino appearing in the final state is extremely relativistic and that the interaction vertex is exactly $V - A$.

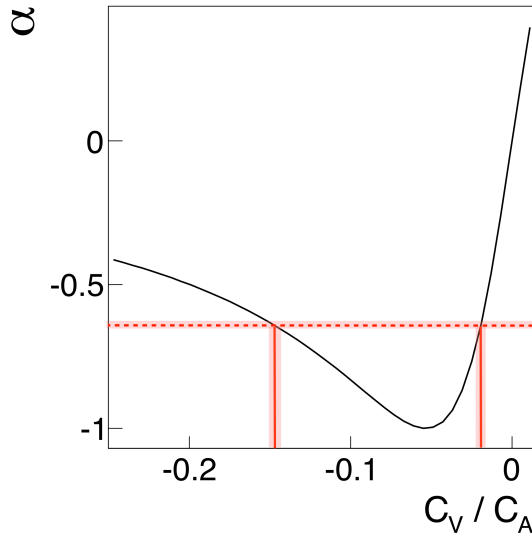


Figure 2.3: The relation of α and the ratio of coupling strength c_V/c_A in the $\Lambda \rightarrow p\pi$ channel, calculated using (2.17). c_V and c_A correspond to the contribution from the parity conservating and parity violating interaction to the decay. The ratio c_V/c_A is two-valued, in any case c_A is dominant, providing the measurement of $\alpha = -0.642 \pm 0.013$.

2.2.3 Comparison with the SG type of spin measurement

Before moving to the detail formalism of Bell's inequality, it worths overviewing the difference between the polarimeter decays and the SG type measurement in the statistical and dynamical property in term of spin measurement.

The most obvious difference at a glance might be that the measurement outcome from the SG interment is digital valued (\pm), while the polarimeter decay returns a consecutive outcome (the pion direction). It is however illustrated as below that as long as QM is concerned, these are equivalent as a measurement.

Suppose a process in which the spin of an isolated fermion, with the polarization vector \mathbf{s} , is measured

by a certain device, say the SG instrument. In the case, taking QA along to direction of measurement (here it is magnetic field) \mathbf{n} , the particle's spin state is represented as

$$|\psi\rangle = \cos\frac{\theta}{2} |\uparrow\rangle_{\mathbf{n}} + e^{i\phi} \sin\frac{\theta}{2} |\downarrow\rangle_{\mathbf{n}}.$$

The probabilities to have the respective outcome \pm is accordingly

$$P_+ = |\langle\uparrow|\psi\rangle|^2 = \cos^2\frac{\theta}{2}$$

$$P_- = |\langle\downarrow|\psi\rangle|^2 = \sin^2\frac{\theta}{2},$$

to sum up,

$$P_{\pm} = \frac{1 \pm \mathbf{s} \cdot \mathbf{n}}{2}.$$

Then, what can we say on \mathbf{s} , giving the measurement outcome \pm ? Naively thinking, if the outcome is $+$, the true spin \mathbf{s} is most likely to point along \mathbf{n} and vice versa. To be more sophisticated, a measure of the "likelihood" is introduced as

$$L = \frac{1 + \mathbf{s} \cdot \mathbf{n}}{2}, \quad (2.18)$$

which is intact the probability that the outcome \pm and the estimation \mathbf{s} are consistent. Here $\mathbf{s} = \mathbf{n}$ leads to the maximum value of L , and it falls down linearly as \mathbf{s} points to an indifferent direction. The estimation power for the likelihood formalism is usually given by the variance of the function L , namely, the region giving $\ln L = \ln L_{\max} - 1/2$ from the maximum L point is equivalent to one standard deviation contour. Likelihood L can be also defined for the case of the polarimeter decay, as the probability of observing the decaying pion to the direction \mathbf{n} , when the Λ spin points to \mathbf{s} . Using the result (2.8),

$$L = \frac{1 + \alpha \mathbf{s} \cdot \mathbf{n}}{4\pi} \quad (2.19)$$

It is therefore found that the likelihood functions are the same with that of the SG type measurement (2.18), except a numerical factor α (as for the $\tau \rightarrow \pi\nu$ channel, $\alpha_{\tau} = 1$ thus completely the same). Hereby, their statistical property, or knowledge from a measurement are equivalent between them, at least at the level of formalism. The phenomenon that a Λ with spin to \mathbf{s} emits a pion to \mathbf{n} , has then just the same structure as an measurement on Λ spin by a SG instrument with the magnetic field pointing \mathbf{n} ($-\mathbf{n}$) and with the outcome of $+$ ($-$). The pion direction plays an equivalent role as the magnetic field of the SG instrument.

On the other hand, there is another important character of spin measurement phenomenology; the dynamics of projection. Recall that in the SG case, the spin state is always projected through the measurement, parallel or anti-parallel with respect to the direction of field \mathbf{n} , and it is the ultimate cause of the non-local effect; the projection is performed even onto the state of the unmeasured spin. In order to test this non-local effect using the polarimeter decays, it has to contain the dynamical mechanism of the projection somehow in itself as well.

As the spin of an already decayed particle is complicated to define, here a two particle state, for simplicity a pair of $\Lambda\bar{\Lambda}$ in the singlet state, is in concern. It is then discussed how the hyperon decayed first Λ_1 has impact on the spin of the opposite hyperon Λ_2 space-likely apart from Λ_1 , analogous to the state projection in the normal active measurements.

First, as already shown many times, the spin state of $\Lambda_1\Lambda_2$ before either of them decays is:

$$|\psi\rangle = \frac{|\uparrow\rangle|\downarrow\rangle - |\downarrow\rangle|\uparrow\rangle}{\sqrt{2}}$$

where the left and right components of sub-ket represent the space of Λ_1 and Λ_2 respectively. Through the

prompt decay $\Lambda_1 \rightarrow p_1\pi_1$, the π_1 direction is determined on \mathbf{n}_1 and the proton p_1 helicity is on s_p , as a consequence, the state of the sub-system Λ_1 is projected into $|\mathbf{n}_1, s_p\rangle$ as:

$$|\psi\rangle \rightarrow |\psi'\rangle = \langle \mathbf{n}_1, s_p | \psi \rangle |\mathbf{n}_1, s_p\rangle. \quad (2.20)$$

The state of the sub-system Λ_2 is therefore

$$|\psi'\rangle = \langle \mathbf{n}_1, s_p | \psi \rangle = \frac{\langle \mathbf{n}_1, s_p | \uparrow \rangle_{\mathbf{n}_1} |\downarrow\rangle_{\mathbf{n}_1} - \langle \mathbf{n}_1, s_p | \downarrow \rangle_{\mathbf{n}_1} |\uparrow\rangle_{\mathbf{n}_1}}{\sqrt{2}}$$

Here the QA is taken to the \mathbf{n}_1 direction as noted by the subscripts, and $|\uparrow\rangle_{\mathbf{n}_1}$ and $|\downarrow\rangle_{\mathbf{n}_1}$ indicate that the polarization vector are respectively along \mathbf{n}_1 and $-\mathbf{n}_1$ in the rest frame.

The amplitude $\langle \mathbf{n}_1, s_p | \uparrow \rangle_{\mathbf{n}_1}$ and $\langle \mathbf{n}_1, s_p | \downarrow \rangle_{\mathbf{n}_1}$ can be straightforwardly calculated from the matrix (2.16). As $|\uparrow\rangle_{\mathbf{n}}$ is the state where \mathbf{n} and the Λ spin is parallel, it reads $\theta = 0$, $\phi = 0$, and thus $\theta^* = \pi - \theta = \pi$, $\phi^* = 0$. $|\downarrow\rangle_{\mathbf{n}}$ leads similarly to $\theta^* = 0$, $\phi^* = 0$. Therefore, they end up in

$$\begin{aligned} \langle \mathbf{n}_1, + | \uparrow \rangle_{\mathbf{n}_1} &= \langle \mathbf{n}_1, - | \downarrow \rangle_{\mathbf{n}_1} = 0 \\ \langle \mathbf{n}_1, - | \uparrow \rangle_{\mathbf{n}_1} &= -c_V - c_A\eta \\ \langle \mathbf{n}_1, + | \downarrow \rangle_{\mathbf{n}_1} &= c_V - c_A\eta \quad \eta := p/(E + m). \end{aligned}$$

It can actually be verified that the spin of Λ_2 is projected to \mathbf{n} or $-\mathbf{n}$ according to the decay of Λ_1 . When the helicity of the final state proton p_1 is $+$ ($s_p = +$),

$$|\psi'\rangle \propto (c_V - c_A\eta) |\downarrow\rangle_{\mathbf{n}_1},$$

and when $s_p = -$,

$$|\psi'\rangle \propto (c_V + c_A\eta) |\uparrow\rangle_{\mathbf{n}_1}.$$

Actually, as the proton helicity s_p is not measured in colliders, the Λ_2 spin can not be concluded to $|\uparrow\rangle_{\mathbf{n}_1}$ or $|\downarrow\rangle_{\mathbf{n}_1}$, with only information of \mathbf{n}_1 , thus the collected sample contains the both case. Note however that, this is no more than a statistical mixture, but never a coherent superposition. There is no ambiguity at event-by-event level, in this sense, the Λ_2 spin is forced to point to \mathbf{n}_1 by the decay.

This is a significant result in that the polarimeter decay is in fact does have the dynamics of projection and the pion direction does perfectly play the role the measurement axis that the SG magnetic field does. The correspondence is not only in form, but is equivalent as long as QM is concerned. However in general, there is a difference in if the observer can control the direction of the measurement axis at one's disposal. For example, in the SG measurement it is easy: the observer has the right to change the B-field direction, while it is never ever possible in the polarimeter decay because the direction of decay products are chosen randomly during the "decoherence" process as they interact macroscopically with the environment. The significance of this difference in testing LHVTs will be argued in section 2.3.2.

As for the case with $\tau\tau$ pair, and the result is even more powerful. Since there are only left-handed neutrino (right-handed anti-neutrino) in the final state, the spin state of τ_2 is singularly determined as

$$|\psi'\rangle \propto (c_V + c_A\eta) |\uparrow\rangle_{\mathbf{n}_1}.$$

if the first tau decays into $\pi^-\nu$, and

$$|\psi'\rangle \propto (c_V - c_A\eta) |\downarrow\rangle_{\mathbf{n}_1},$$

if the first tau decays into $\pi^+\bar{\nu}$, which can be easily distinguished by identifying the charge of the pion.

2.3 Phenomenology in terms of Testing LRTs - Possible Loopholes

According to the discussion so far, it is successfully demonstrated that in QM the polarization decays have the same properties as the direct measurements such as the SG spin measurement or the photon polarization measurement by polarizers. The author is now highly motivated to use these to test LHVTs as soon as possible. However, remember that it is not allowed to test LHVTs with the knowledge of QM in general. Here we want to prove that the formalism of LHVTs contradicts to reality, thus discussion should be confined within the context of LHVTs.

In this section, the interpretation of the polarimeter decays in LHVTs and if there is possible difference from the conventional spin measurements are analyzed. If so, we try to manage by applying additional assumption and specify the loopholes according to it.

2.3.1 Interpretation of the polarizer decay in LHVTs

The first suspicion is if the relation in the polarimeter decays is nevertheless true in LHVTs, that the parent spin and the daughter direction are correlated as:

$$P(\mathbf{n}|\mathbf{s}) = 1 + \alpha \mathbf{n} \cdot \mathbf{s} \quad (2.21)$$

$$P(\mathbf{n}'|\mathbf{s}') = 1 - \alpha \mathbf{n}' \cdot \mathbf{s}'. \quad (2.22)$$

$P(\mathbf{n}|\mathbf{s})$ is the conditional probability density of the daughter particle is found to \mathbf{n} when the parent spin is \mathbf{s} . These are indispensable otherwise there will be no way to get access to the spin of the parent particle. Since it is totally unclear how general LHVTs describe the weak decays, here the possibility to interpret (??) and (2.22) as experimental fact is sought.

As for the experiments measuring (2.21) and (2.22) for the $\Lambda \rightarrow p\pi$ channel, J. W. Cronin (1963) [68] or O. E. Overseth(1967)[69] are well-known where the α_Λ value is obtained as well. In either of those, a polarized ensemble of Λ was prepared, and the decay distribution of $\Lambda \rightarrow p\pi$ was measured. Then, how is the Λ polarization guaranteed? It was not confirmed by direct observation in fact, instead was derived indirectly using QM and some conservation laws as below.

Firstly, the hyperon Λ s are produced through the strong interaction reaction $\pi^-p \rightarrow \Lambda K$ caused by π beam injection to the carbon target. On the target, magnetic field is applied so that the protons inside become magnetized (polarization of each proton is not identical but prefers the B-field direction on average.). Providing that the strong interaction conserves parity, and that π and K are both pseudo-scalar with the intrinsic parity of $-$ while proton and Λ has $+$, it is easily derived that the relative orbital angular momentum between K and Λ is zero. Together with the total angular momentum conservation law, it is then shown that the Λ spin is inherited directly from that of proton which is magnetized. Thus, the Λ polarization can be assured, in a statistical sense.

Can it be reproduced without the concepts of QM but with only fairly general notions? Check the each step of the argument. The magnetization of protons in the target seems to be proper as the magnetization

of matter under magnetic field can at least be available as empirical fact. Next, the parity conservation through the Λ production $\pi^- p \rightarrow \Lambda K$. It is still reasonable to assume in LHVTs, but less trivial than the former one since it is not obvious how to understand the parity of particle generally in LHVTs. However, the spin conservation can be derived directly instead, if assuming the total angular momentum conserves during the process and that the lowest angular momentum component dominantly contributes to the low energy scattering $\pi^- p \rightarrow \Lambda K$ (the S-wave approximation), therefore the polarization of Λ in the experiment can be justified.

Since here only the conservation laws and the S-wave approximation in low energy scatterings are exploited, which are possible to empirically verified and hence universal in LHVTs, it seems still legal to assert the relations (2.21) and (2.22) in the context of LHVTs. This justification is extremely important in that the Bell's inequality used in the experiment highly relies on (2.21) and (2.22), which is shown in chapter 3.

This sort of demonstration is needed for every channel and every experimental setup, however that it is actually not sure if it succeeds in all channels and setup. For example, the case with the τ channels might need some more assumption as illustrated in Able (1992) [64], but anyway empirical, which is by far general than requiring conclusions from QM.

2.3.2 Passiveness of particle decay and the free will loophole

in section 2.2.3, it is proved that the daughter particle direction \mathbf{n} in the polarimeter decay possesses the comparable function that the spin measurement axis in the EPR *gedankenexperiment* provides. However, recall the free will loophole arises (see section 1.3.2) if the axes are fixed during the test. Unfortunately this is exactly the case where \mathbf{n} can not be chosen by the observer at will. This is so called "passiveness of decay" which is the problem almost in every particle experiment using scattering or decays, including ones introduced in the previous chapter.

The even worse thing is that, not only the Bell's inequality can be violated by some LHVTs according to the free will loophole, it is demonstrated by M. Abel *et al.* (1992) [64], H. Dreiner (1992) [65], A. Afriat and F. Sellen (1999) [70] that an explicit model can be constructed which perfectly accords to the prediction of QM, due to the fact that particle direction \mathbf{n} is not an uncommuting observable so that the three components can be determined simultaneously. This is the major conceptual complication of this experiment in testing LHVTs, which eventually discourages the attempt to analyze $Z \rightarrow \tau\tau \rightarrow \pi\nu\pi\nu$ at LEP.

This free will loophole is impossible to close though, it does not have to abandon the whole idea. An assumption with respect to locality is additionally made, so that the LHVTs that fulfill the condition can be tested. There is also the mission of testing quantum non-locality which is free from the loophole arguments. As a sign of gratitude for being allowed to exploit another assumption, in turn, we exhibit our best faith by using only the event sample where the two decays of $\Lambda\bar{\Lambda}$ or $\tau\tau$ are separated space-likely, which strongly justify the use of it. This issue is discussed in detail during chapter 3.

2.3.3 Efficiency loophole in the experiment

Aside from the conceptual problem of the free will, there are also technical complications that let another sorts of loopholes, for example the efficiency loophole or the locality loopholes.

As for the efficiency loophole, the situation is quite different from the cases of photon experiments in that the detection efficiency is usually not the problem in colliders. Apart from some exception such as neutral hadrons, neutrinos, and very soft particles, it is almost 100% since collider has thick enough material to interact with the particle. The bottleneck is the event selection as mention at the begging of the chapter 2.1.1. In this experiment, in particular, a relatively strict selection is required since the BG contamination does has some bad effect on sensitivity (to be shown in section 5.2). In addition, here only the space-like events are in use, as a result, a part of, or possibly vast majority of the signal events will be lost. The collection efficiency of signal events are typically 40% for the Λ series channels where the selection is rather easy, and 15% \sim 20% for the τ series channels with less clues due to the two neutrinos appearing in the final state.

These are far below the decent minimum efficiency in order to violate the Bell type inequalities (for example, $\epsilon_{\min} = 0.67$ (the Eberhard inequality) [27]), without applying the homogenous assumption. This is common to the other experiments in colliders such as one using $K^0\bar{K}^0$, $B^0\bar{B}^0$ (1.3.4).

2.3.4 Space-like separation of decays and the locality loophole

Locality loophole is also the weak point generally in collider experiments since observers can not control the timing of decay, as well as orientation of decay products. However, to our good luck, this can be overcome in this case.

Actually we do have some fraction of the unlucky events where the two decays are time-like, and of course it is impossible to artificially transform them into the space-like events. The fraction is estimated as follows for the Λ series channels $c\bar{c}(\eta_c, \chi_{c0}, J/\psi) \rightarrow \Lambda\bar{\Lambda}$.

Suppose a pair of $\Lambda\bar{\Lambda}$ emerged at $t = 0$ running back-to-back at the same speed $\beta_\Lambda c$ in the $c\bar{c}$ rest frame (c is the light speed.). If the hyperon Λ_1 and Λ_2 decay respectively at $t = t_1, t_2$ ($t_1 < t_2$) and with the decay length x_1, x_2 (see Fig. 2.4)), the condition that they decay in a space-like configuration in space-time is that, Λ_2 decays before the information of Λ_1 decay catches up:

$$\begin{aligned} (t_2 - t_1) c &< x_1 + x_2 \\ &= \beta_\Lambda c(t_1 + t_2) \end{aligned} \quad (2.23)$$

thus,

$$t_2 < \frac{1 + \beta_\Lambda}{1 - \beta_\Lambda} t_1 \quad (2.24)$$

Assuming the exponential decay distribution with the lifetime being τ_Λ , the fraction of the space-like events ω_1 is

$$\begin{aligned} \omega_1 &= \int_0^\infty dt_1 \int_{t_1}^{\frac{1+\beta_\Lambda}{1-\beta_\Lambda} t_1} dt_2 \frac{1}{\tau_\Lambda} \exp\left(-\frac{t_1}{\tau_\Lambda}\right) \frac{1}{\tau_\Lambda} \exp\left(-\frac{t_2}{\tau_\Lambda}\right) \\ &= \frac{\beta_\Lambda}{2}. \end{aligned} \quad (2.25)$$

Note that it is equally likely that Λ_2 decay before Λ_1 does ($t_1 > t_2$), in total, ω_1 is doubled

$$\omega = 2\omega_1 = \beta_\Lambda. \quad (2.26)$$

Note that result will be identical in any reference of frame, due to Lorentz invariance of theory. The space-like fraction ω turns to be β_Λ itself, independent of lifetime τ_Λ . β_Λ , ω etc. for respective charmonium decays are listed as Tab.2.2. The space-like fraction is just 65% \sim 75%, however, those sample can be selectively extracted, by reconstructing the decay point of the hyperons (secondary vertices) with the help of the 4 charged tracks made in the tracker as described in Fig. 2.4. Although the $\Lambda\bar{\Lambda}$ are electrically neutral, leaving no charged tracks, the vertices can be respectively found by extrapolating the tracks of $p\pi^-$ and $\bar{p}\pi^+$ (for the detail on tracker, see the following section). Accordingly, the space-like condition (2.23) reduces into a relation of the decay lengths x_1, x_2 :

$$x_1 + x_2 > \frac{1}{\beta_\Lambda} |x_2 - x_1|. \quad (2.27)$$

Thanks to the fact that Λ and $\bar{\Lambda}$ is long-lived ($\tau_\Lambda = 0.26$ ns), the average length reaches 7–9cm (see Tab.2.2) so that the reconstruction accuracy is not problematic.

Table 2.2: M_ψ is the $c\bar{c}$ mass, β_Λ expresses the Λ velocity in the $c\bar{c}$ rest frame.

Channel	M_ψ (GeV/ c^2)	β_Λ	Average decay length (cm)
$\eta_c \rightarrow \Lambda\bar{\Lambda}$	2.981	0.663	6.91
$\chi_{c0} \rightarrow \Lambda\bar{\Lambda}$	3.415	0.757	9.04
$J/\psi \rightarrow \Lambda\bar{\Lambda}$	3.096	0.693	7.50

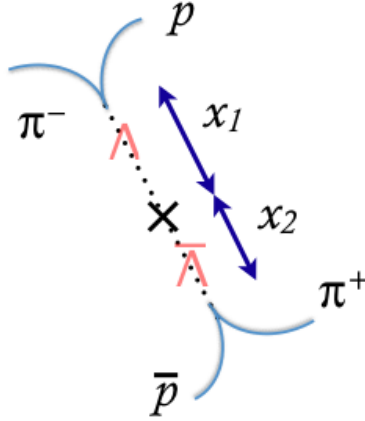


Figure 2.4: A schematic of the process $c\bar{c} \rightarrow \Lambda\bar{\Lambda} \rightarrow p\pi\bar{p}\pi$. $x_{1,2}$ is decay length of $\Lambda_{1,2} = (\Lambda, \bar{\Lambda})$. The blue lines shown the charged tracks created by passages of charged particles in the tracker. Although the $\Lambda\bar{\Lambda}$ are electrically neutral, leaving no charged tracks, the vertices can be respectively found by extrapolating the tracks of $p\pi^-$ and $\bar{p}\pi^+$.

On the other hand, the τ series channels have neutrinos in the final state, instead of p and \bar{p} in the Λ series. As these neutrinos do not interact with matters or gases leaving no signature in the detector, the space-like selection algorithm does not work any more. However, thank to that the taus decaying from Z or the Higgs are extremely fast ($\beta_\tau > 0.999$), almost all events are space-like. The direction production channel $e^+e^- \rightarrow \gamma^* \rightarrow \tau\tau$ needs additional consideration. The space-like fraction $\omega = \beta_\tau$ depends on the center of

mass energy \sqrt{s} as:

$$\begin{aligned}\beta_\tau &= p_\tau/E_\tau \\ &= \sqrt{1 - \frac{m_\tau^2}{E_\tau^2}} \\ &= \sqrt{1 - \frac{4m_\tau^2}{s}}.\end{aligned}\tag{2.28}$$

Assuming the run with $\sqrt{s} = 10.58\text{GeV}$ in the Belle experiment, $\omega = \beta_\tau = 0.94$. The contamination from the time-like events are 6% which is actually not negligible. The impact on sensitivity is quantitative evaluated in section 5.3.

2.3.5 Summary of expected loopholes and comparison with other experiments

The loophole issues discussed above is summarized in the Tab. 2.3, as well as the comparison with the other relevant experiments. Here \times indicates the presence of loophole.

As mentioned, the photon pair experiments nowadays come to close all the three, from which non-optical experiments still suffer much, in particular the locality loophole. However, the experiment proposed in the paper is suppose to close it. The advantage is striking, compared with the other collier experiments such as the $K^0\bar{K}^0$ and $B^0\bar{B}^0$ in terms of loopholes.

Table 2.3: The upper stacks are optical, the lower are non-optical experiments. The raw of Chen(2013) is for the test proposed in the paper. \times means that the respective loophole arises.

Experiments	Exp. type	Efficiency	Locality	Free-will
Aspect <i>et al.</i> (1982) [22]	photon	\times	\times	
Weih's <i>et al.</i> (1998) [30]	photon	\times		
Guistina <i>et al.</i> (2009)	photon		\times	\times
Rowe <i>et al.</i> (2001) [29]	ions		\times	\times
Sakai <i>et al.</i> (2006) [35]	proton		\times	\times
CPLEAR (1999) [36]	$K^0\bar{K}^0$	\times	\times	\times
Belle (2007) [37][38]	$B^0\bar{B}^0$	\times	\times	\times
Chen (2013)	$\Lambda\bar{\Lambda}, \tau^+\tau^-$	\times		\times

2.4 Description of the measurement and the overview of detector

In this experiment, the measured quantities are \mathbf{n} and \mathbf{n}' , the direction of the $\pi^-\pi^+$ from the decay $\Lambda\bar{\Lambda} \rightarrow p\pi^-\bar{p}\pi^+$ or $\tau\tau \rightarrow \pi^-\nu\pi^+\bar{\nu}$ defined in the rest frame of their parent particles such as $\Lambda\bar{\Lambda}$ or $\tau\tau$. To obtain \mathbf{n} and \mathbf{n}' experimentally therefore, the measurement on $\pi^+\pi^-$ direction in the laboratory frame is not sufficient but these the need additional "boost back" with respect to the movement of the parent particle, which means the 3 momenta of $\Lambda\bar{\Lambda}$ or $\tau\tau$ has to be reconstructed. The case of the Λ series channels are easy; measuring the momenta of the recoiled p and \bar{p} is satisfactory. As for the τ series channels, it needs additional technique (kinematical fit) explained in the following.

Fortunately, the detector system in colliders is highly suitable for, or perhaps even specialized in, the detail measurement of particle momenta and direction. Before the detail illustration of reconstruction algorithm of Λ and τ , here an brief overview of a standard detector complex installed in colliders is given.

A typically setup is as follows: the detector is settled around the collision point of the particle beams (Interaction Point: IP) which has a cylindrical shape covering over the beam pipe (see Fig. 2.5). It has a layered structure with detectors serving different functions. Mostly, there is a vertex detector measuring the trajectories and decay positions of particles stalled in the innermost layer, to the outside, a tracker to measure particles momenta; some auxiliary detectors for particle identification such as the time of flight (TOF) or Čerenkov counters; a solenoid magnet providing strong B-field to the inner detectors; a calorimeter for particle energy measurement and a muon detector in the outermost layer.

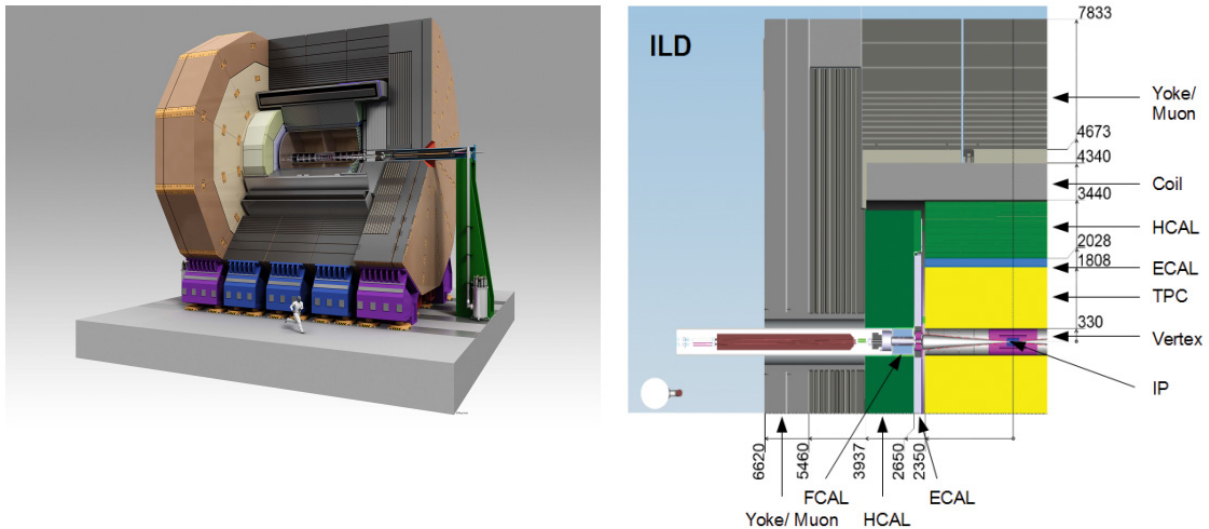


Figure 2.5: The overview of a typical detector in collider experiments. The ILD detector for the future ILC (International Linear Collier) is shown as an example [71]. The left presents the whole module. The beam pipe penetrates the center of the cylinder. The component of each detector is displayed in the right. "ECAL" and "HCAL" are respectively the electro-magnetic and hadronic calorimeter. For the tracker, TPC (time-projection chamber) is design in ILD.

As a matter of course the tracker is the key part here. The tracker is literally a detector measuring tracks, created by passage of charged particles. The most of the trackers are subject to a category called drift chambers. It is filled with gases such as argon or isobutane etc. with electric and magnetic field applied in. When a charged particle crosses through the chamber, it collides and ionizes the gas atoms and the scattered-away electron start to drift along the electric field. They are eventually absorbed by the readout causing an avalanche which is converted into electric signals. For readout, there are typically potential wires put throughout the chamber or silicon PIN diode pads, in which a voltage is applied so as to trigger the avalanche. The signal from a definite wire gives the information of position where the drifting election is absorbed. Together with information of field and the drift time which is measured as the time duration after the trigger of the prompt charged particle passage, the position of ionizations can be reconstructed.

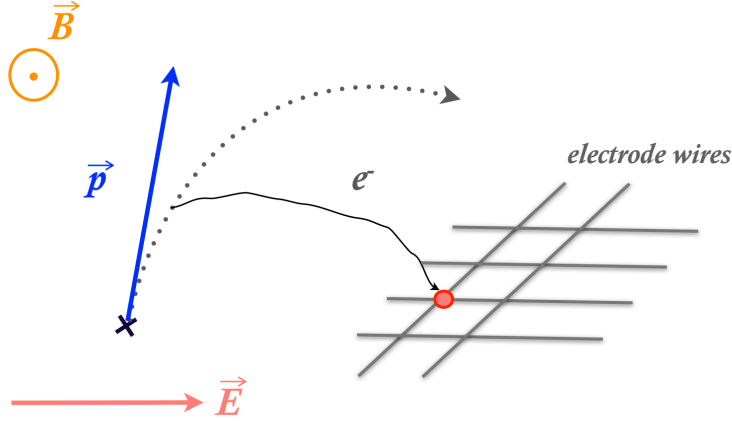


Figure 2.6: Schematic of momentum measurement in a drift chamber. Magnetic field \mathbf{B} is applied in the chamber bending the trajectory of an incident charged particle. The charged particle ionizes the atoms on its path (grey dots), of which electrons are driven into electrodes by electric field applied. Using the two or three dimensional position information of the drift electrons and their drifting time, a track of the charged particle passage (grey dotted line) can be reconstructed. The perpendicular component of the momentum to the B-field P_T is obtained by the curvature radius of the track ρ with 2.29, and the whole three components (blue line) are derived by P_T and the extrapolation of the track to its vertex (cross mark), usually approximated by IP.

Then, how the momentum of the charged particle is measured with the track? It is straightforwardly performed by bending the trajectory with a strong magnetic field \mathbf{B} applied in the chamber (usually the solenoid provided an uniform field to the direction of the beam axis) so that the curvature of the track can tell the momentum component perpendicular to the B-field (P_T), through the relation

$$P_T = eB\rho \quad (2.29)$$

where ρ is the radius curvature of the bent track.

The determination of direction of motion \mathbf{n} is a bit more difficult since the direction before being bent is in interest (the blue arrow in Fig. 2.6). Thus a fitting and an extrapolation to the IP are needed, with the assist from the information of vertex detector around the IP. Note that sometimes the track does not start from IP but from a secondary vertex which is away from IP, just as the pions from Λ or τ as interested here. When it is high momentum, which is the case for the pions from the τ decay, the approximating the secondary vertex with IP or the impact parameter (see Fig. 2.7) is quite sufficient since high momentum tracks are hardly bent. Low momentum tracks need accurate specification of the secondary vertices because the tracks are heavily bent, which the Λ series channels can be implement as described above.

The absolute value of the momentum P is then derived from P_T the direction of motion \mathbf{n} as

$$P = \frac{P_T}{\sin \theta} \quad (2.30)$$

where θ is the angle between \mathbf{n} and \mathbf{B} . Up to today, it has achieved a considerably high resolution, typically for momentum $dp/p = 0.5\% - 1\%$ with charged particles with $1\text{GeV} - 10\text{GeV}$, for direction of motion $\delta\theta, \delta\phi \sim 1\text{mrad}$, which is by far better than the required resolution as confirmed in section 5.4.

Next, the reconstruction of 3 momenta of the decayed parent particles $\Lambda\bar{\Lambda}$ and $\tau\tau$ is discussed. The case

of $\Lambda\bar{\Lambda}$ is simple. It is just the sum of the momenta obtained from the 4 visible tracks \mathbf{p}_p , \mathbf{p}_{π^-} , $\mathbf{p}_{\bar{p}}$ and \mathbf{p}_{π^+} :

$$\begin{aligned}\mathbf{p}_\Lambda &= \mathbf{p}_p + \mathbf{p}_{\pi^-} \\ \mathbf{p}_{\bar{\Lambda}} &= \mathbf{p}_{\bar{p}} + \mathbf{p}_{\pi^+}\end{aligned}\quad (2.31)$$

For the $\tau\tau$ case, to compensate the absence of neutrino tracks, the information of missing energy momentum (missing 4-momentum p_{mis}^μ) is needed. The missing 4-momentum is defined as the energy momentum imbalance between the initial and the final state, from which the sum of the neutrino contribution can be acquired:

$$p_{\text{mis}}^\mu = p_\nu^\mu + p_{\bar{\nu}}^\mu \quad (2.32)$$

if the energy and momentum of the collision have to be well-defined such as e^+e^- colliders.

As for $Z, \gamma^*, H \rightarrow \tau\tau \rightarrow \pi\nu\pi\nu$, the mass shell conditions for $\tau\tau$ can also be used

$$\begin{aligned}m_\tau^2 &= (p_- + p_\nu)^\mu (p_- + p_\nu)_\mu \\ m_\tau^2 &= (p_+ + p_{\bar{\nu}})^\mu (p_+ + p_{\bar{\nu}})_\mu.\end{aligned}\quad (2.33)$$

Considering now the degree of freedom of unknown values is 6 (3-momenta of two neutrinos), there are in fact already sufficient number of conditions (6 conditions) by (2.32) and (2.33), thus it can be analytically solved ideally, however this will be severely suffered from the measurement errors.

In addition to it, there are still other information can be exploited, for example, the decay planes of $\tau^- \rightarrow \pi^-\nu$ and $\tau^+ \rightarrow \pi^+\bar{\nu}$, by specifying the planes in which the pion tracks and their impact parameter vectors are contained in (see Fig. 2.7), which earns 2 more constraints.

These superfluous conditions are important in practice that it allows to perform a kinematical fit rather than an analytical computation with the necessary-sufficient number of conditions. By relaxing the exact relations (2.32) and (2.33) the error propagations are alleviated, that enable a stable reconstruction of $\tau\tau$ 3-momenta.

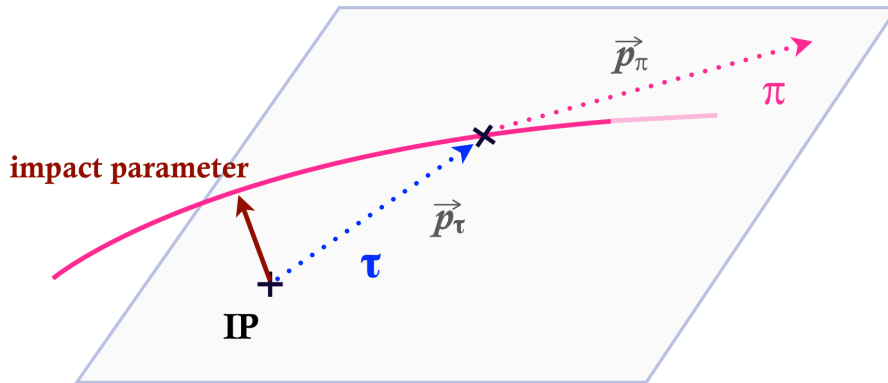


Figure 2.7: Decay plane of $\tau \rightarrow \pi\nu$ and the impact parameter, a plane spanned by the momentum vectors of π (pink dotted line) (or τ , ν) and IP. In experiments, the extrapolated π track (pink solid line) is acquired instead of the momentum vector. Usually, the decay plane is then approximated by a plane spanned by "impact parameter" (a vector from IP to the nearest point of the track) instead.

So far up to now, our conclusion is that we do not have to worry about the performance of the detector system in collider experiments, instead however, the last concern is the effect of strong magnetic field to the Λ or τ spins state. It is true that the state itself will evolve as precession, however the coherence is not

disturbed since in general the field inside the tracker is usually designed to be uniform, where the trajectory is not bent through the magnetic field-magnetic moment interaction as seen in the SG measurement.

To conclude this section, the measurability and accuracy of \mathbf{n} and \mathbf{n}' are fully adequate for either the Λ and τ series, as long as an experiment in a e^+e^- collider is considered.

Chapter 3

Formulation of Bell Inequalities for Our System

3.1 Formulation

In this chapter, the Bell's inequality (BI) is derived, specialized for our own experiment. Apart from the tests reviewed in chapter 1 where discontinuous dichotomic variables are observed, here the continuous $\pi^+\pi^-$ direction \mathbf{n}, \mathbf{n}' are in consideration. It is possible to artificially create a dichotomic variable from continuous observables as seen in the proton pair experiment (section 1.3.3), however here a straightforward way is taken to formulate an inequality with the \mathbf{n} and \mathbf{n}' are directly embedded in, that envisages the clear propagation from the spin correlation of $\Lambda\bar{\Lambda}$ or $\tau\tau$ to the pions direction. For the convenience sake, the formulation entirely proceeds in the example of $c\bar{c} \rightarrow \Lambda\bar{\Lambda} \rightarrow p\pi^- \bar{p}\pi^+$ but it is all true for the τ series channels as well,

Firstly, the relation that the $\Lambda\bar{\Lambda}$ polarization vector \mathbf{s}, \mathbf{s}' are supposed to fulfill is discussed. Defining s_i and s'_j as the projections to arbitrary unit vector (virtual axes) $\mathbf{a}, \mathbf{b}, \mathbf{c}, \mathbf{d}$ as

$$\begin{aligned} s_a &:= \mathbf{s} \cdot \mathbf{a} & s_c &:= \mathbf{s} \cdot \mathbf{c} \\ s'_b &:= \mathbf{s}' \cdot \mathbf{b} & s'_d &:= \mathbf{s}' \cdot \mathbf{d}, \end{aligned} \quad (3.1)$$

the fact $-1 \leq s_a, s'_b, s_c, s'_d \leq 1$ and (1.20) lead to a CHSH type algebraic inequality

$$|\langle s_a s'_b \rangle + \langle s_a s'_d \rangle + \langle s_c s'_b \rangle - \langle s_c s'_d \rangle| \leq 2. \quad (3.2)$$

Note that so far the reality of \mathbf{s} and \mathbf{s}' is not assumed, in other words, \mathbf{s} and \mathbf{s}' do not have to be deterministically valued as vectors in which all the three components are uniquely determined. Here \mathbf{s} and \mathbf{s}' are even allowed to be the polarization vectors in the QM, of which values do not necessarily correspond to the measurement outcome. The requirement is only that there is a three-dimensional vector \mathbf{s} characterizing the orientation spin of a spin one half and it can be assigned to any single particle. As far as this requirement is satisfied, one can immediately arrives at (3.2) as it is merely an algebraic relation.

In the language of LHVT, these \mathbf{s} and \mathbf{s}' are actually ones of hidden variables with respect to the measurement outcome, \mathbf{n} and \mathbf{n}' , which is to say,

$$\mathbf{n} = \mathbf{n}(\mathbf{s}, \mathbf{s}', \lambda), \quad \mathbf{n}' = \mathbf{n}'(\mathbf{s}, \mathbf{s}', \lambda). \quad (3.3)$$

λ represents the other hidden variables, some of which can contained by \mathbf{n} and \mathbf{n}' in common. (3.2) is in

effect the restriction imposed on the hidden variables of \mathbf{n} and \mathbf{n}' .

Next, as discussed in the section 2.3.1, the crucial relation (??) is introduced as an experimental fact that for an isolated system of a Λ with polarization vector \mathbf{s} , the π emerging from the subsequent decay $\Lambda \rightarrow p\pi$ prefers the orientation as

$$P(\mathbf{n}|\mathbf{s}) = 1 + \alpha_\Lambda \mathbf{n} \cdot \mathbf{s}, \quad (3.4)$$

where \mathbf{n} is the π direction (Assumption A). $P(\mathbf{n}|\mathbf{s})$ is the probability density function normalized with

$$\int \frac{d\Omega_{\mathbf{n}}}{4\pi} P(\mathbf{n}|\mathbf{s}) = 1. \quad (3.5)$$

For the $\bar{\Lambda} \rightarrow \bar{p}\pi^+$, it reads similarly

$$P(\mathbf{n}'|\mathbf{s}') = 1 - \alpha_\Lambda \mathbf{n}' \cdot \mathbf{s}'. \quad (3.6)$$

α_Λ is determined as $\alpha_\Lambda = -0.642 \pm 0.013$ through experiment.

Using the relations (2.21) and (2.22), the correlation amplitude $\langle n_a n'_b \rangle$ is written as

$$\begin{aligned} \langle (\mathbf{n} \cdot \mathbf{a})(\mathbf{n}' \cdot \mathbf{b}) \rangle &= \int \frac{d\Omega_{\mathbf{n}}}{4\pi} \frac{d\Omega_{\mathbf{n}'}}{4\pi} (\mathbf{n} \cdot \mathbf{a})(\mathbf{n}' \cdot \mathbf{b}) P(\mathbf{n}, \mathbf{n}') \\ &= \int \frac{d\Omega_{\mathbf{n}}}{4\pi} \frac{d\Omega_{\mathbf{n}'}}{4\pi} \frac{d\Omega_{\mathbf{s}}}{4\pi} \frac{d\Omega_{\mathbf{s}'}}{4\pi} (\mathbf{n} \cdot \mathbf{a})(\mathbf{n}' \cdot \mathbf{b}) P(\mathbf{n}, \mathbf{n}'|\mathbf{s}, \mathbf{s}') P(\mathbf{s}, \mathbf{s}'). \end{aligned} \quad (3.7)$$

with $P(x)$ notes the probability density function (PDF) with respect to the variable x . Here it is then shown that the inequality with respect to \mathbf{s} and \mathbf{s}' (3.3) obtained above can be translated into one written in the language of \mathbf{n} and \mathbf{n}' , by introducing the second assumption that if the two decays of Λ and $\bar{\Lambda}$ are in a space-like configuration in space-time, the pions orientations \mathbf{n} and \mathbf{n}' depends only on the spin of their respective parents hyperons, namely,

$$\mathbf{n} = \mathbf{n}(\mathbf{s}, \lambda) \quad \mathbf{n}' = \mathbf{n}'(\mathbf{s}', \lambda) \quad (3.8)$$

(Assumption B). This is a comparable condition to the locality principle. Hereby, the probabilistic behavior of \mathbf{n} and \mathbf{n}' are assured to be independent, and the factorization of the joint-PDF can be performed as

$$P(\mathbf{n}|\mathbf{s})P(\mathbf{n}'|\mathbf{s}') = P(\mathbf{n}, \mathbf{n}'|\mathbf{s}, \mathbf{s}') \quad (3.9)$$

Note that this assumption B is fairly reasonable in terms of LHVT, however, here the author would like to lay emphasis again on that there could be the LHVT models that elude the constrains due to the passiveness of decays, as pointed out in section 2.3.2 (the "free will" loophole). Those would be such models that the direction of $\pi^+\pi^-$ is determined beforehand, before the interaction between Λ and $\bar{\Lambda}$ is switched off, thus the pion can in principle have the dependence on the opposite hyperon spin, in which (3.8) is not true anymore.

Now forget the loophole for a while. For the LHVTs which follows the relation 3.8, with the help of (3.9), (3.7) becomes

$$\begin{aligned} &\langle (\mathbf{n} \cdot \mathbf{a})(\mathbf{n}' \cdot \mathbf{b}) \rangle \\ &= \int \frac{d\Omega_{\mathbf{n}}}{4\pi} \frac{d\Omega_{\mathbf{n}'}}{4\pi} \frac{d\Omega_{\mathbf{s}}}{4\pi} \frac{d\Omega_{\mathbf{s}'}}{4\pi} (\mathbf{n} \cdot \mathbf{a})(\mathbf{n}' \cdot \mathbf{b}) P(\mathbf{n}|\mathbf{s}) P(\mathbf{n}'|\mathbf{s}') P(\mathbf{s}, \mathbf{s}') \end{aligned} \quad (3.10)$$

Plugging (2.21) and (2.22) in,

$$= \int \frac{d\Omega_{\mathbf{n}}}{4\pi} \frac{d\Omega_{\mathbf{n}'}}{4\pi} \frac{d\Omega_{\mathbf{s}}}{4\pi} \frac{d\Omega_{\mathbf{s}'}}{4\pi} (\mathbf{n} \cdot \mathbf{a})(\mathbf{n}' \cdot \mathbf{b})(1 + \alpha_\Lambda \mathbf{n} \cdot \mathbf{s})(1 - \alpha_\Lambda \mathbf{n}' \cdot \mathbf{s}') P(\mathbf{s}, \mathbf{s}').$$

Representing \mathbf{n} and \mathbf{n}' with the polar coordinates (θ, ϕ) and (θ', ϕ') with \mathbf{s} and \mathbf{s}' being the zeniths respectively, and with integrating over $d\Omega_{\mathbf{n}}d\Omega_{\mathbf{n}'}$, it leads to

$$\begin{aligned} & \langle (\mathbf{n} \cdot \mathbf{a})(\mathbf{n}' \cdot \mathbf{b}) \rangle \\ &= \int \frac{d \cos \theta d\phi}{4\pi} \frac{d \cos \theta' d\phi'}{4\pi} \frac{d\Omega_{\mathbf{s}}}{4\pi} \frac{d\Omega_{\mathbf{s}'}}{4\pi} (a_1 \sin \theta \cos \phi + a_2 \sin \theta \sin \phi + a_3 \cos \theta) \\ & \quad \times (b_1 \sin \theta' \cos \phi' + b_2 \sin \theta' \sin \phi' + b_3 \cos \theta') (1 + \alpha_{\Lambda} \cos \theta)(1 - \alpha_{\Lambda} \cos \theta') P(\mathbf{s}, \mathbf{s}') \end{aligned}$$

Here $\cos \phi$ and $\sin \phi$ vanish with ϕ integration. As $a_3 = \mathbf{a} \cdot \mathbf{s} = s_a$, $b_3 = \mathbf{b} \cdot \mathbf{s}' = s'_b$,

$$\begin{aligned} & \langle (\mathbf{n} \cdot \mathbf{a})(\mathbf{n}' \cdot \mathbf{b}) \rangle \\ &= \left(\int \frac{d \cos \theta}{2} \frac{d \cos \theta'}{2} (1 + \alpha_{\Lambda} \cos \theta)(1 - \alpha_{\Lambda} \cos \theta') \cos \theta \cos \theta' \right) \\ & \quad \times \left(\int \frac{d\Omega_{\mathbf{s}}}{4\pi} \frac{d\Omega_{\mathbf{s}'}}{4\pi} s_a s'_b P(\mathbf{s}, \mathbf{s}') \right) \\ &= -\frac{\alpha_{\Lambda}^2}{9} \langle s_a s'_b \rangle. \end{aligned}$$

Hence, the $\pi^+\pi^-$ direction correlation $\langle s_i s_j \rangle$ is successfully tied to the $\Lambda\bar{\Lambda}$ spin correlation $\langle s_i s_j \rangle$ with a beautiful proportional relation

$$\langle n_i n_j \rangle = -\frac{\alpha_{\Lambda}^2}{9} \langle s_i s_j \rangle \quad (i = a, c; \quad j = b, d). \quad (3.11)$$

This formula is first derived by J. P. Baranov (2008) [59] with arguing the correlation of measured spin values of $\Lambda\bar{\Lambda}$: $\langle A(\mathbf{a})B(\mathbf{b}) \rangle$, instead of $\langle s_i s'_j \rangle$. There are some suspicious points in the paper:

- Measurements on the $\Lambda\bar{\Lambda}$ spins before they decay are assumed, which is never the case in reality.
- Spins are described to point to the measurement axis when they are measured, which is the notion of QM.

Then the author and Y. Nakaguchi provided the new version of the proof [72] as above.

With (3.11), the inequality for the $\Lambda\bar{\Lambda}$ spins (3.2) is transformed into

$$Q := |\langle n_a n'_b \rangle + \langle n_a n'_d \rangle + \langle n_c n'_b \rangle - \langle n_c n'_d \rangle| \leq \frac{2\alpha_{\Lambda}^2}{9} \quad (3.12)$$

Q is defined as the LHS of the inequality. This is the BI that is used in the experiment. In contrast to 3.2, it is written in the language of experimentally observable \mathbf{n} and \mathbf{n}' . The classical limit is $2\alpha^2/9$ (CL), while in QM, due to the immediate non-local spin flip as described in 2.2.3, the correlation is enhanced such that the LHS of (3.12) can reach $2\sqrt{2}\alpha^2/9$ when the Λ and $\bar{\Lambda}$ spins are in singlet, which is referred as the quantum limit (QL). This BI is extended to the other channels with reading α_{Λ} to the respective α value. Several comments are attached to this inequality.

- Thank to the fact that the hyperon spins \mathbf{s} , \mathbf{s}' are not measured directly, the inequality can be derived without requiring them to be realistic. Here the only what they are required to be is to satisfy 3.4 and 3.6 and the rest of the properties belonging to \mathbf{s} and \mathbf{s}' are not assumed. Thus inequality (3.12) could be more general than the ordinary BI formulation that requires the reality of spins as well as the locality, which is to say, it can serve to test general HVTs rather than LHVTs that are tested with the

conventional BIs. However, as this generality problem is a complicated subject, here for simplicity, the range in interest is confined in testing LHVTs, since it is plausible that (3.12) is at least valid for any LHVTs that satisfy the assumption A and B.

- To realize the condition described in the assumption B (3.8) (the locality condition), the hyperons decays should be space-like, otherwise it requires by far strong assumption to assure the factorization (3.9). It is illustrated in the previous chapter that it is experimentally possible to extract only the space-like events as for the Λ series channels, and the contamination from the time-like events are negligible as for the τ series channels except for the $e^+e^- \rightarrow \gamma^* \rightarrow \tau\tau$. The time-like contamination in fact requires the modification on the RHS of (3.12), which is discussed in the later section 5.3.
- BG events generally do not follow the BI (3.12) since the assumption A (2.21) (2.22) are not valid for those events. As a result, the restriction imposed on them becomes looser than (3.12). The reflection of the BG events to the BI is argued in the section 5.2
- One remarkable character of this BI is that, the relative magnitude of the violation does not depend on the channel of polarimeter decay. The ratio of the QL to the CL is always $\sqrt{2}$, regardless of the value of α^2 . This is because, as discussed more in detail in chapter 4, $\langle n_i n'_j \rangle$ has the same dependency (proportional to α^2) as the CL ($2\alpha^2/9$). Hence when α^2 decreases, $\langle n_i n'_j \rangle$ and the CL decline by the same extent. This fact implies that the BI (3.12) is essentially an inequality in terms of the hyperons spins, which is just converted into one with respect to the pions correlation with (3.11). Therefore, not only $\Lambda \rightarrow p\pi$ and $\tau \rightarrow \pi\nu$ but any other weak decays even with small α^2 value can violate the BI in principle. This is an important conclusion in that potentially there are more channels available, which expands the opportunity to test LHVTs and the quantum non-locality in various systems.
- Thus theoretically, the BI (3.12) can violate if only α^2 is not zero. But it would be extremely difficult to confirm it in experiment since the absolute disparity between the QL and the CL $2(\sqrt{2} - 1)\alpha^2/9$ close to zero as $\alpha^2 \rightarrow 0$. After all, large α^2 is preferred.
- From view of experimental feasibility, a noticeable character in the test using BI (3.12) is that the overall 4 terms can be measured at one run, in contrast to the ones measuring the coincidence rate such as the photon pair experiments. The axes configuration $\mathbf{a}, \mathbf{b}, \mathbf{c}, \mathbf{d}$ can be chosen after the data taking, and the data can be applied to each of the setting. Thus, it is 4 times more economical in statistics than the coincident rate type experiments. Considering that the statistics is limited in the collider experiments, this 4 times difference is huge.

Here $\mathbf{a}, \mathbf{b}, \mathbf{c}, \mathbf{d}$ are the virtual measurement axes, as seen in the proton pair experiment (section 1.3.3), which have no impact on the measure net outcome therefore play no physical role, in construct to the magnetic field of the SG instrument. The maximum value or the dependence of Q on the axes $\mathbf{a}, \mathbf{b}, \mathbf{c}, \mathbf{d}$ are determined uniquely if the data of \mathbf{n}, \mathbf{n}' are taken. Thus it is expected to be more economical to fix the axes in such a configuration that the Q is maximized, and eliminate them from the representation. In the

next section, it is demonstrated that this optimization can be performed totally analytically and the BI is reduced into an extremely concise representation which allow us to recognize the BI is violated at a glance.

3.2 Axes optimization using the method of C matrix

This section is entirely about linear algebra. The theme is to find the configuration of unit vectors \mathbf{a} , \mathbf{b} , \mathbf{c} , \mathbf{d} that maximize a value

$$Q := |\langle n_a n'_b \rangle + \langle n_a n'_d \rangle + \langle n_c n'_b \rangle - \langle n_c n'_d \rangle|.$$

Before computing, let me re-write the correlation amplitude $\langle n_a n'_b \rangle$ in terms of a 3×3 matrix \hat{C} defined as

$$\hat{C}_{ij} := \langle n_i n'_j \rangle$$

where the indices $i, j = 1, 2, 3$ correspond to x, y, z in the Cartesian coordinates respectively. With the correlation matrix C , $\langle n_a n'_b \rangle$ is reduced into the form of a bilinear

$$\langle n_a n'_b \rangle = \sum_{i=1}^3 \sum_{j=1}^3 a_i b_j \langle n_i n'_j \rangle = \mathbf{a}^T \hat{C} \mathbf{b}. \quad (3.13)$$

Accordingly, Q becomes

$$Q = |\mathbf{a}^T \hat{C} (\mathbf{b} + \mathbf{d}) + \mathbf{c}^T \hat{C} (\mathbf{b} - \mathbf{d})|. \quad (3.14)$$

Here the physical part (\hat{C}) and the rest ($\mathbf{a}, \mathbf{b}, \mathbf{c}, \mathbf{d}$) are well separated.

Next, find the maximum Q . It is obvious that considering Q as $Q = \mathbf{a}^T \hat{C} (\mathbf{b} + \mathbf{d}) + \mathbf{c}^T \hat{C} (\mathbf{b} - \mathbf{d})$ instead do not lose any generality. Also, as Q will be absolute-valued eventually, here we do not care if the obtained value is the maximum or the minimum (A simple symmetry argument proves they are identical).

The method of Lagrange multipliers (MLM) is utilized. The constraint conditions are:

$$\begin{aligned} \mathbf{a}^T \mathbf{a} &= 1, & \mathbf{b}^T \mathbf{b} &= 1 \\ \mathbf{c}^T \mathbf{c} &= 1, & \mathbf{d}^T \mathbf{d} &= 1. \end{aligned} \quad (3.15)$$

With the respective multipliers ξ_a, ξ_b, ξ_c and ξ_d , one builds a scalar function L as:

$$L = \mathbf{a}^T \hat{C} (\mathbf{b} + \mathbf{d}) + \mathbf{c}^T \hat{C} (\mathbf{b} - \mathbf{d}) \quad (3.16)$$

$$- \frac{1}{2} \xi_a (\mathbf{a}^T \mathbf{a} - 1) - \frac{1}{2} \xi_b (\mathbf{b}^T \mathbf{b} - 1) - \frac{1}{2} \xi_c (\mathbf{c}^T \mathbf{c} - 1) - \frac{1}{2} \xi_d (\mathbf{d}^T \mathbf{d} - 1). \quad (3.17)$$

Setting all the derivatives of L to zero,

$$\frac{\partial L}{\partial \mathbf{a}^T} = 0 \quad \iff \quad \hat{C} (\mathbf{b} + \mathbf{d}) - \xi_a \mathbf{a} = 0 \quad (3.18)$$

$$\frac{\partial L}{\partial \mathbf{b}} = 0 \quad \iff \quad (\mathbf{a} + \mathbf{c})^T \hat{C} - \xi_b \mathbf{b}^T = 0 \quad (3.19)$$

$$\frac{\partial L}{\partial \mathbf{c}^T} = 0 \quad \iff \quad \hat{C} (\mathbf{b} - \mathbf{d}) - \xi_c \mathbf{c} = 0 \quad (3.20)$$

$$\frac{\partial L}{\partial \mathbf{d}} = 0 \quad \iff \quad (\mathbf{a} - \mathbf{c})^T \hat{C} - \xi_d \mathbf{d}^T = 0 \quad (3.21)$$

$$\frac{\partial L}{\partial \xi_\alpha} = 0 \quad \iff \quad (3.15) \quad (\alpha = a, b, c, d).$$

Multiplying $\mathbf{a}^T, \mathbf{c}^T(\mathbf{b}, \mathbf{d})$ from the LHSs of (3.18)~(3.21) and using (3.15), the multipliers ξ_α are shown to be

$$\begin{aligned}\xi_a &= \mathbf{a}^T \hat{C}(\mathbf{b} + \mathbf{d}) & \xi_c &= \mathbf{c}^T \hat{C}(\mathbf{b} - \mathbf{d}) \\ \xi_b &= (\mathbf{a} + \mathbf{c})^T \hat{C}\mathbf{b} & \xi_d &= (\mathbf{a} - \mathbf{c})^T \hat{C}\mathbf{d}.\end{aligned}\tag{3.22}$$

Substituting these back into (3.19) and (3.21) gives

$$\begin{aligned}\mathbf{b} &= \frac{\hat{C}^T(\mathbf{a} + \mathbf{c})}{(\mathbf{a} + \mathbf{c})^T \hat{C}\mathbf{b}} =: \frac{\hat{C}^T(\mathbf{a} + \mathbf{c})}{\rho} \\ \mathbf{d} &= \frac{\hat{C}^T(\mathbf{a} - \mathbf{c})}{(\mathbf{a} - \mathbf{c})^T \hat{C}\mathbf{d}} =: \frac{\hat{C}^T(\mathbf{a} - \mathbf{c})}{\sigma}.\end{aligned}\tag{3.23}$$

\mathbf{b} and \mathbf{d} are parallel to $\hat{C}^T(\mathbf{a} + \mathbf{c})$ and $\hat{C}^T(\mathbf{a} - \mathbf{c})$ respectively. The normalization factor ρ and σ are taken to keep $|\mathbf{b}|$ and $|\mathbf{d}|$ being 1:

$$\rho = \sqrt{(\mathbf{a} + \mathbf{c})^T \hat{C}^T \hat{C} (\mathbf{a} + \mathbf{c})} \quad \sigma = \sqrt{(\mathbf{a} - \mathbf{c})^T \hat{C}^T \hat{C} (\mathbf{a} - \mathbf{c})}\tag{3.24}$$

Here, a 3×3 symmetric matrix $S := \hat{C}^T \hat{C} = \hat{C} \hat{C}^T$ is introduced. Eliminating \mathbf{b} and \mathbf{d} in (3.18) and (3.20), with (3.22) and (3.23), one finds

$$\begin{aligned}(\sigma + \rho)S\mathbf{a} + (\sigma - \rho)S\mathbf{c} &= \mu\mathbf{a} \\ (\sigma - \rho)S\mathbf{a} + (\sigma + \rho)S\mathbf{c} &= \nu\mathbf{c},\end{aligned}\tag{3.25}$$

where

$$\begin{aligned}\mu &:= (\sigma + \rho)\mathbf{a}^T S\mathbf{a} + (\sigma - \rho)\mathbf{a}^T S\mathbf{c} \\ \nu &:= (\sigma + \rho)\mathbf{c}^T S\mathbf{a} + (\sigma - \rho)\mathbf{c}^T S\mathbf{c}.\end{aligned}\tag{3.26}$$

These end up in the eigen-equations with respect to \mathbf{a} and \mathbf{c} as

$$\begin{aligned}[-4\rho\sigma S^2 + (\sigma + \rho)(\mu + \nu)S]\mathbf{a} &= \mu\nu\mathbf{a} \\ [4\rho\sigma S^2 + (\sigma + \rho)(\mu + \nu)S]\mathbf{c} &= \mu\nu\mathbf{c}.\end{aligned}\tag{3.27}$$

Seemingly these have a terribly intricate structure, since ρ , σ , μ and ν all contain \mathbf{a} and \mathbf{c} in a very complicated way. However, a simple attempt of applying the LHS of (3.27) as $T := \pm 4\rho\sigma S^2 + (\sigma + \rho)(\mu + \nu)S$ to the eigenvectors of S : \mathbf{v}_i reveals

$$[\pm 4\rho\sigma S^2 + (\sigma + \rho)(\mu + \nu)S]\mathbf{v}_i = [\pm 4\rho\sigma\lambda_i^2 + (\sigma + \rho)(\mu + \nu)\lambda_i]\mathbf{v}_i,\tag{3.28}$$

with λ_i being the eigenvalues of S and the relation $S\mathbf{v}_i = \lambda_i\mathbf{v}_i$. This shows that, every eigenvector of S is the eigenvector of R as well. Though \mathbf{v}_i are illustrated to be necessary, whether they provide sufficient solutions for (3.27) needs a little more argument. First, when S has three independent eigenvectors, it is obviously the case that \mathbf{v}_i has 1 to 1 correspondence to the eigenvectors of T thus no other solutions exist. When S possesses less than two independent eigenvectors is a bit problematic, however in the case, S is the projection operator into the eigenspace R_S . According to the nature of projector, S^2 and thus the linear combination of S^2 and S are also shown to be the projector into R_S , so is T . Therefore, the class of T is proven to be at least no more than that of S in general, which guarantees that \mathbf{v}_i gives the full description of solutions for (3.27).

As the norm of \mathbf{a} and \mathbf{c} are 1,

$$\begin{aligned}\mathbf{a} &= \pm \mathbf{v}_i \\ \mathbf{c} &= \pm \mathbf{v}_j \\ |\mathbf{v}_i| &= 1 \quad (i, j = 1, 2, 3).\end{aligned}\tag{3.29}$$

Plugging these into (3.23) and (3.24), one obtains \mathbf{b} , \mathbf{d} and the other coefficients. Considering the case with $(\mathbf{a}, \mathbf{c}) = (\mathbf{v}_i, \mathbf{v}_j)$ first,

$$\begin{aligned}\rho &= \sqrt{(\lambda_i + \lambda_j)(1 + \mathbf{v}_i^T \cdot \mathbf{v}_j)} \\ \sigma &= \sqrt{(\lambda_i + \lambda_j)(1 - \mathbf{v}_i^T \cdot \mathbf{v}_j)}\end{aligned}$$

When (i) $\mathbf{a} = \mathbf{c}$ ($i = j$),

$$\begin{aligned}\rho &= 2\sqrt{\lambda_i} & \sigma &= 0 \\ \mathbf{b} &= \frac{\hat{C}^T \mathbf{v}_i}{\sqrt{\lambda_i}} & \mathbf{d} &= (\text{arbitrary unit vector}) \\ Q &= 2\mathbf{a}^T \hat{C} \mathbf{b} = 2\sqrt{\lambda_i}.\end{aligned}\tag{3.30}$$

When (ii) $\mathbf{a} \neq \mathbf{c}$ ($i \neq j$),

$$\begin{aligned}\rho &= \sigma = \sqrt{\lambda_i + \lambda_j} \\ \mathbf{b} &= \frac{\hat{C}^T (\mathbf{v}_i + \mathbf{v}_j)}{\sqrt{\lambda_i + \lambda_j}} & \mathbf{d} &= \frac{\hat{C}^T (\mathbf{v}_i - \mathbf{v}_j)}{\sqrt{\lambda_i + \lambda_j}} \\ Q &= 2\sqrt{\lambda_i + \lambda_j}.\end{aligned}\tag{3.31}$$

Here the fact is used that $S = \hat{C}^T \hat{C}$ is a symmetric matrix which has eigenvectors orthogonal to each other ($\mathbf{v}_i^T \cdot \mathbf{v}_j = \delta_{ij}$).

The other combinations $(\mathbf{a}, \mathbf{c}) = (\mathbf{v}_i, -\mathbf{v}_j)$, $(-\mathbf{v}_i, \mathbf{v}_j)$, $(-\mathbf{v}_i, -\mathbf{v}_j)$ lead to the same result. The maximum Q is derived from (3.31), with letting λ_i and λ_j being the two largest eigenvalues of S .

Lastly, a typical concern with respect to MLM is reviewed that generally maxima (minima) derived from MLM could be local (fake) maxima where the real maximum (minimum) value does not sit at extrema but at the boundary of parameter space. However it is not case here, since the parameter space of \mathbf{a} , \mathbf{b} , \mathbf{c} , and \mathbf{d} are consecutive "spheres" that have no boundary.

To summarize,

$$Q_{\max} = 2\sqrt{\lambda_1 + \lambda_2} \leq \frac{2\alpha^2}{9}.\tag{3.32}$$

where λ_1 and λ_2 are the largest two eigenvalues of $\hat{C}^T \hat{C}$. It is not pleasant to contain values with measurement error in the upper limit, dividing with the LHS of (3.32),

$$\begin{aligned}C_{ij} &= \frac{9}{2\alpha^2} \langle n_i n'_j \rangle \quad (i, j = 1, 2, 3) \\ Q_{\max} &= 2\sqrt{\lambda_1 + \lambda_2} \\ Q_{\max} &\leq 1.\end{aligned}\tag{3.33}$$

This is the target expression. The classical limit is 1, while the QM reaches $\sqrt{2}$ at maximum.

Chapter 4

QM Analyses and the Violation of the Bell Inequality

In this chapter, a series of QM calculation is carried out to illustrate the pattern of spin entanglement of $\Lambda\bar{\Lambda}$ or $\tau\tau$ in the candidate channels; $\chi_{c0}, \eta_c, J/\psi \rightarrow \Lambda\bar{\Lambda}$; $Z, H \rightarrow \tau\tau$; $e^+e^- \rightarrow \gamma^* \rightarrow \tau\tau$, as well as to find out if they actually give the large Q_{\max} values that violate the BI derived in the previous chapter (3.33). Since QM is assumed to be the "truth" here, these are therefore the expected Q_{\max} values in experiment.

Specifically, for each channel, the distribution of $\pi^+\pi^-$ in the final state is calculated using the method of S-matrix in QFT, from which a C matrix is build

$$C = \begin{pmatrix} \langle n_x n'_x \rangle & \langle n_x n'_y \rangle & \langle n_x n'_z \rangle \\ \langle n_y n'_x \rangle & \langle n_y n'_y \rangle & \langle n_y n'_z \rangle \\ \langle n_z n'_x \rangle & \langle n_z n'_y \rangle & \langle n_z n'_z \rangle \end{pmatrix}$$

and the Q_{\max} value is specified as $Q_{\max} = 2\sqrt{\lambda_1 + \lambda_2}$ ($\lambda_{1,2}$ is the largest two eigenvalues of $C^T C$). The channel giving Q_{\max} larger than the classical limit 1 is entitled to be an possible experiment channel, which will be scrutinized further in chapter 5.

The result for the scalar channels $\eta_c, \chi_{c0} \rightarrow \Lambda\bar{\Lambda}$ and $H \rightarrow \tau\tau$ is trivial and boring that these apparently gives $Q_{\max} = \sqrt{2}$, the quantum limit. This can be easily derived with some symmetry arguments, however it is still pedagogical since the entanglement structure is clear and gives a good insight for the non-trivial channels such as ones with vector initial state.

The vector channels are interesting since the relativistic effect comes into play where the orbital angular momentum intervenes into the spin state creating highly non-trivial pattern of entanglement. Experimentally, these vector initial states have much more magnitude of statistics than the scalar channels. The result is important in considering the experimental feasibility.

The calculation itself is nothing but nasty, however the structure and the implication arising during the process is amusing.

4.1 $\chi_{c0} \rightarrow \Lambda \bar{\Lambda}$

Begin with the simplest case; the scalar initial state channel $\chi_{c0} \rightarrow \Lambda \bar{\Lambda} \rightarrow p\pi\bar{p}\pi$. The total matrix element \mathcal{M} is the product of sub-matrices corresponding to each decay:

$$\mathcal{M} = \sum_{i,j} \mathcal{M}_{\Lambda}^i \mathcal{M}_{\chi_{c0}}^{ij} \mathcal{M}_{\bar{\Lambda}}^j \quad (4.1)$$

$i, j = \pm$ denote the helicity of Λ and $\bar{\Lambda}$ respectively, of which sum are taken in the total matrix since they are unobserved intermediate modes. The sub-matrices are written as below:

$$\mathcal{M}_{\chi_{c0}}^{ij} \propto \bar{u}_{\Lambda}^i v_{\bar{\Lambda}}^j \quad (4.2)$$

$$\mathcal{M}_{\Lambda}^i \propto \bar{u}_p^{s_p} (1 + c_{\Lambda} \gamma^5) u_{\Lambda}^i \quad (4.3)$$

$$\mathcal{M}_{\bar{\Lambda}}^j \propto \bar{v}_{\bar{\Lambda}}^j (1 + c_{\bar{\Lambda}} \gamma^5) v_{\bar{p}}^{s_{\bar{p}}} \quad (4.4)$$

u and v are the 4-spinor of particle or anti-particle, s_p and $s_{\bar{p}}$ the helicity of p and \bar{p} in the final state respectively. In forming the vertex of $\chi_{c0} \rightarrow \Lambda \bar{\Lambda}$, the effective Lagrangian approach is adopted since hadrons are composite particles bounded by the strong force in which the perturbation is not guaranteed to work. With the fact that χ_{c0} is scalar and an assumption that $\chi_{c0} \rightarrow \Lambda \bar{\Lambda}$ conserve parity, the coupling can be uniquely determined as Yukawa coupling. Note that the parity conservation should not be taken for granted in general since the weak interaction could come into play. Fortunately from theoretical and experimental observation, it is well-known that the electro-magnetic interaction (EM) and the strong interaction contribute in the charmonium annihilation $c\bar{c} \rightarrow \Lambda \bar{\Lambda}$ dominantly [73], thus this parity conservation assumption is supposed to safely holds for the case here.

The matrix (4.3) is the same as (2.10) in the chapter 2. c_{Λ} $c_{\bar{\Lambda}}$ are related to c_V and c_A appearing in (2.10) through

$$c_{\Lambda} := -c_{\bar{\Lambda}} = \frac{c_A}{c_V}. \quad (4.5)$$

Start with $\chi_{c0} \rightarrow \Lambda \bar{\Lambda}$ first. Suppose that Λ flies with the momentum \mathbf{p} and $\bar{\Lambda}$ the $-\mathbf{p}$ which is back-to-back each other in the χ_{c0} rest frame (χ_{c0} -RF), and recalling that the notation of helicity of anti-particle and anti-spinor is opposite [74]

$$v^j = \begin{pmatrix} \sqrt{p \cdot \sigma} \xi^{-j} \\ -\sqrt{p \cdot \bar{\sigma}} \xi^{-j} \end{pmatrix}, \quad (4.6)$$

the sub-matrix turns to be

$$\begin{aligned} \mathcal{M}_{\chi_{c0}}^{ij} &= \bar{u}_{\Lambda}^i(\mathbf{p}) v_{\bar{\Lambda}}^j(-\mathbf{p}) \\ &= \frac{E+m}{2} ((1 \mp \eta) \xi_{\mathbf{p}}^{\dagger i}, (1 \pm \eta) \xi_{\mathbf{p}}^{\dagger i}) \gamma^0 \begin{pmatrix} (1 \pm \eta) \xi_{-\mathbf{p}}^{-i} \\ -(1 \mp \eta) \xi_{-\mathbf{p}}^{-i} \end{pmatrix} \\ &= \frac{E+m}{2} ((1 \pm \eta) \xi_{\mathbf{p}}^{\dagger i}, (1 \mp \eta) \xi_{\mathbf{p}}^{\dagger i}) \begin{pmatrix} (1 \pm \eta) \xi_{-\mathbf{p}}^{-i} \\ -(1 \mp \eta) \xi_{-\mathbf{p}}^{-i} \end{pmatrix} \end{aligned} \quad (4.7)$$

where E_{Λ} , p_{Λ} and m_{Λ} are Λ ($\bar{\Lambda}$) energy, momentum and mass respectively. Here the 2-spinor $\xi_{\mathbf{p}}^{\pm}$ is defined the same as (2.14) in chapter 2, so as $\eta := p_{\Lambda}/(E_{\Lambda} + m_{\Lambda})$. Representing \mathbf{p} with polar angle coordinates (θ, ϕ) , one finds that $-\mathbf{p}$ corresponds to $(\pi - \theta, \phi + \pi)$, thus

$$\xi_{-\mathbf{p}}^+ = \xi_{\mathbf{p}}^- \quad \xi_{-\mathbf{p}}^- = -\xi_{\mathbf{p}}^+ \quad (4.8)$$

Plugging these into the above,

$$\begin{aligned}\mathcal{M}_{\chi_{c0}}^{ij} &= \frac{E+m}{2}((1\pm\eta)\xi_{\mathbf{p}}^{\dagger i}, (1\mp\eta)\xi_{\mathbf{p}}^{\dagger i}) \begin{pmatrix} \pm(1\pm\eta)\xi_{\mathbf{p}}^i \\ \mp(1\mp\eta)\xi_{\mathbf{p}}^i \end{pmatrix} \\ &= [(1+\eta)^2 - (1-\eta)^2] \delta_{ij} \\ &= 2p_{\Lambda} \cdot \delta_{ij}\end{aligned}\tag{4.9}$$

Letting $|\psi_{\Lambda\bar{\Lambda}}\rangle$ note the $\Lambda\bar{\Lambda}$ helicity state, as $\mathcal{M}_{\chi_{c0}}^{ij}$ is proportional to the coefficients of the helicity eigenstate $i, j = \pm$,

$$\mathcal{M}_{\chi_{c0}}^{ij} \propto \langle i, j | \psi_{\Lambda\bar{\Lambda}} \rangle.$$

Therefore

$$\begin{aligned}|\psi_{\Lambda\bar{\Lambda}}\rangle &= \sum_{i,j} \langle i, j | \psi_{\Lambda\bar{\Lambda}} \rangle |i, j\rangle \\ &\propto \frac{|++\rangle + |--\rangle}{\sqrt{2}}.\end{aligned}$$

This is the helicity triplet state with maximal entanglement, which is equivalent to the spin triplet state

$$|\psi_{\Lambda\bar{\Lambda}}\rangle \rightarrow \frac{|\uparrow\downarrow\rangle - |\downarrow\uparrow\rangle}{\sqrt{2}}.\tag{4.10}$$

if boosting back to their respective Λ rest frame.

It sounds a bit weird that the outcome of composite spin of the 2 Λ s is not zero despite they are born from a spin 0 particle. An ad hoc explanation is provided from parity transformation property of Yukawa, similar to the discussion in section 2.2.1. Because of that the parity is conserved through $\chi_{c0} \rightarrow \Lambda\bar{\Lambda}$ and that the intrinsic parity of χ_{c0} , Λ and $\bar{\Lambda}$ are respectively $+$, $+$, $-$, the relative orbital angular momentum between $\Lambda\bar{\Lambda}$ has to be $l = 1$, which immediately leads to the total spin $S = 1$.

On the other hand, we know the spin conservation rule in non-relativistic system, however, these two seemingly contradicting facts are barely reconciled, since $\mathcal{M}_{\chi_{c0}} \rightarrow 0$ when $p_{\Lambda} \rightarrow 0$.

Next we come to the total matrix \mathcal{M} and obtain the $\pi^+\pi^-$ angular distribution. The relation between them is

$$\begin{aligned}\frac{d\sigma}{d\Omega_n d\Omega_{n'}} &\propto \sum_{s_p, s_{\bar{p}}} |\mathcal{M}|^2 =: \overline{|\mathcal{M}|^2} \\ &= \sum_{i,j,i',j'} \left[\overline{\mathcal{M}_{\Lambda}^{*i'} \mathcal{M}_{\Lambda}^i \mathcal{M}_{\chi_{c0}}^{ij} \mathcal{M}_{\Lambda}^{*j} \mathcal{M}_{\Lambda}^{j'} \mathcal{M}_{\chi_{c0}}^{*ij}} \right].\end{aligned}\tag{4.11}$$

Note that the sum of $s_p, s_{\bar{p}}$, expressed by the over line, is take after squaring \mathcal{M} while the helicity of $\Lambda\bar{\Lambda}$ is summed before it. Accordingly, there becomes two types of terms in (4.11); terms such as $|\mathcal{M}_{\Lambda}^+|^2$ which can be interpreted by itself as the transition probability from Λ with the helicity $+$ to $p\pi$ ("direct terms") and the others such as $\mathcal{M}_{\Lambda}^{*+} \mathcal{M}_{\Lambda}^-$ which do not mean straightforwardly the transition probability. ("interference terms"). This is the essential part of the QM formalism that the spin coherence of $\Lambda\bar{\Lambda}$ is considered to keep during the decay process and the helicity of intermediate $\Lambda\bar{\Lambda}$ state is not defined. As seen later, this interference terms play a role in enhancing the correlation amplitude Q_{\max} , giving the major impetus to the BI violation.

Define L and \bar{L} as $L_{ii'} := \overline{\mathcal{M}_{\Lambda}^{*i'} \mathcal{M}_{\Lambda}^i}$ and $\bar{L} := \overline{\mathcal{M}_{\Lambda}^{*j} \mathcal{M}_{\Lambda}^{j'}}$ and substitute (4.9) into (4.11),

$$\overline{|\mathcal{M}|^2} = 4p_{\Lambda}^2 [L_{++}\bar{L}_{++} + L_{--}\bar{L}_{--} + L_{-+}\bar{L}_{+-} + L_{+-}\bar{L}_{-+}].\tag{4.12}$$

Here $L_{\pm\pm}$ corresponds to the direct terms while $L_{\pm\mp}$ to the interference terms.

A great advantage in using S-matrix is that every sub-matrices are guaranteed to be invariant under any proper Lorentz transformations, that is to say, we are allowed to evaluate each individual piece of the matrix in different respective frame. For example, $\mathcal{M}_{\chi_{c0}}$ is calculated in the χ_{c0} -RF above, as for \mathcal{M}_Λ and $\mathcal{M}_{\bar{\Lambda}}$ we can jump the other frame, namely the Λ and the $\bar{\Lambda}$ -RF respectively.

$$\begin{aligned}
L_{ii'} &:= \overline{\mathcal{M}_\Lambda^{*i'} \mathcal{M}_\Lambda^i} \\
&= \sum_{s_p} \bar{u}_\Lambda^i (1 - c_\Lambda^* \gamma^5) \bar{u}_p^{s_p} u_p^{s_p} (1 + c_\Lambda \gamma^5) u_\Lambda^{i'} \\
&= \bar{u}_\Lambda^i (1 - c_\Lambda^* \gamma^5) (\not{p}_p + m_p) (1 + c_\Lambda \gamma^5) u_\Lambda^{i'} \\
&= \bar{u}_\Lambda^i \begin{pmatrix} 1 + c_\Lambda^* & \\ & 1 + c_\Lambda^* \end{pmatrix} \begin{pmatrix} m_p & p_p^\mu \cdot \sigma_\mu \\ p_p^\mu \cdot \bar{\sigma}_\mu & m_p \end{pmatrix} \begin{pmatrix} 1 + c_\Lambda & \\ & 1 + c_\Lambda \end{pmatrix} u_\Lambda^{i'} \\
&= \bar{u}_\Lambda^i \begin{pmatrix} m_p(1 + c_\Lambda^*)(1 - c_\Lambda) & p_p \cdot \sigma |1 + c_\Lambda|^2 \\ p_p \cdot \bar{\sigma} |1 - c_\Lambda|^2 & m_p(1 - c_\Lambda^*)(1 + c_\Lambda) \end{pmatrix} u_\Lambda^{i'}. \tag{4.13}
\end{aligned}$$

As the Λ -RF is considered, $u_\Lambda^\pm = \sqrt{m_\Lambda}^T (\xi_\Lambda^\pm, \xi_\Lambda^\pm)$. Here the "direction of boost" is defined as the direction of relative movement of the Λ -RF to the χ_{c0} -RF, and the z -axis is taken to it as well. Denoting ξ^\pm as the eigenspinor along or against the z -axis,

$$\xi_\Lambda^+ = \begin{pmatrix} 1 \\ 0 \end{pmatrix}, \quad \xi_\Lambda^- = \begin{pmatrix} 0 \\ 1 \end{pmatrix}. \tag{4.14}$$

Using these relations, one arrives

$$\begin{aligned}
L_{ii'} &= 2m_\Lambda \xi_\Lambda^{i\dagger} ((1 - |c|^2)m_p + (1 + |c|^2)E_p - (c + c^*)\mathbf{p}_p \cdot \boldsymbol{\sigma}) \xi_\Lambda^{i'} \\
&= 2m_\Lambda K \xi_\Lambda^{i\dagger} (1 - \alpha_\Lambda \mathbf{n} \cdot \boldsymbol{\sigma}) \xi_\Lambda^{i'} \\
&= \begin{cases} L_{\pm\pm} = 2m_\Lambda K (1 \pm \alpha_\Lambda n_z) \\ L_{\pm\mp} = 2m_\Lambda K \alpha_\Lambda n_\pm. \end{cases} \quad (n_\pm := n_x \pm i n_y) \tag{4.15}
\end{aligned}$$

with K , α_Λ and \mathbf{n} being

$$\begin{aligned}
K &:= (1 - |c|^2)m_p + (1 + |c|^2)E_p \\
\alpha_\Lambda &:= (c + c^*)/K \\
\mathbf{n} &:= \frac{\mathbf{p}_\pi}{p_\pi} = -\frac{\mathbf{p}_p}{p_p}. \tag{4.16}
\end{aligned}$$

Same calculation is carried out for \bar{L} in the $\bar{\Lambda}$ -RF:

$$\begin{aligned}
\bar{L}_{jj'} &= \overline{\mathcal{M}_{\bar{\Lambda}}^j \mathcal{M}_{\bar{\Lambda}}^{j'}} \\
&= \sum_{s_{\bar{p}}} \left(\bar{v}_{\bar{\Lambda}}^j (1 - c_\Lambda \gamma^5) v_{\bar{p}}^{s_{\bar{p}}} \right) \left(\bar{v}_{\bar{\Lambda}}^{j'} (1 - c_\Lambda \gamma^5) v_{\bar{p}}^{s_{\bar{p}}} \right)^* \\
&= \bar{v}_{\bar{\Lambda}}^j (1 - c_\Lambda \gamma^5) (\not{p}_{\bar{p}} - m_p) (1 + c_\Lambda^* \gamma^5) v_{\bar{\Lambda}}^{j'} \\
&= 2m_\Lambda \xi_{\bar{\Lambda}}^{-j\dagger} K (1 + \alpha_\Lambda \mathbf{n}' \cdot \boldsymbol{\sigma}) \xi_{\bar{\Lambda}}^{-j'}. \tag{4.17}
\end{aligned}$$

Here the coordinate system is taken the same as one introduced in the calculation in the Λ -RF above, in order to visualize more clearly the relation of Λ and $\bar{\Lambda}$ spin as well as the direction of π^+ and π^- . As the direction of Λ boost is taken to the z -axis, that for $\bar{\Lambda}$ becomes the $-z$ direction. The x, y axes are taken such that (x, y, z) forms a right-handed coordinate system. Fig. 4.1 is the summary of these relations. For

the sake of consistency, define $\xi_{\bar{\Lambda}}^{\pm}$ as the state where the spin points to the $\bar{\Lambda}$ direction ($-z$ direction):

$$\xi_{\bar{\Lambda}}^+ = \begin{pmatrix} 0 \\ 1 \end{pmatrix}, \xi_{\bar{\Lambda}}^- = \begin{pmatrix} 1 \\ 0 \end{pmatrix}. \quad (4.18)$$

With these expressions, one obtains

$$\begin{cases} \bar{L}_{\pm\pm} = 2m_{\Lambda}K(1 \pm \alpha_{\Lambda}n'_z) \\ \bar{L}_{\pm\mp} = -2m_{\Lambda}K\alpha_{\Lambda}n'_{\mp} \end{cases} \quad (n'_{\pm} := n'_x \pm in'_y). \quad (4.19)$$

The result of L and \bar{L} (4.15),(4.19) can be summarized as a 2×2 matrix as below, with the helicity indices of Λ and $\bar{\Lambda}$ being the legs:

$$L = \begin{pmatrix} 1 + \alpha_{\Lambda}n_z & \alpha_{\Lambda}n_+ \\ \alpha_{\Lambda}n_- & 1 - \alpha_{\Lambda}n_z \end{pmatrix}, \quad \bar{L} = \begin{pmatrix} 1 + \alpha_{\Lambda}n'_z & -\alpha_{\Lambda}n'_- \\ -\alpha_{\Lambda}n'_+ & 1 - \alpha_{\Lambda}n'_z \end{pmatrix} \quad (4.20)$$

The diagonals and the off-diagonals corresponds to the direct and the interference terms respectively.

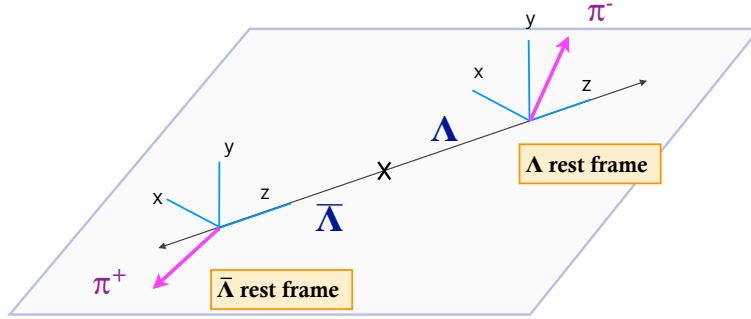


Figure 4.1: The coordinate system in the Λ and $\bar{\Lambda}$ RF. z -axis is defined as the orientation of Λ boost which is the direction of the relative movement of Λ -RF to the χ_{c0} -RF. The x, y axes are taken such that (x, y, z) forms a right-handed coordinate system.

Now all preparation has been done. With (4.15) and (4.19) thrown into (4.12), one eventually arrives at

$$\begin{aligned} \frac{d\sigma}{d\Omega_n d\Omega_{n'}} &\propto |\overline{\mathcal{M}}|^2 \\ &= 16p_{\Lambda}^2 m_{\Lambda}^2 K^2 [(1 + \alpha_{\Lambda}n_z)(1 + \alpha_{\Lambda}n'_z) + (1 - \alpha_{\Lambda}n_z)(1 - \alpha_{\Lambda}n'_z) - \alpha_{\Lambda}^2(n_+n'_- + n_-n'_+)] \\ &= 1 + \alpha_{\Lambda}^2 n_z n'_z - \alpha_{\Lambda}^2 (n_x n'_x + n_y n'_y) \\ &\propto 1 + \alpha_{\Lambda}^2 (-n_x n'_x - n_y n'_y + n_z n'_z) \end{aligned} \quad (4.21)$$

The interpretation of this $\pi^+\pi^-$ distribution is fairly clear. With respect to the Λ and $\bar{\Lambda}$ boost direction ("longitudinal direction"), π^- and π^+ tend to be in the same orientation, while they prefer to be anti-parallel with respect to the "transverse" direction. Recall that π^- disfavors the Λ spin direction and that π^+ favors $\bar{\Lambda}$ spin direction, this is nothing but the demonstration of $\Lambda\bar{\Lambda}$ spin triple state. (Fig. 4.2)

The first two terms $L_{++}\bar{L}_{++}$ and $L_{--}\bar{L}_{--}$ in (4.21) originates from the direct terms, while the latter two $L_{-+}\bar{L}_{+-}$ and $L_{+-}\bar{L}_{-+}$ are from the interference terms. The direct terms only responsible for longitudinal correlation as they describe the mode where $\Lambda\bar{\Lambda}$ helicities are determined respectively to $(+, -)$ or $(-, +)$, which are the spin eigen-states along boost directions thus never create correlation to the transverse direction.

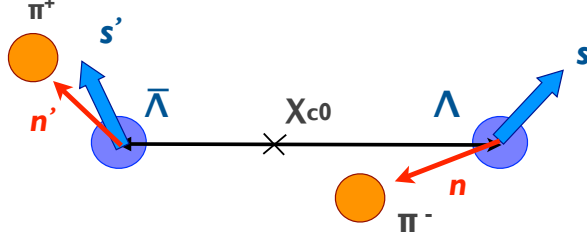


Figure 4.2: The relation of $\Lambda\bar{\Lambda}$ spins and $\pi^+\pi^-$ directions in the $\chi_{c0} \rightarrow \Lambda\bar{\Lambda} \rightarrow p\pi\bar{p}\pi$ channel.

Finally, a C matrix is obtained as

$$\begin{aligned}
 C_{ij} &= \frac{9}{\alpha_\Lambda^2} \langle n_i n'_j \rangle \\
 &= \frac{9}{\alpha_\Lambda^2} \int d\Omega_n d\Omega_{n'} n_i n'_j \left(\frac{d\sigma}{d\Omega_\Lambda d\Omega_n d\Omega_{n'}} / \sigma_{tot} \right) \\
 &= \frac{9}{\alpha_\Lambda^2} \frac{\int d\Omega_n d\Omega_{n'} n_i n'_j |\overline{\mathcal{M}}|^2}{\int d\Omega_\Lambda d\Omega_n d\Omega_{n'} |\overline{\mathcal{M}}|^2},
 \end{aligned} \tag{4.22}$$

therefore,

$$C = \begin{pmatrix} 1/2 & & \\ & 1/2 & \\ & & 1/2 \end{pmatrix} \tag{4.23}$$

C_{11} and C_{22} correspond to the transverse, C_{33} to the longitudinal correlation. This unambiguous way of representing correlation is the biggest advantage of introducing the C matrix.

Q_{\max} is derived by finding the two largest eigenvalues of $C^T C$. Here it is simply

$$\begin{aligned}
 C^T C &= \text{diag}(1/4, 1/4, 1/4) \\
 \lambda_1 &= \lambda_2 = \frac{1}{4} \\
 Q_{\max} &= \sqrt{2} > 1
 \end{aligned} \tag{4.24}$$

As expected, Q_{\max} overwhelms the classical upper bound that the BI describes, and it is identical to the quantum limit $\sqrt{2}$.

Here one can learn that interference terms give the important contribution. Without them, which is the case of the most simple LHVT model,

$$\begin{aligned}
 C &= \begin{pmatrix} & & \\ & & \\ & & 1/2 \end{pmatrix} \\
 Q_{\max} &= 1
 \end{aligned} \tag{4.25}$$

The longitudinal correlation is maximum though, Q_{\max} can only reach the classical limit.

4.2 $\eta_c \rightarrow \Lambda\bar{\Lambda}$

The analysis of $\eta_c \rightarrow \Lambda\bar{\Lambda}$ is quite similar to the $\chi_{c0} \rightarrow \Lambda\bar{\Lambda}$ channel. In fact the only difference from $\chi_{c0} \rightarrow \Lambda\bar{\Lambda}$ is that η_c is pseudo-scalar. The total matrix reads

$$\mathcal{M} = \mathcal{M}_\Lambda^i \mathcal{M}_{\eta_c}^{ij} \mathcal{M}_{\bar{\Lambda}}^j \quad (4.26)$$

$$\mathcal{M}_{\eta_c}^{ij} \propto \bar{u}_\Lambda^i \gamma^5 v_{\bar{\Lambda}}^j \quad (4.27)$$

Again, assuming the parity conservation in $\eta_c \rightarrow \Lambda\bar{\Lambda}$, the pseudo-Yukawa type of vertex is obtained. \mathcal{M}_Λ and $\mathcal{M}_{\bar{\Lambda}}$ are same as ones in the previous section (4.3) and (4.4). The sub-matrix $\mathcal{M}_{\eta_c} \rightarrow \Lambda\bar{\Lambda}$ becomes

$$\begin{aligned} \mathcal{M}_{\eta_c}^{ij} &= \bar{u}_\Lambda^i(\mathbf{p}) \gamma^5 v_{\bar{\Lambda}}^j(-\mathbf{p}) \\ &= \frac{E+m}{2} \left((1 \mp \eta) \xi_{\mathbf{p}}^{\dagger i}, (1 \pm \eta) \xi_{\mathbf{p}}^{i, \dagger} \right) \gamma^0 \gamma^5 \begin{pmatrix} (1 \pm \eta) \xi_{-\mathbf{p}}^{-i} \\ -(1 \mp \eta) \xi_{-\mathbf{p}}^{-i} \end{pmatrix} \\ &= \frac{E+m}{2} \left((1 \pm \eta) \xi_{\mathbf{p}}^{\dagger i}, (1 \mp \eta) \xi_{\mathbf{p}}^{\dagger i} \right) \begin{pmatrix} -(1 \pm \eta) \xi_{-\mathbf{p}}^{-i} \\ -(1 \mp \eta) \xi_{-\mathbf{p}}^{-i} \end{pmatrix}. \end{aligned} \quad (4.28)$$

Using $\xi_{-\mathbf{p}}^+ = \xi_{\mathbf{p}}^-$, $\xi_{-\mathbf{p}}^- = -\xi_{\mathbf{p}}^+$ (4.8),

$$\begin{aligned} &= \frac{E+m}{2} \left((1 \pm \eta) \xi_{\mathbf{p}}^{\dagger i}, (1 \mp \eta) \xi_{\mathbf{p}}^{\dagger i} \right) \begin{pmatrix} \mp(1 \pm \eta) \xi_{\mathbf{p}}^i \\ \mp(1 \mp \eta) \xi_{\mathbf{p}}^i \end{pmatrix} \\ &= \delta_{ij} \begin{cases} -(1+\eta)^2 - (1-\eta)^2 = -2E_\Lambda & (i=j=+) \\ (1-\eta)^2(1+\eta)^2 = -2E_\Lambda & (i=j=-) \end{cases} \end{aligned} \quad (4.29)$$

Just as in the case of $\chi_{c0} \rightarrow \Lambda\bar{\Lambda}$, only the terms which have the same helicity for Λ and $\bar{\Lambda}$ survive. With a careful observation on the signs, the helicity state of $\Lambda\bar{\Lambda}$ reads

$$|\psi_{\Lambda\bar{\Lambda}}\rangle \propto \frac{|++\rangle - |--\rangle}{\sqrt{2}}, \quad (4.30)$$

which is the helicity singlet state with the maximal entanglement. Using L and \bar{L} , the total matrix is written as

$$|\overline{\mathcal{M}}|^2 = 4E_\Lambda^2 [L_{++}\bar{L}_{++} + L_{--}\bar{L}_{--} - L_{-+}\bar{L}_{+-} - L_{+-}\bar{L}_{-+}] \quad (4.31)$$

The only difference from the χ_{c0} channel is the opposite sign of the interference terms. Plugging the result (4.15) obtained in the previous section,

$$\begin{aligned} |\overline{\mathcal{M}}|^2 &= 16E_\Lambda^2 m_\Lambda^2 K^2 [(1 + \alpha_\Lambda n_z)(1 + \alpha_\Lambda n'_z) - (1 - \alpha_\Lambda n_z)(1 - \alpha_\Lambda n'_z) + \alpha_\Lambda^2 (n_+ n'_- + n_- n'_+)] \\ &= 32E_\Lambda^2 m_\Lambda^2 K^2 [1 + \alpha_\Lambda^2 n_z n'_z + \alpha_\Lambda^2 (n_x n'_x + n_y n'_y)] \\ &\propto (1 + \alpha_\Lambda^2 n_z n'_z) + \alpha_\Lambda^2 (n_x n'_x + n_y n'_y) \\ &= 1 + \alpha_\Lambda^2 (n_x n'_x + n_y n'_y + n_z n'_z) \end{aligned} \quad (4.32)$$

The transverse correlation (correlation to the x, y direction, perpendicular to the $\Lambda\bar{\Lambda}$ movement) is opposite to the $\chi_{c0} \rightarrow \Lambda\bar{\Lambda}$ case, thus the \mathbf{n} and \mathbf{n}' prefer to be anti-parallel. This results from the fact that Λ and $\bar{\Lambda}$ are in helicity singlet state (Fig. 4.3).

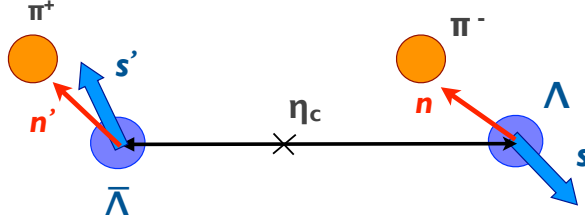


Figure 4.3: The relation of $\Lambda\bar{\Lambda}$ spins and $\pi^+\pi^-$ directions in the $\eta_c \rightarrow \Lambda\bar{\Lambda} \rightarrow p\bar{p}\pi\pi$ channel.

The C matrix and Q_{\max} value is therefore

$$C = \begin{pmatrix} 1/2 & & \\ & 1/2 & \\ & & 1/2 \end{pmatrix}$$

$$Q_{\max} = \sqrt{2}. \quad (4.33)$$

It again reaches the quantum limit and the BI is again maximally violated.

4.3 $J/\psi \rightarrow \Lambda\bar{\Lambda}$

The case with J/ψ is a bit complicated since it depends on its initial polarization. A brilliant analysis valid for arbitrary J/ψ polarization is delivered by N. A. Tornqvist [56], however here rather the structure of entanglement is in interest, we still keep our straightforward approach.

We first start with the fact that J/ψ s has to be in either pure left-handed or pure right-handed transverse polarization, as far as they are directly produced via $e^+e^- \rightarrow \gamma^* \rightarrow J/\psi$ Fig. 4.4 from e^+e^- collision. This is essentially due to the helicity structure of EM coupling that only (e_R^+, e_L^-) and (e_L^+, e_R^-) contribute to e^+e^- annihilation (L/R denote the left/right helicity) when they are highly relativistic. Consider J/ψ mass is $\sim 3\text{GeV}$ and thus the e^+e^- have to be typically 1.5GeV , this assumption is fairly reasonable ($m_e/E_e < 10^{-6}$). The coupling of $e_L^+e_R^-$ gives rise of right-handed, and $e_R^+e_L^-$ of the left-handed J/ψ . As long as an unpolarized e^+e^- beam is assumed (which is more common than not in practice), they are equally produced. Note that here "unpolarized" means a statistical mixture of equal number of left and right-handed e^+e^- in the beam, therefore the polarization of J/ψ is definitely R or L event by event, rather than in the coherent superposition state. This is an extremely important difference so that here no interference should be considered between the two polarizations L and R for J/ψ s.

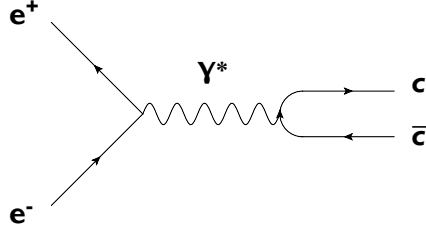


Figure 4.4: Diagram of the charmonium production. e^+e^- do not directly couple to quarks for the lepton number conservation. Thus the intermediation of virtual photon γ^* is needed.

Coming to the matrix of $J/\psi \rightarrow \Lambda\bar{\Lambda}$, generally it has the form of:

$$\mathcal{M}_{\psi,s}^{ij} \propto \epsilon_{s\mu} \bar{u}_{\Lambda}^i \left(\gamma^{\mu} + \frac{a_{\psi}}{2p_{\Lambda}} q^{\mu} \right) v_{\bar{\Lambda}}^j \quad (4.34)$$

$i, j = \pm$ are the indices of $\Lambda\bar{\Lambda}$ helicity and $s = L, R$ notes the J/ψ polarization.

This vertex is less trivial than the case of $\chi_{c0}, \eta_c \rightarrow \Lambda\bar{\Lambda}$ but the terms can be enormously limited giving parity conservation (EM and strong interaction is dominant). As J/ψ is vector (parity $-$, spin 1), it has to be vector coupling. (without parity conservation, pseudo-vector coupling is also available). To the lowest order of the effective Lagrangian, the J/ψ field A^{μ} only couples to the current made of Λ the field ψ

$$\bar{\psi} \gamma^{\mu} \psi, \quad \bar{\psi} \partial^{\mu} \psi. \quad (4.35)$$

Therefore, the interaction terms in the effective Lagrangian are written using coefficients c_1, c_2 as

$$c_1 A_{\mu} \bar{\psi} \gamma^{\mu} \psi + c_2 A_{\mu} \bar{\psi} \partial^{\mu} \psi. \quad (4.36)$$

The vertex factor in the matrix is identical to those represented in the momentum space:

$$\epsilon_{\mu} \bar{u} (c_1 \gamma^{\mu} + c_2 q^{\mu}), \quad (4.37)$$

where q^{μ} is momentum transfer $q^{\mu} := p_{\Lambda}^{\mu} - p_{\bar{\Lambda}}^{\mu}$. (4.34) is then derived with re-parametrizing c_1 and c_2 into a_{ψ} .

For simplicity, consider the first term in (4.34) for now; $\epsilon_{\mu s} \bar{u}_{\Lambda}^i \gamma^{\mu} v_{\bar{\Lambda}}^j$ is calculated. As the $\Lambda\bar{\Lambda}$ go back-to-back in the J/ψ rest frame,

$$\begin{aligned} \bar{u}_{\Lambda}^i(\mathbf{p}) \gamma^{\mu} v_{\bar{\Lambda}}^j(-\mathbf{p}) &= \frac{E+m}{2} ((1 \mp \eta) \xi_{\mathbf{p}}^{\dagger i}, (1 \pm \eta) \xi_{\mathbf{p}}^{\dagger i}) \gamma^0 \gamma^{\mu} \begin{pmatrix} (1 \pm \eta) \xi_{-\mathbf{p}}^{-j} \\ -(1 \mp \eta) \xi_{-\mathbf{p}}^{-j} \end{pmatrix} \\ &= \frac{E+m}{2} ((1 \mp \eta) \xi_{\mathbf{p}}^{\dagger i}, (1 \mp \eta) \xi_{\mathbf{p}}^{\dagger i}) \begin{pmatrix} \sigma^{\mu} \\ \bar{\sigma}^{\mu} \end{pmatrix} \begin{pmatrix} (1 \pm \eta) \xi_{\mathbf{p}}^j \\ -(1 \mp \eta) \xi_{\mathbf{p}}^j \end{pmatrix}. \end{aligned} \quad (4.38)$$

Note that $\sigma^{\mu} = (1, -\boldsymbol{\sigma})$, $\bar{\sigma}^{\mu} = (1, \boldsymbol{\sigma})$.

For the terms with $i = j = \pm$, one obtains

$$\begin{aligned}\bar{u}_\Lambda^i(\mathbf{p})\gamma^\mu v_\Lambda^I(-\mathbf{p}) &= \frac{E+m}{2}(1-\eta^2)(\xi_{\mathbf{p}}^{\dagger i}\sigma^\mu\xi_{\mathbf{p}}^i - \xi_{\mathbf{p}}^{\dagger i}\bar{\sigma}^\mu\xi_{\mathbf{p}}^i) \\ &= \begin{pmatrix} 0 \\ -2m_\Lambda\xi_{\mathbf{p}}^{\dagger i}\boldsymbol{\sigma}\xi_{\mathbf{p}}^i \end{pmatrix} \\ &= 2m_\Lambda \begin{pmatrix} 0 \\ \mp \sin\theta \\ 0 \\ \mp \cos\theta \end{pmatrix}.\end{aligned}\quad (4.39)$$

Here θ is the polar angle with e^- beam direction defined as z -axis (zenith).

For the terms with $i \neq j$ ($i = -j = \pm$),

$$\begin{aligned}\bar{u}_\Lambda^i(\mathbf{p})\gamma^\mu v_\Lambda^j(-\mathbf{p}) &= \frac{E+m}{2}[(1\mp\eta)\xi_{\mathbf{p}}^{\dagger i}\sigma^\mu\xi_{\mathbf{p}}^j - (1\pm\eta)\xi_{\mathbf{p}}^{\dagger i}\bar{\sigma}^\mu\xi_{\mathbf{p}}^j] \\ &= \begin{pmatrix} \mp 2p_\Lambda\xi_{\mathbf{p}}^{\dagger i}\xi_{\mathbf{p}}^j \\ \mp 2E_\Lambda\xi_{\mathbf{p}}^{\dagger i}\boldsymbol{\sigma}\xi_{\mathbf{p}}^j \end{pmatrix} \\ &= \begin{pmatrix} 0 \\ \mp 2E_\Lambda\xi_{\mathbf{p}}^{\dagger i}\boldsymbol{\sigma}\xi_{\mathbf{p}}^j \end{pmatrix} \\ &= 2E_\Lambda \begin{pmatrix} 0 \\ -\cos\theta \\ \pm i \\ \pm \sin\theta \end{pmatrix}\end{aligned}\quad (4.41)$$

Here the notation $\epsilon_{L,R}^\mu =^T (0, 1, \pm i, 0)/\sqrt{2}$ is employed (\pm in the RHS corresponds to L, R in the LHS respectively). $\epsilon_{s\mu}\bar{u}_\Lambda^i\gamma^\mu v_\Lambda^j$ with respective i, j, s turns to as in the Tab. 4.1. Following the presentation

Table 4.1: $\epsilon_{s\mu}\bar{u}_\Lambda^i\gamma^\mu v_\Lambda^j$ for each polarization of J/ψ and e^+e^-

(i, j)	$s = R$	$s = L$
$(+, +)$	$\sqrt{2}m_\Lambda \sin\theta$	$\sqrt{2}m_\Lambda \sin\theta$
$(+, -)$	$\sqrt{2}E_\Lambda(1 + \cos\theta)$	$-\sqrt{2}E_\Lambda(1 - \cos\theta)$
$(-, +)$	$-\sqrt{2}E_\Lambda(1 - \cos\theta)$	$\sqrt{2}E_\Lambda(1 + \cos\theta)$
$(-, -)$	$-\sqrt{2}m_\Lambda \sin\theta$	$-\sqrt{2}m_\Lambda \sin\theta$

above, The $\Lambda\bar{\Lambda}$ helicity state is

$$|\psi_{\Lambda\bar{\Lambda}}\rangle_R \propto \sqrt{2}m_\Lambda \sin\theta |++\rangle - \sqrt{2}m_\Lambda \sin\theta |--\rangle + \sqrt{2}E_\Lambda(1 + \cos\theta) |+-\rangle - \sqrt{2}E_\Lambda(1 - \cos\theta) |-+\rangle \quad (4.42)$$

$$|\psi_{\Lambda\bar{\Lambda}}\rangle_L \propto \sqrt{2}m_\Lambda \sin\theta |++\rangle - \sqrt{2}m_\Lambda \sin\theta |--\rangle - \sqrt{2}E_\Lambda(1 - \cos\theta) |+-\rangle + \sqrt{2}E_\Lambda(1 + \cos\theta) |-+\rangle. \quad (4.43)$$

It is terribly non-trivial if it is entangled, though it is visually entangled in that it has a complicated dependence on kinematical factors (m_Λ , E_Λ and θ) and is seemingly impossible to factorize into a product of two kets. Here an example is demonstrated that the visual impression has nothing to do with the extend of entanglement.

Suppose a non-relativistic limit ($E_\Lambda \rightarrow m_\Lambda$). As mentioned above, $\Lambda\bar{\Lambda}$ helicity eigenstates reduce to spin eigenstates with respect to $\Lambda\bar{\Lambda}$ orientation,

$$|+\rangle_\Lambda \rightarrow |\uparrow\rangle_\Lambda, \quad |-\rangle_\Lambda \rightarrow |\downarrow\rangle_\Lambda \quad (4.44)$$

The subscripts indicate the choice of the QA. Re-writing into a representation with the beam direction being the QA, (4.44) becomes

$$|+\rangle_{\Lambda} = |\uparrow\rangle_{\Lambda} = \cos \frac{\theta}{2} |\uparrow\rangle_e + e^{i\phi} \sin \frac{\theta}{2} |\downarrow\rangle_e, \quad |-\rangle_{\Lambda} = |\downarrow\rangle_{\Lambda} = -e^{-i\phi} \sin \frac{\theta}{2} |\uparrow\rangle_e + \cos \frac{\theta}{2} |\downarrow\rangle_e \quad (4.45)$$

where (θ, ϕ) is the polar and azimuthal angles with respect to the beam axis (see Fig. 4.5). The spin state for $\bar{\Lambda}$ is obtained by replacing $\theta \rightarrow \pi - \theta$, $\phi \rightarrow -\phi$ in (4.45).

$$|+\rangle_{\bar{\Lambda}} = \sin \frac{\theta}{2} |\uparrow\rangle_e - e^{i\phi} \cos \frac{\theta}{2} |\downarrow\rangle_e, \quad |-\rangle_{\bar{\Lambda}} = e^{-i\phi} \cos \frac{\theta}{2} |\uparrow\rangle_e + \sin \frac{\theta}{2} |\downarrow\rangle_e. \quad (4.46)$$

Applying these to (4.45) and (4.46), one finds

$$|\psi_{\Lambda\bar{\Lambda}}\rangle_R \propto |\uparrow\uparrow\rangle_e, \quad |\psi_{\Lambda\bar{\Lambda}}\rangle_L \propto |\downarrow\downarrow\rangle_e. \quad (4.47)$$

These are actually product states. Physically, this is the conclusion from the spin conservation law in the non-relativistic limit, therefore it is deterministically predicted that $\Lambda\bar{\Lambda}$ spin state is $|\uparrow\uparrow\rangle_e$ when J/ψ polarization is R (spin 1 pointing to the $+z$ direction), vice versa. This result implicates the vector initial state is just boring if non-relativistic, at the same, that the $\Lambda\bar{\Lambda}$ helicity may be entangled with the relativistic effect that mixing spin and orbital angular momentum.

As shown above, it is generally challenging to systematically evaluate the entanglement from the state vector directly though ¹, (4.43) and (4.42) nevertheless allows us to infer the property qualitatively.

For instance, the terms proportional to m_{Λ} forms the helicity singlet regardless of the Λ direction θ . Here we call this "scalar mode" as it looks spin singlet.

In contrast, the latter two terms proportional to E_{Λ} are complicated. First of all, the entanglement depends on θ . It is enhanced when the Λ goes to the transverse direction and the state comes asymptotically to $2\sqrt{E_{\Lambda}}(|+-\rangle - |-+\rangle)$ as $\theta \sim \pi/2$, on the other hand, it is suppressed when Λ is forward and dissolved into a product state with being $\theta \sim 0, \pi$. For the sake of convenience, here the contribution from these terms is defined "vector mode". In a non-relativistic limit the scalar mode and the vector mode contribute equally, while the vector mode overcomes when the system becomes relativistic.

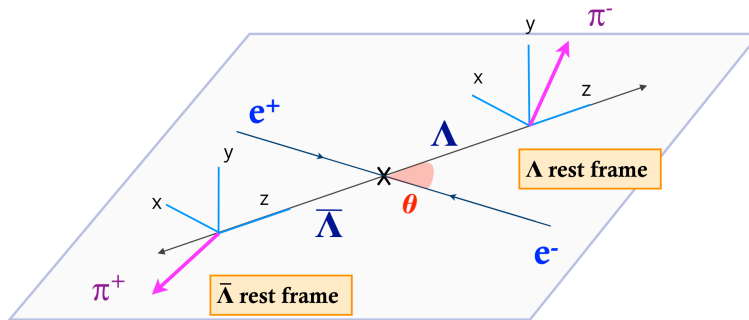


Figure 4.5: The coordinates system in the Λ and $\bar{\Lambda}$ RF. x, z axes are taken such that they span the $ee \rightarrow J/\psi \rightarrow \Lambda\bar{\Lambda}$ reaction plane. z -axis is referred to the orientation of Λ boost which is the direction of the relative movement of Λ -RF to the χ_{c0} -RF. The y axis are taken such that (x, y, z) forms a right-handed coordinate system.

¹There does exist a formula that decides if the state is entangled [75], however no well-defined measure of entanglement has been established yet.

Phenomenologically, this power balance can be understood by the angular distribution of $\Lambda\bar{\Lambda}$.

$$\begin{aligned}
\frac{d\sigma}{d\Omega_\Lambda} &\propto |\langle\psi_{\Lambda\bar{\Lambda}}|\psi_{\Lambda\bar{\Lambda}}\rangle|_R^2 + |\langle\psi_{\Lambda\bar{\Lambda}}|\psi_{\Lambda\bar{\Lambda}}\rangle|_L^2 \\
&= 8m_\Lambda^2 \sin^2 \theta + 4E_\Lambda^2(1 + \cos^2 \theta) \\
&\propto (E_\Lambda^2 + m_\Lambda^2) + (E_\Lambda^2 - m_\Lambda^2) \cos^2 \theta \\
&\propto 1 + \frac{E_\Lambda^2 - m_\Lambda^2}{E_\Lambda^2 + m_\Lambda^2} \cos^2 \theta.
\end{aligned} \tag{4.48}$$

The scalar mode contribute to the factor $\sin^2 \theta$, while the vector mode to the $1 + \cos^2 \theta$ dependency. In a non-relativistic limit the both dependency cancels each other leading to an isotropic distribution, where no angular orbital momentum comes into effect, consistent to the spin conservation rule. The angular dependence give rise as becoming relativistic, and in an ultra-relativistic limit, it comes to a pure P-wave distribution $1 + \cos^2 \theta$. Now that we almost understand the behavior, let the second term of (4.34) $\frac{a_\psi}{2p_\Lambda} \epsilon^\mu q_\mu$ join in the game. Since it does not have the legs of spinor space, it is essentially Yukawa coupling, thus the result of $\chi_{c0} \rightarrow \Lambda\bar{\Lambda}$ (4.9) can be simply referred.

The factor $\epsilon^\mu q_\mu$ is computed as below, with the taking a certain notion of ϵ^μ

$$q_\mu = p_\Lambda^\mu - p_{\bar{\Lambda}}^\mu = {}^T(0, 2p_\Lambda) \tag{4.49}$$

$$\epsilon_L^\mu q_\mu = -\sqrt{2}(p_x - ip_y) = -\sqrt{2}p_\Lambda e^{-i\phi} \sin \theta \tag{4.50}$$

$$\epsilon_R^\mu q_\mu = -\sqrt{2}(p_x + ip_y) = -\sqrt{2}p_\Lambda e^{i\phi} \sin \theta. \tag{4.51}$$

Therefore, the matrix $\epsilon^\mu q_\mu \bar{u}v$ becomes

$$\epsilon_s^\mu \bar{u}_\Lambda^i \left(a_\psi \frac{q_\mu}{2p_\Lambda} \right) v_\Lambda^j = \mp \sqrt{2} a_\psi p_\Lambda \sin \theta \cdot \delta_{ij} \quad (s = L, R; i = j = \pm) \tag{4.52}$$

Here the ϕ is set to zero, exploiting the rotational invariance of the system. According to (4.52), it apparently contributes to the terms of scalar mode only. Effectively, it replaces the Λ mass m_Λ in the Tab. 4.1 with $m'_\Lambda := m_\Lambda - a_\psi p_\Lambda$.

Similar to L and \bar{L} , the result of the overall matrix 4.34 can be summarized in a 2×2 matrix whose components corresponds to the $\Lambda\bar{\Lambda}$ helicity (i, j) as

$$\begin{aligned}
\mathcal{M}_{\psi,R} &:= \begin{pmatrix} \mathcal{M}_{\psi,R}^{++} & \mathcal{M}_{\psi,R}^{+-} \\ \mathcal{M}_{\psi,R}^{-+} & \mathcal{M}_{\psi,R}^{--} \end{pmatrix} = \begin{pmatrix} \sqrt{2}m'_\Lambda \sin \theta & \sqrt{2}E_\Lambda(1 + \cos \theta) \\ -\sqrt{2}E_\Lambda(1 - \cos \theta) & -\sqrt{2}m'_\Lambda \sin \theta \end{pmatrix} \\
\mathcal{M}_{\psi,L} &:= \mathcal{M}_{\psi,R}^\dagger.
\end{aligned} \tag{4.53}$$

which will be utilized later on.

The modification $m_\Lambda \rightarrow m'_\Lambda$ due to the second term in (4.34) also requires change in $J/\psi \rightarrow \Lambda\bar{\Lambda}$ angular distribution, since the parameter m'_Λ tunes the ratio of contribution from the scalar mode to the vector mode.

$$\begin{aligned}
\frac{d\sigma}{d\Omega_\Lambda} &\propto 1 + \frac{E_\Lambda^2 - m_\Lambda'^2}{E_\Lambda^2 + m_\Lambda'^2} \cos^2 \theta \\
&= 1 + A \cos^2 \theta.
\end{aligned} \tag{4.54}$$

In fact $m_\Lambda'^2$ is determined through the measurement of this distribution. The recent result is $A = 0.65 \pm 0.11(stat.) \pm 0.03(syst.)$ (BES2) [76], giving $m_\Lambda'^2 = 0.51_{-0.19}^{+0.22}$. m'_Λ is two value at the moment with ambiguity

in the sign, however as pointed later, the sign of m'_Λ contributes to the interference term of $J/\psi \rightarrow \Lambda \bar{\Lambda} \rightarrow p\pi^- \bar{p}\pi^-$ hence it explicitly effects to the correlation pattern of $\pi^+\pi^-$ direction, which can easily be observed.

Finally, the total matrix $J/\psi \rightarrow \Lambda \bar{\Lambda} \rightarrow p\pi^- \bar{p}\pi^-$ is

$$\begin{aligned}
|\overline{\mathcal{M}}|_s^2 &= \sum_{s_p, s_{\bar{p}}} \sum_{i, j, i', j'} \left(\mathcal{M}_\Lambda^i \mathcal{M}_{\psi, s}^{ij} \mathcal{M}_{\bar{\Lambda}}^j \right) \left(\mathcal{M}_\Lambda^{*j'} \mathcal{M}_{\psi, s}^{*i'j'} \mathcal{M}_{\bar{\Lambda}}^{*i'} \right) \\
&= \sum_{i, j, i', j'} \overline{\mathcal{M}_\Lambda^{*i'} \mathcal{M}_\Lambda^i \mathcal{M}_{\psi, s}^{ij} \mathcal{M}_{\bar{\Lambda}}^j \mathcal{M}_\Lambda^{*j'} \mathcal{M}_{\psi, s}^{*i'j'}} \\
&= \sum_{i, j, i', j'} L_{i'i} \mathcal{M}_{\psi, s}^{ij} \bar{L}_{jj'} \mathcal{M}_{\psi, s}^{*i'j'} \\
&= \text{Tr} \left[L \mathcal{M}_{\psi, s} \bar{L} \mathcal{M}_{\psi, s}^\dagger \right].
\end{aligned} \tag{4.55}$$

Here L and \bar{L} is as defined in (4.20). Together with (4.53) one arrives at

$$\begin{aligned}
|\overline{\mathcal{M}}|_s^2 &= \text{Tr} \left[L \mathcal{M}_\psi \bar{L} \mathcal{M}_\psi^\dagger \right] \\
&= 8m_\Lambda^2 K^2 \text{Tr} \left[\begin{pmatrix} 1 + \alpha_\Lambda n_z & \alpha_\Lambda n_+ \\ \alpha_\Lambda n_- & 1 - \alpha_\Lambda n_z \end{pmatrix} \begin{pmatrix} m'_\Lambda \sin \theta & E_\Lambda (1 + \cos \theta) \\ -E_\Lambda (1 - \cos \theta) & -m'_\Lambda \sin \theta \end{pmatrix} \right. \\
&\quad \left. \begin{pmatrix} 1 + \alpha_\Lambda n'_z & -\alpha_\Lambda n'_- \\ -\alpha_\Lambda n'_+ & 1 - \alpha_\Lambda n'_z \end{pmatrix} \begin{pmatrix} m'_\Lambda \sin \theta & -E_\Lambda (1 - \cos \theta) \\ E_\Lambda (1 + \cos \theta) & -m'_\Lambda \sin \theta \end{pmatrix} \right].
\end{aligned} \tag{4.56}$$

When $s = R$, this comes eventually to

$$\begin{aligned}
|\overline{\mathcal{M}}|_R^2 &= 16m_\Lambda^2 K^2 E^2 [(1 + \cos^2 \theta)(1 - \alpha_\Lambda^2 n_z n'_z) + \alpha_\Lambda^2 \sin^2 \theta (-n_x n'_x + n_y n'_y) + 2\alpha_\Lambda \cos \theta (n_z - n'_z) \\
&\quad + \Gamma^2 [1 + \alpha_\Lambda^2 (-n_x n'_x - n_y n'_y + n_z n'_z)] \sin^2 \theta \\
&\quad + \Gamma (\alpha_\Lambda^2 \sin 2\theta (n_x n'_z + n_z n'_x) - 2\alpha_\Lambda \sin \theta (n_x - n'_x))]
\end{aligned} \tag{4.57}$$

Note that $\Gamma := m'_\Lambda/E_\Lambda$. The first line shows the contribution from the vector mode ($\propto E_\Lambda^2$), the second line is from the scalar mode ($\propto m_\Lambda^2$) and the third is from their interference ($\propto E_\Lambda m'_\Lambda$).

The case of $s = L$ is the same except the opposite sign of $2\alpha_\Lambda \cos \theta (n_z - n'_z)$ and $-2\alpha_\Lambda \sin \theta (n_x - n'_x)$ in (4.57) (which corresponds to the third term in the first line, the second term in the third line respectively). These terms cancel, provided that J/ψ is produced through unpolarized e^+e^- beam, and the distribution of $\pi^+\pi^-$ results in

$$\begin{aligned}
\frac{d\sigma}{d\Omega_\Lambda d\Omega_n d\Omega_{n'}} &\propto \frac{1}{2} \sum_{s=L, R} |\overline{\mathcal{M}}|_s^2 \\
&\propto (1 + \cos^2 \theta)(1 - \alpha_\Lambda^2 n_z n'_z) + \alpha_\Lambda^2 \sin^2 \theta (-n_x n'_x + n_y n'_y) \\
&\quad + \Gamma^2 [1 + \alpha_\Lambda^2 (-n_x n'_x - n_y n'_y + n_z n'_z)] \sin^2 \theta \\
&\quad + \Gamma \sin 2\theta (n_x n'_z + n_z n'_x)
\end{aligned} \tag{4.58}$$

Integrating over $d\Omega_\Lambda$, the $\pi^+\pi^-$ distribution is obtained as

$$\begin{aligned}
\frac{d\sigma}{d\Omega_n d\Omega_{n'}} &\propto 2(1 - \alpha_\Lambda^2 n_z n'_z) + \alpha_\Lambda^2 (-n_x n'_x + n_y n'_y) \\
&\quad + \Gamma^2 [1 + \alpha_\Lambda^2 (-n_x n'_x - n_y n'_y + n_z n'_z)]
\end{aligned} \tag{4.59}$$

Here the interference term of scalar and the vector mode vanishes as $\sin 2\theta$ is odd with respect to θ . The C

matrix is found to be

$$C = \frac{1}{2(2 + \Gamma^2)} \begin{pmatrix} -1 - \Gamma^2 & & \\ & 1 - \Gamma^2 & \\ & & -2 + \Gamma^2 \end{pmatrix} \quad (4.60)$$

$C_{11}^2 > C_{22}^2$ can be easily confirmed provided $\Gamma^2 > 0$. Thus Q_{\max} is

$$Q_{\max} = 2\sqrt{C_{11}^2 + C_{33}^2} = \frac{\sqrt{5 - 2\Gamma^2 + 2\Gamma^4}}{2 + \Gamma^2}. \quad (4.61)$$

With the measured value of $\Gamma^2 = m_\Lambda^2/E_\Lambda^2 = 0.212_{-0.080}^{+0.092}$,

$$Q_{\max} = 0.976 \pm 0.048.$$

The result is subtle to the hell. The Q_{\max} is consistent to either above or below 1. This is highly unfortunate case: if there is only the contribution from the vector mode (comparable to the case with $\Gamma = 0$ here), the C matrix is

$$C_v = \begin{pmatrix} -1/4 & & \\ & 1/4 & \\ & & -1/2 \end{pmatrix} \quad (4.62)$$

or if with only scalar mode, (comparable to the case with $\Gamma \rightarrow \infty$ here)

$$C_s = \begin{pmatrix} -1/2 & & \\ & -1/2 & \\ & & 1/2 \end{pmatrix}. \quad (4.63)$$

The corresponding Q_{\max} values are $Q_{\max} = \sqrt{5}/2$ and $Q_{\max} = \sqrt{2}$ respectively, thus both violate the BI by themselves. In this case in question, the contributions are mixed weighted with $1 : \Gamma/2$, as a result, the most powerful correlation C_{33} cancel partially, suppressing Q_{\max} . The relation between Q_{\max} and Γ is shown in Fig.4.6. Since the measurement uncertainty on the parameter m_Λ^2 is still huge, the possibility of having Q_{\max} far exceeding 1 has not been excluded. Though $J/\psi \rightarrow \Lambda\bar{\Lambda}$ has enormous statistics ($\sim 10^6$), $\sim 2\sigma$ deviations is at least needed for realistic experimentally observable violation, which is not promising.

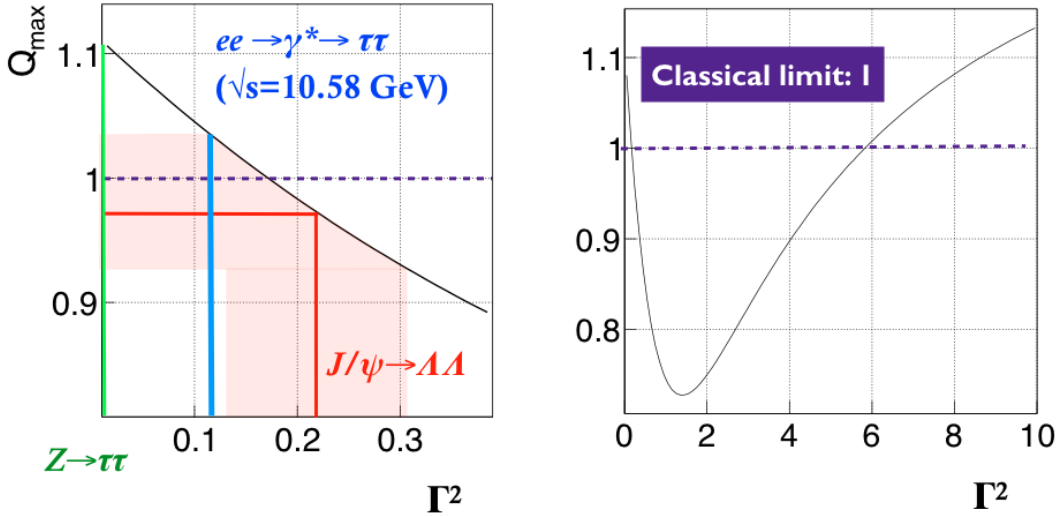


Figure 4.6: Dependence of Q_{\max} on Γ^2 . Γ^2 is $m_\Lambda^2/E_\Lambda^2 = (m_\Lambda - a_\psi p_\Lambda)^2/E_\Lambda^2$ in the $J/\psi \rightarrow \Lambda\bar{\Lambda}$ channel, $\Gamma^2 = m_\tau^2/E_\tau^2$ in the $Z, \gamma^* \rightarrow \tau\tau$ channel. The colored lines are the measured or theoretical values of their Γ , and the red band means the error for the $J/\psi \rightarrow \Lambda\bar{\Lambda}$ channel.

Well, can we save the J/ψ by any chance? For example, what if only the events with Λ oriented to a specific direction are sampled? According to (4.58), the C matrix without integrating over θ is

$$C(\theta) = \frac{1}{2(1 + \Gamma^2) + 2(1 - \Gamma^2) \cos^2 \theta} \begin{pmatrix} -(1 + \Gamma^2) \sin^2 \theta & 0 & \Gamma \sin 2\theta \\ 0 & (1 - \Gamma^2) \sin^2 \theta & 0 \\ \Gamma \sin 2\theta & 0 & -2 + (1 + \Gamma^2) \sin^2 \theta \end{pmatrix} \quad (4.64)$$

in which the explicit dependence of θ is contained. Fig. 4.7 displays the dependency for all components of $C(\theta)$.

As $C(\theta)$ has non-zero values in the off-diagonals C_{13}, C_{31} , to obtain Q_{\max} , $C^T C$ has to be diagonalized and the largest two eigenvalues λ_1, λ_2 have to be specified by definition. The result of $Q_{\max} = \sqrt{\lambda_1 + \lambda_2}$ is shown in Fig. 4.8 (red solid line). For any θ , Q_{\max} surpasses the classical limit 1. This is of representative that $\Lambda \bar{\Lambda}$ is actually entangled. The black points and the error bar are the result of one pseudo-experiment with 10^6 events using MC simulation. The bin of $\cos \theta = 0$ gives the largest violation with 7.5σ standard deviation.

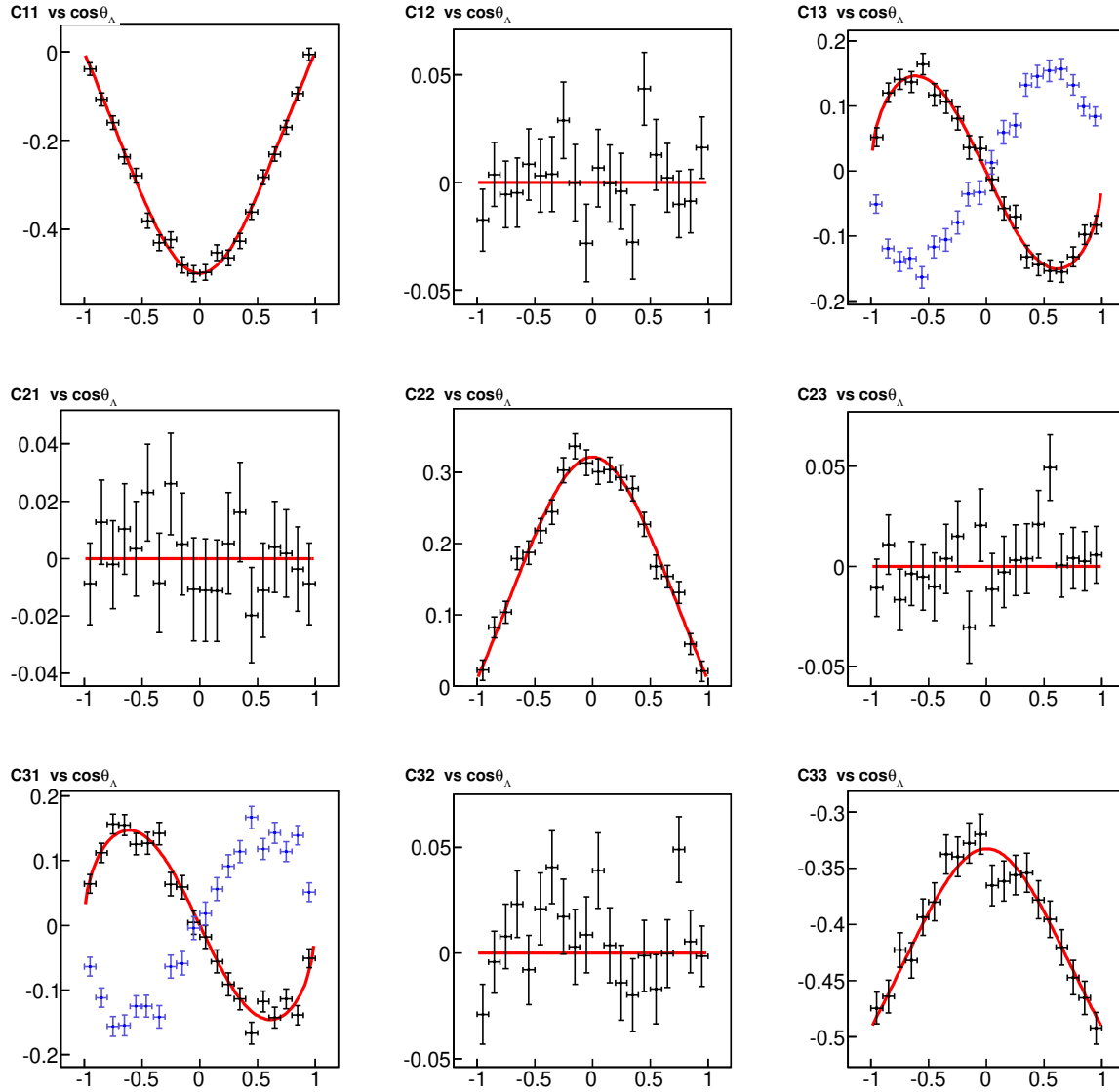


Figure 4.7: Dependency of each components of $C(\theta)$ against $\cos\theta$. The red line the calculated theoretical line from (4.64), the black points and the error bars are the result of one pseudo-experiment with 10^6 events using MC simulation. For C_{13} and C_{31} , two cases $\Gamma > 0$ (red line and black points) and $\Gamma < 0$ (blue line and blue points) are considered.

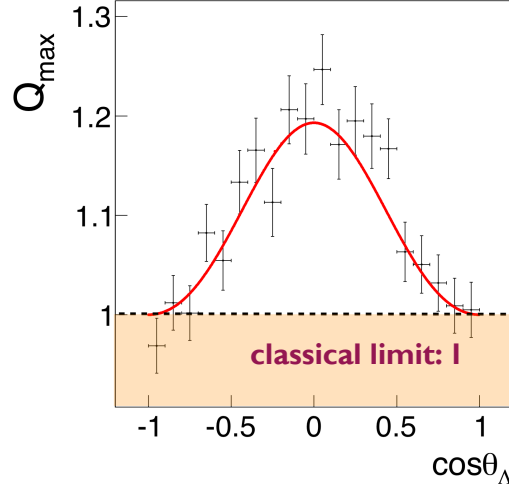


Figure 4.8: Q_{\max} calculated with events sampled with a specific range of θ . The red line is theoretical prediction $Q_{\max} = 2\sqrt{\lambda_1(\theta) + \lambda_2(\theta)}$ ($\lambda_{1,2}$ is the largest two eigenvalues of $C^T(\theta)C(\theta)$), and the black points corresponds to the result of one pseudo-experiment with 10^6 events using MC simulation

This result is perfectly preferable, but only if the procedure of the arbitrary θ sampling is legal in LHVT. Actually it is substantially doubtful, as θ should be regarded as a hidden variable in principle. Thus letting samples with a specific value of θ represent the entire ensemble is just equivalent with setting the homogeneous assumption as referred in section 1.3.2. It is true that a subclass of LHVT models which is homogeneous in θ follows the $Q_{\max} \leq 1$ in any θ , however it is not the case in general, and practically impossible to deduce how large the subclass is.

Moreover as J/ψ is vector which is not homogenous in direction, the assumption of having same correlation value in any θ is much less plausible compared with the case of χ_{c0} or η_c which are isotropic scalar. In fact, this result of QM is a very good counter-example to it: the correlation amplitude could be Q_{\max} biased by an arbitrary sampling of events.

To conclude, it does have some conceptual failure to test LHVT using this channel. However it is still interesting in the texture of testing QM non-locality, since it predicts the non-trivial θ dependence of Q_{\max} (Fig. 4.8) and the modulation of $C(\theta)$ (Fig. 4.7), which is sensitive to the decoherence of $\Lambda \bar{\Lambda}$. To test the change in modulation amplitude, one needs large statistics in order to cope with the binning. Fortunately the J/ψ channel perfectly fulfills the requirement that the expected available sample size 10^6 is demonstrated to be enough.

An additional bonus for this channel, though it has nothing to do with neither LHVT nor QM non-icality, is that the unknown sign of the parameter Γ or m'_Λ can be unambiguously determined by the sign of the C_{31} and C_{13} modulation (Fig. 4.7). The red line is theoretical prediction if Γ is positive, while the blue line is the case with negative Γ . The black points are the result of a pseudo-experiment with 10^6 events using MC simulation. The error bars are safely small enough to distinguish the sign of Γ .

4.4 $e^+e^- \rightarrow \gamma^* \rightarrow \tau\tau$

In this and next section, the direct production of $\tau\tau$ pair through the s-channel annihilation of e^+e^- is in discuss. There are two processes with different intermediate gauge particles: (i) the $e^+e^- \rightarrow \gamma^* \rightarrow \tau\tau$ and the (ii) $e^+e^- \rightarrow Z \rightarrow \tau\tau$. Generally, there exists the interfere with each other, however, here the argument is confine to only two scenario:

1. The center of mass energy of $e^+e^- \sqrt{s}$ is far below the weak scale m_Z ($\sim 90\text{GeV}$). ($s \ll m_Z^2$)
2. The center of mass energy of e^+e^- is around the Z resonance. ($s \sim m_Z^2$)

In fact, the center mass energy for most of the e^+e^- collider experiments subject to either of the condition, since there has been supposed to be little physics motivation in the energy region between the two. In either case the contribution from the interference is negligible since one of the two is dominant compared with the other. This section discusses the case 1. and 2. will be analyzed in the next section.

The matrices of each sub-processes of $e^+e^- \rightarrow \gamma^* \rightarrow \tau\tau$ are

$$\mathcal{M}_\gamma^{ij} \propto \epsilon_{s\mu} \bar{u}_\tau^i \gamma^\mu v_\tau^j \quad (4.65)$$

$$\mathcal{M}_\tau^i \propto \bar{u}_\tau^{s\nu} (1 - \gamma^5) u_\tau^i \quad (4.66)$$

$$\mathcal{M}_\tau^j \propto \bar{v}_\tau^j (1 - \gamma^5) v_\tau^{s\bar{\nu}} \quad (4.67)$$

In (4.65), only the tree-level process is considered. For the same reason with the $ee \rightarrow J/\psi$ as illustrated above, when ee are relativistic, only the combinations (e_L^+, e_R^-) and (e_R^+, e_L^-) contribute to the annihilation. Thus effectively, the intermediate photon γ^* only has transverse polarization R or L , represented by $\epsilon_{s\mu}$ in (4.65).

We do not have to be obsessed with the calculation since it can be settled almost entirely in analogy of $J/\psi \rightarrow \Lambda\bar{\Lambda}$: Firstly, the result of (4.65) is the same as the first term of (4.34). (4.66) and (4.67) corresponds to (4.3) and (4.4) with substituting $c_\Lambda = 1$ and $c_{\bar{\Lambda}} = -1$ respectively. c_{lm} and $c_{\bar{\Lambda}}$ only accounts for the polarimeter performance α of which the C matrix, Q_{\max} and the BI are all independent. Therefore, from now on, the only thing we have to do is interpreting the entire result of the $J/\psi \rightarrow \Lambda\bar{\Lambda}$ channel with replacing $\Gamma = m'_\Lambda/E_\Lambda$ to $\Gamma = m_\tau/E_\tau$. Accordingly the C matrix and Q_{\max} end up in

$$C = \frac{1}{2(2 + \Gamma^2)} \begin{pmatrix} -1 - \Gamma^2 & & \\ & 1 - \Gamma^2 & \\ & & -2 + \Gamma^2 \end{pmatrix}$$

$$Q_{\max} = \frac{\sqrt{5 - 2\Gamma^2 + 2\Gamma^4}}{2 + \Gamma^2} \quad (4.68)$$

The dependency of Q_{\max} against Γ is illustrated in Fig. 4.6. Here Γ , the ratio of contribution from the scalar and the vector mode can be tuned by the beam energy. By (4.68), one finds $Q_{\max} > 1$ is fulfilled when

$$\Gamma^2 > 3 + 2\sqrt{2} \quad \text{or} \quad \Gamma^2 < 3 - 2\sqrt{2}.$$

Using $0 < \Gamma = m_\tau/E_\tau < 1$, $\sqrt{s} = 2E_\tau$, it turns out that the center mass energy

$$\sqrt{s} > \frac{2m_\tau}{\sqrt{2} - 1} = 8.58(\text{GeV}) \quad (4.69)$$

is at least needed to violate the BI and greater \sqrt{s} is preferred. From view of \sqrt{s} and statistics, the most

promising candidate is the Belle experiment with $\sqrt{s} = 10.58(\text{GeV})$, which gives

$$Q_{\max} = 1.037.$$

With the massive statistics in Belle, this much of violation may enough for experimental sensitivity, however here only the tree-level diagram is considered thus the minor change from loop correction can potentially change the conclusion, for example, the anomalous magnetic moment of electron or tau give rise a term just as the second term in (4.34) which can slightly tune Γ . Since the violation is tiny if any, the result is highly sensitive to the minor uncertainty. Further study such as including loop corrections is needed.

4.5 $Z \rightarrow \tau\tau$

In the previous section 4.4, an important fact is derived that faster τ suppresses the Γ value, in other words, enhances the contribution from the vector mode and Q_{\max} . From the viewpoint, $Z \rightarrow \tau\tau$ is a premium channel in that the two τ s are so fast that the approximation of ultra-relativistic limit can be adopted. ($\beta \simeq 0.999, \Gamma := m_\tau^2/E_\tau^2 \simeq 0.0015$).

The matrix for $Z \rightarrow \tau\tau \rightarrow \pi\nu\pi\nu$ is all the same to $ee \rightarrow \gamma^* \rightarrow \tau\tau \rightarrow \pi\nu\pi\nu$, except the sub-matrix of $Z \rightarrow \tau\tau$ is

$$\begin{aligned} \mathcal{M}_{Z,s}^{ij} &\propto \epsilon_{s,\mu} \bar{u}_\tau^i \gamma^\mu (c_V - c_A \gamma^5) v_\tau^j \\ c_V &= T_3 - 2Q \sin^2 \theta_w = 0.0378 \\ c_A &= T_3 = -\frac{1}{2}. \end{aligned} \quad (4.70)$$

s denotes the polarization of the Z ($s = L, R$) and $\sin^2 \theta_w$ is the Weinberg angle, with valued as $\sin^2 \theta_w = 0.2397 \pm 0.0013$ [48]. The first term, the vector current term, is proportional to the first term in (4.34) which results in Tab. 4.1. The latter term, the axial current term is then

$$\begin{aligned} \bar{u}_\tau^i(\mathbf{p}) \gamma^\mu \gamma^5 v_\tau^j(-\mathbf{p}) &= \frac{E+m}{2} \left((1 \mp \eta) \xi_{\mathbf{p}}^{\dagger i}, (1 \pm \eta) \xi_{\mathbf{p}}^{\dagger i} \right) \gamma^0 \gamma^5 \gamma^\mu \begin{pmatrix} (1 \pm \eta) \xi_{-\mathbf{p}}^{-j} \\ -(1 \mp \eta) \xi_{-\mathbf{p}}^{-j} \end{pmatrix} \\ &= \frac{E+m}{2} \left((1 \mp \eta) \xi_{\mathbf{p}}^{\dagger i}, (1 \pm \eta) \xi_{\mathbf{p}}^{\dagger i} \right) \begin{pmatrix} -\sigma^\mu & \\ & \bar{\sigma}^\mu \end{pmatrix} \begin{pmatrix} (1 \pm \eta) \xi_{\mathbf{p}}^i \\ -(1 \mp \eta) \xi_{\mathbf{p}}^i \end{pmatrix}. \end{aligned}$$

For the case with $i = j = \pm$,

$$\begin{aligned} \bar{u}_\tau^i(\mathbf{p}) \gamma^\mu \gamma^5 v_\tau^i(-\mathbf{p}) &= \frac{E+m}{2} (1-\eta^2) (-\xi_{\mathbf{p}}^{\dagger i} \sigma^\mu \xi_{\mathbf{p}}^i - \xi_{\mathbf{p}}^{\dagger i} \bar{\sigma}^\mu \xi_{\mathbf{p}}^i) \\ &= \delta_{ij} \begin{pmatrix} -2m_\tau \\ 0 \\ 0 \\ 0 \end{pmatrix} \end{aligned} \quad (4.71)$$

For the case with $i \neq j$, ($i = -j = \pm$)

$$\begin{aligned}
\bar{u}_\tau^i(\mathbf{p})\gamma^\mu\gamma^5v_\tau^i(-\mathbf{p}) &= \frac{E+m}{2} [-(1 \mp \eta)\xi_{\mathbf{p}}^{\dagger i}\sigma^\mu\xi_{\mathbf{p}}^j - (1 \pm \eta)\xi_{\mathbf{p}}^{\dagger i}\bar{\sigma}^\mu\xi_{\mathbf{p}}^j] \\
&= \begin{pmatrix} 0 \\ \mp 2p_\Lambda\xi_{\mathbf{p}}^{\dagger i}\sigma\xi_{\mathbf{p}}^j \end{pmatrix} \\
&= 2p_\tau \begin{pmatrix} 0 \\ -\cos\theta \\ \pm i \\ \pm \sin\theta \end{pmatrix}.
\end{aligned} \tag{4.72}$$

Summing up the two terms, the value of the matrix \mathcal{M}_Z is found to be as Tab. 4.2 for respective s, i, j .

Table 4.2: The result of $\epsilon_{s,\mu}\bar{u}_\tau^i\gamma^\mu(c_V - c_A\gamma^5)v_\tau^j$

(i, j)	$s = R$	$s = L$
(+, +)	$\sqrt{2}m_\tau \sin\theta$	$\sqrt{2}m_\tau \sin\theta$
(+, -)	$\sqrt{2}(c_V E_\tau + c_A p_\tau)(1 + \cos\theta)$	$-\sqrt{2}(c_V E_\tau + c_A p_\tau)(1 - \cos\theta)$
(-, +)	$-\sqrt{2}(c_V E_\tau + c_A p_\tau)(1 - \cos\theta)$	$\sqrt{2}(c_V E_\tau + c_A p_\tau)(1 + \cos\theta)$
(-, -)	$-\sqrt{2}m_\tau \sin\theta$	$-\sqrt{2}m_\tau \sin\theta$

Under the ultra-relativistic limit $m_\Lambda \rightarrow 0$, terms of $(i, j) = (+, +), (-, -)$ vanish. Comparing the two tables Tab. 4.1 and Tab. 4.2 in the limit, they are proportional to each other, thus the angular distribution in $\pi^+\pi^-$ in the $Z \rightarrow \tau\tau \rightarrow \pi\nu\pi\nu$ channel corresponds to the result of the $J/\psi \rightarrow \Lambda\bar{\Lambda} \rightarrow p\pi p\pi$ channel with replacing the α_Λ in (4.57) with $\alpha_\tau = 1$ and with Γ being 0:

$$|\overline{\mathcal{M}}|_R^2 = 16m_\Lambda^2 K^2 E^2 [(1 + \cos^2\theta)(1 - \alpha_\tau^2 n_z n'_z) + \alpha_\tau^2 \sin^2\theta(-n_x n'_x + n_y n'_y) + 2\alpha_\Lambda \cos\theta(n_z - n'_z)] \tag{4.73}$$

$$|\overline{\mathcal{M}}|_L^2 = 16m_\Lambda^2 K^2 E^2 [(1 + \cos^2\theta)(1 - \alpha_\tau^2 n_z n'_z) + \alpha_\tau^2 \sin^2\theta(-n_x n'_x + n_y n'_y) - 2\alpha_\Lambda \cos\theta(n_z - n'_z)] \tag{4.74}$$

Assuming it is produced via unpolarized e^+e^- annihilation. However, unlike the example of $ee \rightarrow J/\psi$ above, since the coupling strength of Z to $e_L^- e_R^+$ and to $e_R^- e_L^+$ are different, the number of outgoing left-handed and right-handed Z bosons are not equal (note that helicity of Z is still deterministic by each event). However this asymmetry has no impact eventually, since the differences between L (4.74) and R (4.73) are only in terms linear to n_i or n'_j which vanishes with integral $\int d\Omega_n d\Omega_{n'}$ when computing the C matrix.²

Therefore, it simply reduces to the case of $J/\psi \rightarrow \Lambda\bar{\Lambda}$ (4.60) with $\Gamma \rightarrow 0$:

$$\begin{aligned}
C &= \begin{pmatrix} -1/4 & & \\ & 1/4 & \\ & & -1/2 \end{pmatrix} \\
Q_{\max} &= \frac{\sqrt{5}}{2} \simeq 1.118 > 1.
\end{aligned} \tag{4.75}$$

Although the correlation is weaker than the channels with scalar initial state such as χ_{c0} and η_c , it is enough to overcome the classical limit.

²The contribution from longitudinal polarization mode of Z ($\sim O(\frac{m_\tau^2}{m_Z^2})$) is negligible.

4.6 $H \rightarrow \tau\tau$

As long as the CP-even SM Higgs is concerned, the result is identical to the case of the $\chi_{c0} \rightarrow \Lambda\bar{\Lambda}$ channel (4.23),

$$C = \begin{pmatrix} -1/2 & & \\ & -1/2 & \\ & & 1/2 \end{pmatrix} \quad (4.76)$$

$$Q_{\max} = \sqrt{2},$$

resulting in maximal violation of the BI.

Though now it seems less likely giving the result from LHC [77], in principle Higgs is possible to contain the CP-odd component as well. For pure pseudo-scalar Higgs (purely CP-odd), the result will be identical to the case of $\eta_c \rightarrow \Lambda\bar{\Lambda}$ (4.2):

$$C = \begin{pmatrix} 1/2 & & \\ & 1/2 & \\ & & 1/2 \end{pmatrix} \quad (4.77)$$

$$Q_{\max} = \sqrt{2}.$$

The case of the mixture is a bit bothering as it is a coherent superposition of CP-even and CP-odd that is not equal to a simple averaging of (4.76) and (4.77) thus we trace back to the matrix for $H \rightarrow \tau\tau$:

$$\mathcal{M} \propto \bar{u}_\tau(a + b\gamma^2)v_\tau. \quad (4.78)$$

Matrices corresponding to the $\tau^- \rightarrow \pi^- \nu$ and $\tau^+ \rightarrow \pi^+ \bar{\nu}$ are (4.66) and (4.67) respectively. Fortunately the result of the χ_{c0} channel (4.12) and the η_c channel (4.31) can be referred and the total matrix is derived to

$$|\overline{\mathcal{M}}|^2 \propto L_{++}\bar{L}_{++} + L_{--}\bar{L}_{--} + r(L_{-+}\bar{L}_{+-} + L_{+-}\bar{L}_{-+}) \quad (4.79)$$

$$r := \frac{a^2 E_\tau^2 - b^2 p_\tau^2}{a^2 E_\tau^2 + b^2 p_\tau^2} \simeq \frac{a^2 - b^2}{a^2 + b^2}.$$

It is worth pointing that the interference terms ($L_{-+}\bar{L}_{+-} + L_{+-}\bar{L}_{-+}$) are weakened due to the mixing of CP phase. As the direct term, ($L_{++}\bar{L}_{++} + L_{--}\bar{L}_{--}$) contributes to C_{33} , while the interference terms to C_{11} and C_{22} , it is shown that

$$C = \begin{pmatrix} \frac{1}{2}r & & \\ & \frac{1}{2}r & \\ & & \frac{1}{2} \end{pmatrix}$$

$$Q_{\max} = \sqrt{1 + r^2} \geq 1 \quad (4.80)$$

where $r = 1$ with the SM Higgs. The violation of the BI is substantially suppressed if the Higgs CP is highly mixed.

Chapter 5

Discussion on Experimental Feasibility

Theoretical analysis in the previous section reveals that all candidates except $J/\psi \rightarrow \Lambda\bar{\Lambda}$ have $Q_{\max} > 1$. In addition to it, this section tries to include numerous experimental effects and discusses the realistic sensitivity, to be specific, it proceeds as:

- Estimation on required and available statistics to confirm $Q_{\max} > 1$ with a certain level of significance.
- Evaluation of effect from the contamination of background events.
- Evaluation of effect from finite detector resolution.

5.1 Distribution of C_{11} , C_{33} , Q_{\max} and Sensitivity

Our top-most interest is Q_{\max} , which is calculated from the C matrix. Here we start with the basic elements of C matrix $\langle n_i n'_j \rangle$, ($i, j = 1, 2, 3$), observing the statistical behavior in detail. In practical situations, these correlation amplitudes can only be estimated from simple algebraic averaging

$$\langle n_i n'_j \rangle = \frac{1}{N} \sum_{k=1}^N (n_i n'_j)_k.$$

which will inevitably suffer from limited precision due to the statistical fluctuation when the available sample size is finite.

5.1.1 Shape of $n_i n'_j$ distribution

Before heading to correlation $\langle n_i n'_j \rangle$, the event-by-event distribution of $n_i n'_j$ is worth noting, in that it has a terribly non-trivial shape and statistical features.

According to the result of chapter 4, the distribution of \mathbf{n} and \mathbf{n}' can be generally reduced to

$$\frac{d\sigma}{d\Omega_n d\Omega_{n'}} \propto 1 + \alpha^2 \sum_{i,j} w_{ij} n_i n'_j. \quad (5.1)$$

Here $i, j = 1, 2, 3$ correspond to the Cartesian coordinates x, y, z in their parent rest frame as defined before. The projection to the 2 variable space of n_i, n'_j is made by integrating over the rest of all degree of freedom

(DOF). For instance, the angular distribution for $\eta_c \rightarrow \Lambda\bar{\Lambda}$ channel

$$\frac{d\sigma}{d\Omega_n d\Omega_{n'}} \propto 1 + \alpha_\Lambda^2 (n_x n'_x + n_y n'_y + n_z n'_z)$$

has 4 DOFs, corresponding to the 2 π s direction (θ, ϕ) , (θ', ϕ') . The 2D joint probability density function (PDF) for $n_z =: \cos\theta$ and $n'_z =: \cos\theta'$ is straightforwardly obtained by integrating with the other DOFs (ϕ, ϕ') , thus

$$P(n_z, n'_z) = \int d\phi d\phi' \frac{d\sigma}{d\Omega_n d\Omega_{n'}} \propto 1 + \alpha_\Lambda^2 n_z n'_z$$

with a smooth slope as shown in Fig. 5.1. The 1D PDF with respect to $x := n_z n'_z$ is then derived via a normal procedure of variable transformation in which a factor responsible for metric variation (see Fig. 5.2)

$$M(x) = \frac{dx}{dn_z dn'_z} = 2 \int_x^1 dn_z \left(\frac{x + dx}{n_z} - \frac{x}{n_z} \right) = 2 \ln \frac{1}{|x|} dx$$

is applied, therefore,

$$\begin{aligned} P(x) &= P(n_z, n'_z) M(x) \\ &\propto (1 + \alpha^2 x) \ln \frac{1}{|x|}. \end{aligned}$$

It is illustrated that the singularity at $x = 0$ in the distribution (Fig.5.3) purely arises from the metric factor $M(x)$ but physical consequences.

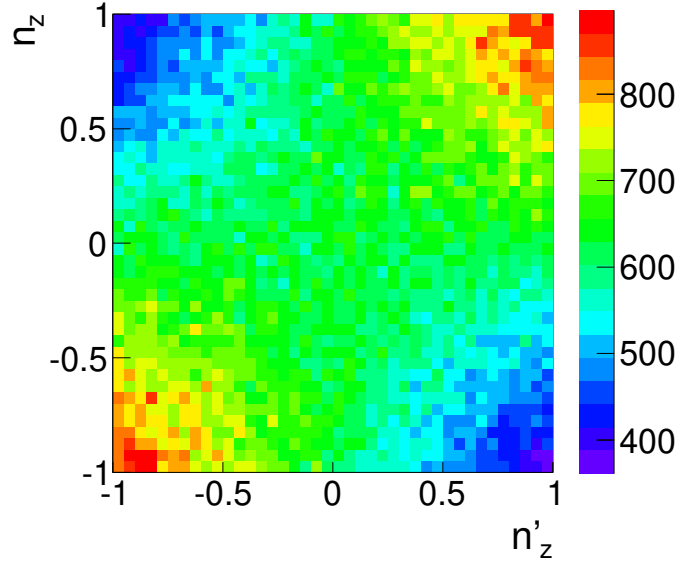


Figure 5.1: 2D PDF of n_z, n'_z in the $\eta_c \rightarrow \Lambda\bar{\Lambda} \rightarrow p\pi^-\bar{p}\pi^+$ channel: $P(n_z, n'_z) = 1 + \alpha^2 n_z n'_z$

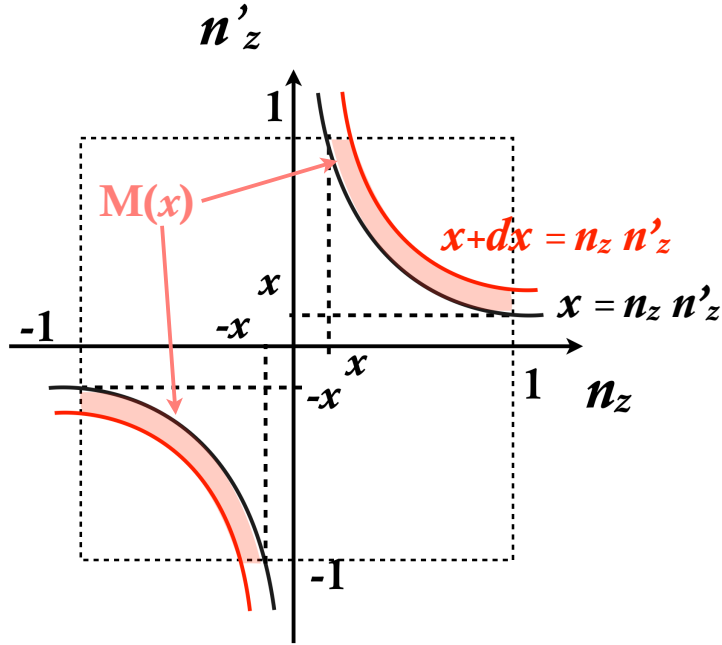


Figure 5.2: The metric factor $M(x) = dx/dn_z dn'_z$ corresponding to the transformation $x := n_z n'_z$

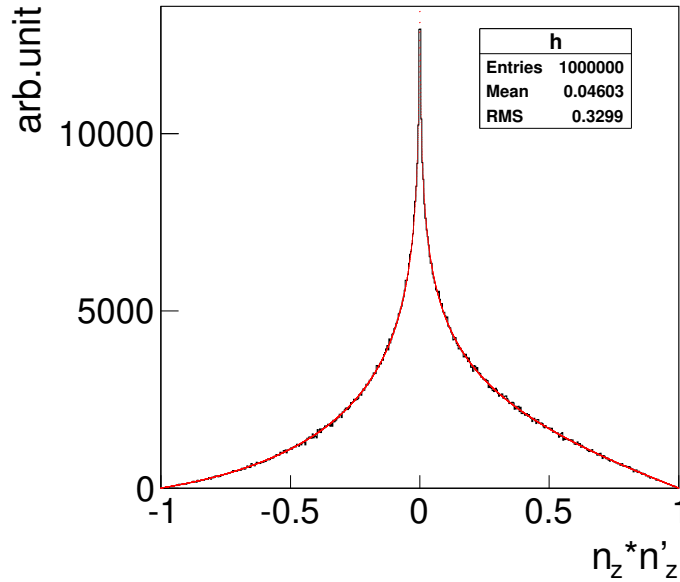


Figure 5.3: Distribution of $x := n_z n'_z$ in the $\eta_c \rightarrow \Lambda \bar{\Lambda} \rightarrow p \pi^- \bar{p} \pi^+$ channel. The black histogram shows MC simulation, while the red line is the fit by function $P(x) \propto (1 + \alpha^2 x) \ln \frac{1}{|x|}$ with perfect accordance.

It has long tails in the both side and diverges at $x = 0$. The asymmetry represents the correlation of $\pi\pi$ in their direction. With a closer analysis, one easily finds

- In spite of the divergence at $x = 0$, the integration over $x \in [-1, 1]$ is finite, with a constant value

independent of α .

$$\begin{aligned}
\int_{-1}^1 dx(1 + \alpha^2 x) \ln \frac{1}{|x|} &= \int_{-1}^1 dx \left[\frac{(1 + \alpha^2 x)^2}{2\alpha^2} \right]' \ln \frac{1}{|x|} \\
&= \left[\frac{(1 + \alpha^2 x)^2}{2\alpha^2} \ln \frac{1}{|x|} \right]_{-1}^1 - \frac{1}{2\alpha^2} \int_{-1}^1 dx(1 + \alpha^2 x)^2 \frac{-1}{x} \\
&= \frac{1}{\alpha^2} \int_0^1 dx 2\alpha^2 \\
&= 2
\end{aligned} \tag{5.2}$$

- $P(x)$ is positive throughout $x \in [-1, 1]$, when $\alpha^2 \leq 1$.

This is the case here that $\alpha \leq 1$ is guaranteed by physics (see 2.2) and $|x| \leq 1$ is a trivial fact as $|n_z|, |n'_z| \leq 1$.

Accordingly, $P(x)$ is likely to have good reason to be treated as a PDF, though strange to some extent. It seems to be something like delta-function. Normalizing with (5.2)

$$P(x) = \frac{1}{2}(1 + \alpha^2 x) \ln \frac{1}{|x|}. \tag{5.3}$$

The expectation value μ and RMS σ are

$$\mu = \int_{-1}^1 dx xP(x) = \frac{\alpha^2}{9} \tag{5.4}$$

$$\begin{aligned}
\sigma^2 &= \int_{-1}^1 dx (x - \mu)^2 P(x) = \frac{1}{9} \left(1 - \frac{\alpha^4}{9} \right) \\
\sigma &= \frac{1}{3} \sqrt{1 - \frac{\alpha^4}{9}}
\end{aligned} \tag{5.5}$$

This μ is the true value of $\langle n_z n'_z \rangle$ (estimated value with infinitely large sample size). It greatly depends on the performance of polarimeter α^2 because good polarimeter results in larger asymmetry of distribution hence larger μ value. The notable fact is in the RMS. The distribution has a substantial extended width and the dependence on α^2 is almost nothing. $\alpha^2 = 1$ gives the minimum width of $\sigma = 0.3305$ while the maximum is $\sigma = 0.3333$ with $\alpha^2 = 0$. This extended intrinsic width is the nature of statistics rather than physics.

The other combinations of $n_i n'_j$ $i, j = 1, 2, 3$ follow the same argument and their distributions are described as

$$P(x) = \frac{1}{2}(1 + w_{ij}\alpha^2 x) \ln \frac{1}{|x|} \tag{5.6}$$

where w_{ij} are the same as in (5.1). As later discussed, the large intrinsic width in the distributions deduces a significant conclusion: Since there is already a heavy fluctuation even with ideal measurement in infinite accuracy, the smearing effect from measurement error of \mathbf{n}, \mathbf{n}' to $n_i n'_j$ is almost negligible.

5.1.2 Shape of C_{11}, C_{33} distribution vs number of events

Following the result above, uncertainty of the estimation for $\langle n_i n'_j \rangle$ in an experiment with sample size N is studied, which is namely the statistical fluctuation of $y = \frac{1}{N} \sum_{k=1}^N (n_i n'_j)_k$ over many pseudo-experiments.

According to the central limit theorem (CLT), with large enough sample size N , the distribution of y (defined as $Q(y)$) converge into a Gaussian with the mean value μ' and RMS σ' of

$$\begin{aligned}\mu' &= \mu = \frac{\alpha^2}{9} \\ \sigma' &= \sigma/\sqrt{N} = \frac{1}{3\sqrt{N}}\sqrt{1 - \frac{\alpha^4}{9}}\end{aligned}\tag{5.7}$$

where μ, σ is the mean and RMS of $n_i n'_j$ distribution, equal to (5.4) and (5.5) respectively.

How much N is then needed for this conversion and that the approximation (5.7) holds? Here a MC simulation is carried out and $Q(y)$ over pseudo-experiments are given in Fig. 5.4. The convergence is amazingly fast so that $Q(y)$ is already nearly Gaussian with $N \sim 2, 3$ and Fig. 5.5 shows that it perfectly agrees with the approximation of CLT when $N \geq 2$. $P(x)$ is revealed to have an extremely convergence property.

Since C_{33} is just proportional to $\langle n_z n'_z \rangle$:

$$C_{33} = \frac{9}{2\alpha} \langle n_z n'_z \rangle,$$

the distribution is a one with $Q(x)$ scaled by the factor $\frac{9}{2\alpha^2}$. The mean and RMS are

$$\begin{aligned}\mu_{33} &= \frac{1}{2} \\ \sigma_{33} &= \frac{1}{2\sqrt{N}}\sqrt{\frac{9}{\alpha^4} - 1}.\end{aligned}\tag{5.8}$$

The mean μ_{33} is equal to the true value thus it is unbiased regardless of N . The other components of C matrix follow the same distribution, namely Gaussians centered around the true values fluctuating with the magnitude of $\sigma_{33} = \frac{1}{2\sqrt{N}}\sqrt{\frac{9}{\alpha^4} - 1}$.

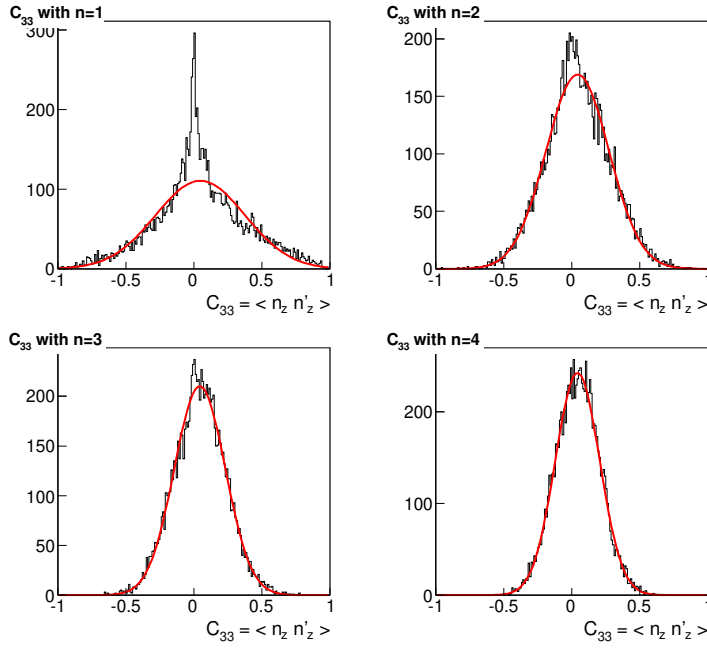


Figure 5.4: Distribution $Q(y)$ in the $\eta_c \rightarrow \Lambda \bar{\Lambda} \rightarrow p\pi^- \bar{p}\pi^+$ channel. y is an algebraic average of $n_z n'_z$ which follows according to (5.3). Each histogram show the case with $N = 1, 2, 3, 4$, the sample size used to calculate y . $N = 1$ gives the same distribution as (5.3). Center limit is already confirmed with $N \geq 2$.

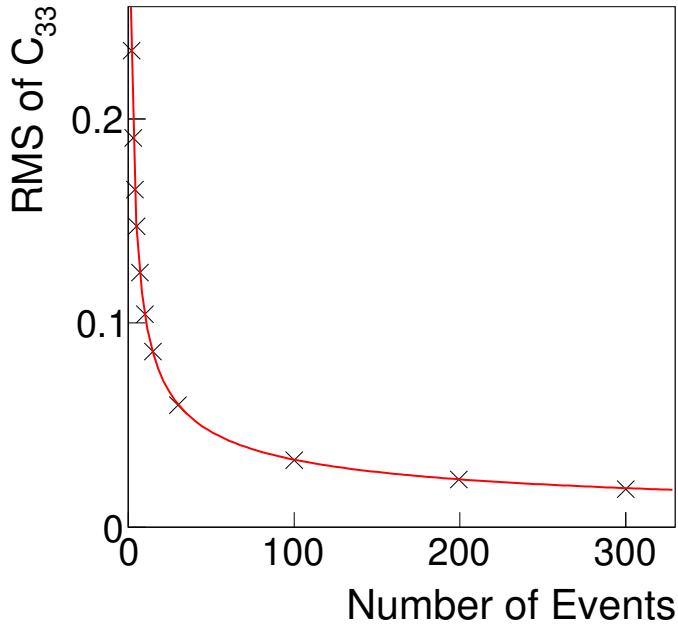


Figure 5.5: RMS of $Q(y)$ distribution with respect to sample size N . The red line is the approximated value from the CLT: $\sigma = \frac{1}{3\sqrt{N}} \sqrt{1 - \frac{\alpha^4}{9}}$.

5.1.3 Estimator for Q_{max}

All preparation for analyzing statistical behavior of Q_{max} is now done, except one thing: the choice of estimator for Q_{max} is not trivial and actually problematic. There are two candidate methods to define:

- Following the definition of Q_{max} literally. That is to say, estimating all components of C matrix, building $S = C^t C$ then take the two biggest eigenvalue of S matrix λ_1, λ_2 to form the estimator of Q_{max}

$$Q_{\text{max}}^M = 2\sqrt{\lambda_1 + \lambda_2}.$$

- On the other hand, in either 6 channels studied in chapter 4, QM predicts the zero values of off-diagonals in C matrix, leading Q_{max} to

$$Q_{\text{max}}^D = \sqrt{C_{11}^2 + C_{33}^2}.$$

The other possible way to estimating Q_{max} is use this value, in other word ignoring the off-diagonal components of C , even if the measured values are non-zero.

Naively thinking, there is no reason to take Q_{max}^D for solution because $Q_{\text{max}} = Q_{\text{max}}^D$ is not valid in theory other than QM in general. It sounds logically failed to use a measure only valid in QM to test the other theories. However as demonstrated in 3.2, the configuration maximizing Q value for a given C is case where $S = C^T C$ is strictly diagonalized. So it is always $Q_{\text{max}}^D \leq Q_{\text{max}}^M$. Q_{max}^D always gives conservative estimation but never ever cheating.

This is as well the reason why Q_{max}^M should not use. Since the contribution of non-zero off-diagonal component always enhance the Q_{max}^M value, statistical fluctuation of off-diagonals only to biases Q_{max}^M positively. To summarize, Q_{max}^D is at least no less conservative than Q_{max}^M and as long as QM prediction, where the off-diagonals are all zero, is supposed to be true, Q_{max}^M will suffer from heavier bias than Q_{max}^D . Fig. 5.6 and Fig. 5.7 are the comparison of Q_{max}^M (blue) and Q_{max}^D (red) distribution over pseudo-experiments and their mean/RMS respectively for $\eta_c \rightarrow \Lambda\bar{\Lambda}$ channel. The dotted line is the true value QM predicts, from which deviation means the bias. Though Q_{max}^M experience less statistical fluctuation, it has apparently more severe bias and slower center limit than Q_{max}^D . This is the reason Q_{max}^D is more suitable as the estimator of Q_{max} . Fig. 5.8 and Fig. 5.9 are same plots for the $Z \rightarrow \tau\tau$ channel, which shows the same tendency.

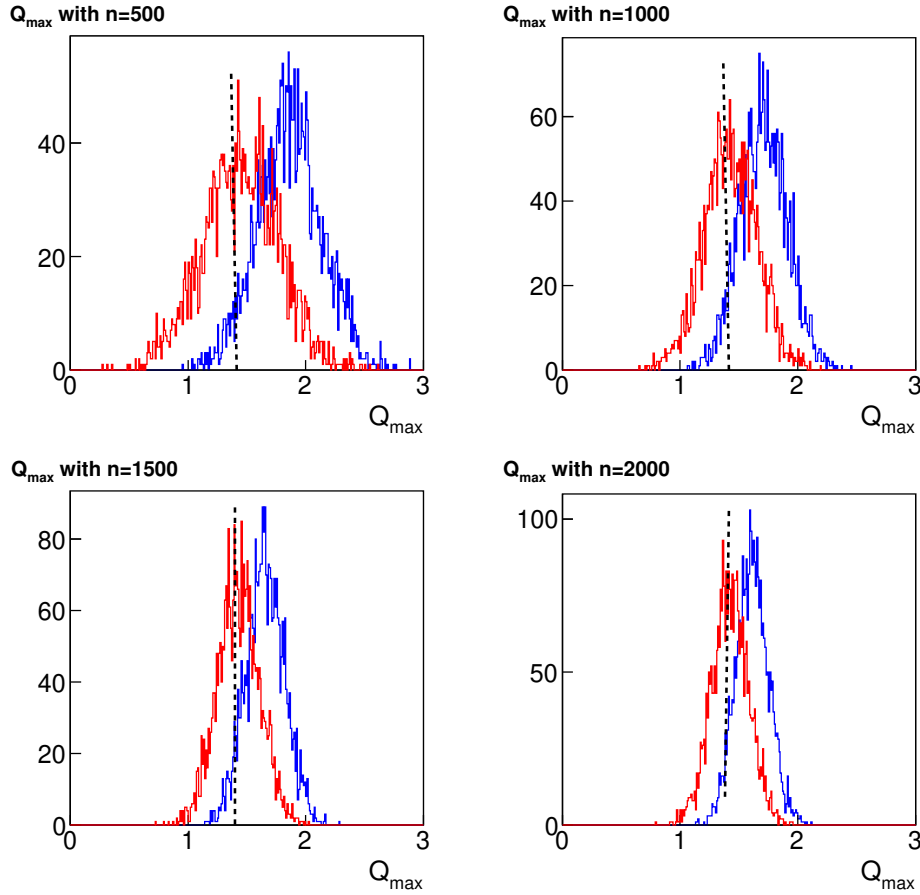


Figure 5.6: Distribution of Q_{\max}^M (blue) and Q_{\max}^D (red) for the $\eta_c \rightarrow \Lambda\bar{\Lambda}$ channel. The dotted line means the true (theoretical) value of Q_{\max} in QM.

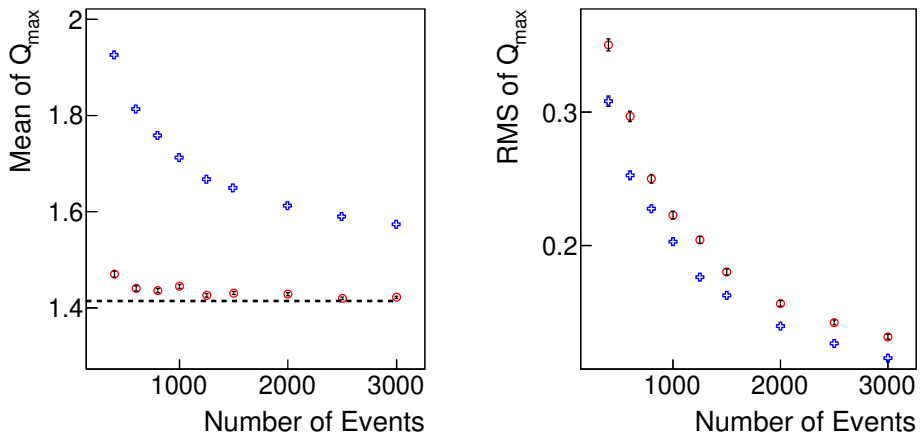


Figure 5.7: Mean and RMS of Q_{\max}^M (blue) and Q_{\max}^D (red) distribution for the $\eta_c \rightarrow \Lambda\bar{\Lambda}$ channel. The dotted line means the true (theoretical) value of Q_{\max} in QM. The case with $\chi_{c0} \rightarrow \Lambda\bar{\Lambda}$ is exactly the same.

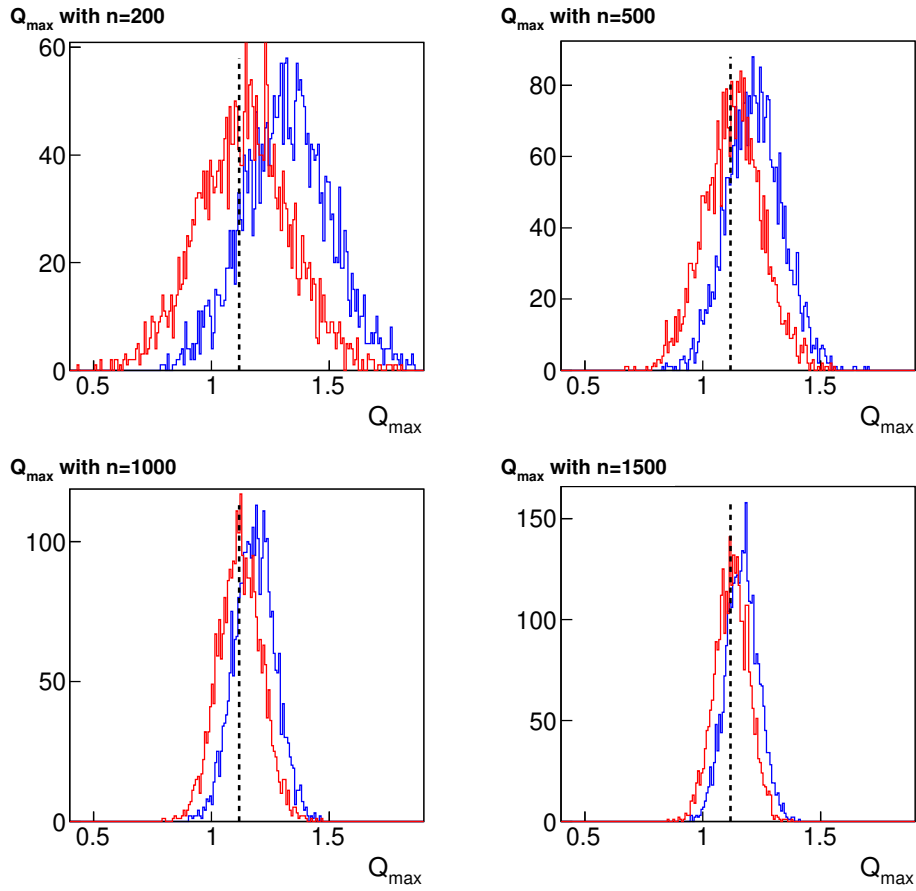


Figure 5.8: Distribution of Q_{max}^M (blue) and Q_{max}^D (red) for the $Z \rightarrow \tau\tau$ channel. The dotted line means the true (theoretical) value of Q_{max} in QM.

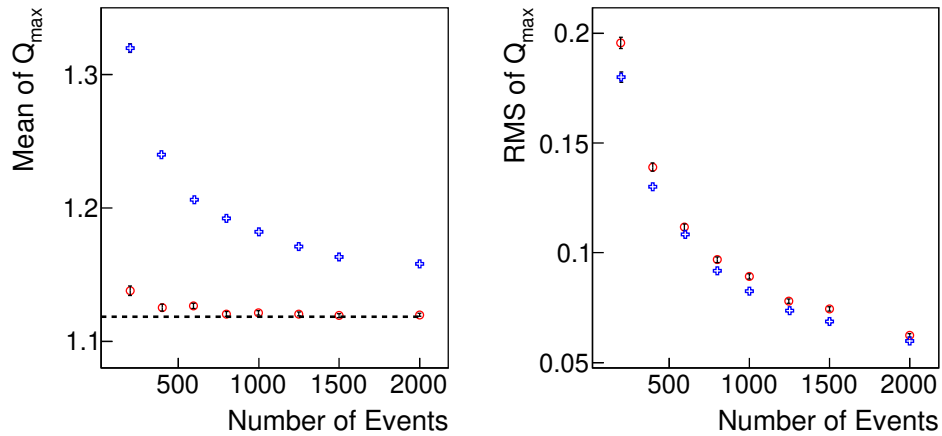


Figure 5.9: Mean and RMS of Q_{max}^M (blue) and Q_{max}^D (red) distribution for the $Z \rightarrow \tau\tau$ channel. The dotted line means the true (theoretical) value of Q_{max} in QM. The case with $ee \rightarrow \gamma^* \rightarrow \tau\tau$ and $H \rightarrow \tau\tau$ are exactly the same.

Several comments on statistical properties of Q_{max}^D are attached.

- As Q_{\max}^D depends on C_{11} and C_{33} in a non-linear way,

$$Q_{\max}^D = 2\sqrt{C_{11}^2 + C_{33}^2}$$

it does suffer from some bias and a positive non-Gaussian in the distribution when N is small, despite C_{11} and C_{33} always follow a bias-free Gaussian. In most the case, this non-Gaussianity vanishes because the expected available sample is sufficiently abundant. The only exception is $H \rightarrow \tau\tau$ where the sample size could be poor as $N \sim 20$).

- The non-Gaussianity vanishes almost with

$$N \sim \begin{cases} 150 & (\Lambda \text{ series}) \\ 20 & (\tau \text{ series}). \end{cases} \quad (5.9)$$

See also Fig. 5.10 and Fig. 5.11 where the explicit convergence of the distribution is shown. The non-Gaussianity arise from the fluctuation of C_{11} and C_{33} . Since the extent only depends on α (5.8), the performance of polarimeter, it is common with the channels in the same series.

- The RMS of Q_{\max}^D distribution is easily found when it converges into Gaussian, considering error propagation from C_{11} and C_{33} . Assuming no statistical correlation between C_{11} and C_{33} ,

$$\begin{aligned} \sigma(Q_{\max}^D)^2 &= \left(\frac{\partial Q_{\max}^D}{\partial C_{11}} \right)^2 \sigma_{11}^2 + \left(\frac{\partial Q_{\max}^D}{\partial C_{33}} \right)^2 \sigma_{33}^2 \\ &= \left(2 \frac{C_{11}}{\sqrt{C_{11}^2 + C_{33}^2}} \right)^2 \sigma_{11}^2 + \left(2 \frac{C_{33}}{\sqrt{C_{11}^2 + C_{33}^2}} \right)^2 \sigma_{33}^2 \\ &= \frac{4}{C_{11}^2 + C_{33}^2} (C_{11}^2 \sigma_{11}^2 + C_{33}^2 \sigma_{33}^2). \end{aligned}$$

σ_{11} and σ_{33} are referred from (5.8) then

$$\begin{aligned} \sigma_{11} = \sigma_{33} &= \frac{1}{2\sqrt{N}} \sqrt{\frac{9}{\alpha^4} - 1} \\ &=: \sigma_C. \end{aligned}$$

Therefore

$$\begin{aligned} \sigma(Q_{\max}^D)^2 &= 4\sigma_C^2 \\ \sigma(Q_{\max}^D) &= 2\sigma_C \\ &= \frac{1}{\sqrt{N}} \sqrt{\frac{9}{\alpha^4} - 1} \end{aligned} \quad (5.10)$$

To conclude, one defines the experimental value of Q_{\max} as Q_{\max}^D . From now on, Q_{\max} designates Q_{\max}^D if no special remark accompanies.

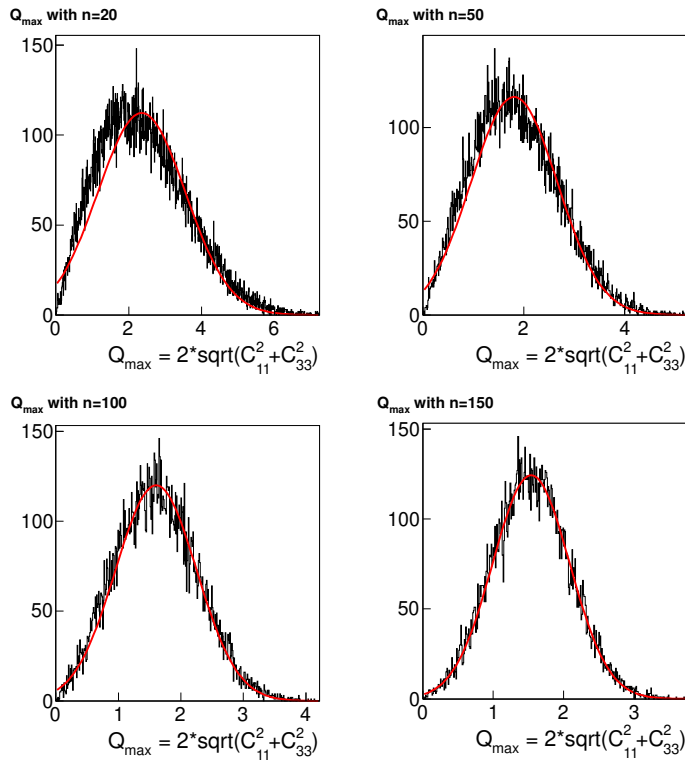


Figure 5.10: Q_{\max}^D distribution with sample size of $N = 20, 50, 100, 150$ in case of channels of the Λ series. It comes to Gaussian around $N \sim 150$.

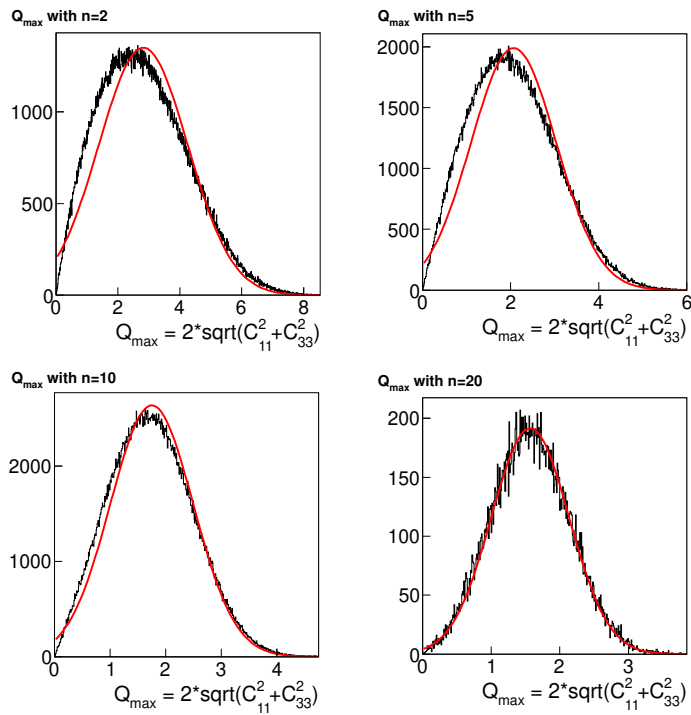


Figure 5.11: Q_{\max}^D distribution with sample size of $N = 2, 5, 10, 20$ in channels of the τ series. It comes to Gaussian around $N \sim 20$.

5.1.4 Significance and the master formula

Here we finally derive the expected significance of observed violation of BI, with respect to sample size N . The significance is defined as:

$$\Delta =: \frac{\mu(Q_{\max}) - CL}{\sigma(Q_{\max})} \quad (5.11)$$

When N is sufficiently large so that Q_{\max} distributes according to Gaussian, this is just the standard deviation, for example, $\Delta = 1$ means 1σ deviation. When N is not enough large then it is not the case, (5.11) gives a more conservative evaluation of significance since the non-Gaussian tail enhance the value of $\sigma(Q_{\max})$.

In an ideal setup, $\mu(qmax)$ is identical with the theoretical Q_{\max} value derived in chapter 4:

$$\mu(Q_{\max}) = \begin{cases} \sqrt{2} & (\eta_c, \chi_{c0} \rightarrow \Lambda\bar{\Lambda}; H \rightarrow \tau\tau) \\ \sqrt{5} & (Z \rightarrow \tau\tau) \\ \frac{2}{\sqrt{5 - 2\Gamma^2 + 2\Gamma^4}}; \Gamma^2 := \frac{4m_\tau^2}{s} & (e^+e^- \rightarrow \gamma^* \rightarrow \tau\tau) \end{cases}$$

\sqrt{s} is the e^+e^- center of mass energy. Assuming $\sqrt{s} = 10.58(\text{GeV})$ of Belle experiment, $\mu(Q_{\max}) = 1.037$. CL is the classical limit of BI: 1, in an ideal case.

When N is larger than the threshold (5.9) and Q_{\max} distributes according asymptotically to Gaussian, substituting (5.10) gives

$$\Delta =: (\mu(Q_{\max}) - CL) \frac{\alpha^2}{\sqrt{9 - \alpha^4}} \sqrt{N}. \quad (5.12)$$

This is the master formula of significance.

One finds the dependency of (5.12) can be factorized in the 3 factors; the first part $\mu(Q_{\max}) - CL$ represents the extent of spin entanglement of $\Lambda\bar{\Lambda}$ or $\tau\tau$ pair, the indispensable component for violating BI; the second factor $\alpha^2/\sqrt{9 - \alpha^4}$ indicates the dependence on the polarimeter power of decay $\Lambda \rightarrow p\pi$ or $\tau \rightarrow \pi\nu$, in which larger α^2 reflects the spin entanglement more to the observable Q_{\max} , enhancing the significance; the last factor is statistics, with the \sqrt{N} dependency. The function relation to N with respect to each channel is illustrated in Fig. 5.12. The sample size giving 1σ , 2σ , 3σ significance is as in Tab. 5.1.

Table 5.1: Sample size corresponds to 1σ , 2σ , 3σ significance with respect to each channel

Channel	N(1σ)	N(2σ)	N(3σ)
$\eta_c, \chi_{c0} \rightarrow \Lambda\bar{\Lambda}$	600	2200	5000
$Z \rightarrow \tau\tau$	300	1200	1700
$ee \rightarrow \gamma^* \rightarrow \tau\tau$	6000	26500	60000
$H \rightarrow \tau\tau$	45	180	400

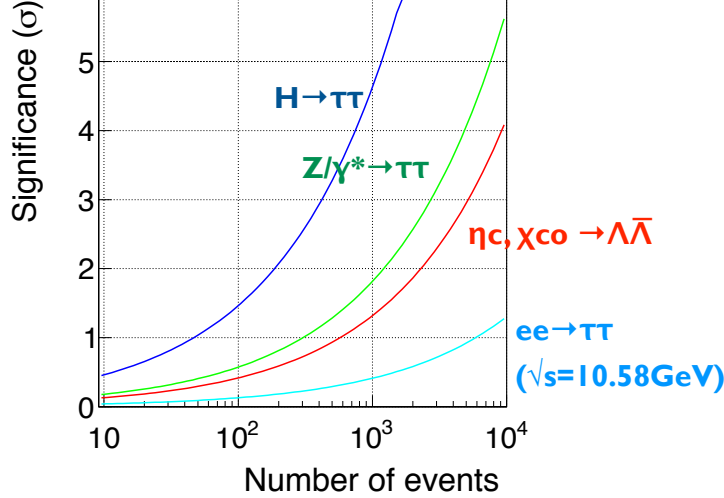


Figure 5.12: The significance Δ in the function of sample size N with respect to each channel

5.2 Effect from Background

There are two independent effects brought by BG.

- (i) Correlation amplitude $\langle n_i n'_j \rangle$ will be smeared, reducing the Q_{\max} value. BG events tend to be accidental where the two pions candidate are less like to correlated. Therefore the observed correlation amplitude $\langle n_i n'_j \rangle$ is supposed to be diluted. Here a BG model is assumed in which the two pions candidate have no correlation: $\langle n_i n'_j \rangle = 0$, giving the most conservative estimation of the smearing effect. The distribution of $x = n_i n'_j$ for BG events comes to

$$P(x) = \frac{1}{2} \ln \frac{1}{|x|}.$$

which is same as (5.3) with $\alpha = 0$. The distribution of $x = n_i n'_j$ for signal events is (5.3). Assuming a simple mixture of signal and BG events, the observed distribution of $x = n_i n'_j$ will be

$$\begin{aligned} P_b(x) &= (1-b) \frac{1}{2} (1 + \alpha^2 x) \ln \frac{1}{|x|} + b \frac{1}{2} \ln \frac{1}{|x|} \\ &\propto \frac{1}{2} (1 + (1-b)^2 \alpha^2 x) \ln \frac{1}{|x|} \end{aligned} \quad (5.13)$$

where b represent the fraction of BG events. So, it effectively shifts the α value in the distribution for signal events as

$$\alpha^2 \rightarrow (1-b)\alpha^2.$$

The mean value and the RMS are

$$\begin{aligned} \mu &= (1-b) \frac{\alpha^2}{9} \\ \sigma &= \frac{1}{3} \sqrt{1 - (1-b)^2 \left(\frac{\alpha^2}{9} \right)^2} \end{aligned} \quad (5.14)$$

Hence the $C_{ij} = \frac{9}{2\alpha^2} \langle n_i n'_j \rangle$ has the mean and RMS of

$$\begin{aligned}\mu &= (1-b)\tilde{C}_{ij} \\ \sigma &= \frac{1}{2\sqrt{N}} \sqrt{\frac{9}{\alpha^4} - (1-b)^2}\end{aligned}\tag{5.15}$$

respectively. The tilde mark represent theoretical value. The statistical behavior of Q_{\max} is found, repeating the argument in 5.1.3

$$\mu(Q_{\max}) = (1-b)\tilde{Q}_{\max}\tag{5.16}$$

$$\sigma(Q_{\max}) = \frac{1}{\sqrt{N}} \sqrt{\frac{9}{\alpha^4} - (1-b)^2}.\tag{5.17}$$

As smeared by BG, the mean value $\mu(Q_{\max})$ scale down from theoretical value \tilde{Q}_{\max} by the factor $1-b$. On the other hand RMS is almost independent of b , remains the same magnitude as the case without BG. The significance curves with different BG levels b are illustrated as Fig. 5.13~5.17 for each channel individually.

The expected BG level is, for the $\eta_c, \chi_{c0} \rightarrow \Lambda\bar{\Lambda}$ channel, less than 0.5% in current analysis. (though the signal selection criteria might be too strict for our analysis).

The situation in the τ series channel are more severe as only $\pi^+\pi^-$ appear in the final state. Nevertheless, the BG level can be managed to keep below 2% in the $Z \rightarrow \tau\tau$ at LEP and the $e^+e^- \rightarrow \gamma^* \rightarrow \tau\tau$ at Belle, with appropriate procedures.

$H \rightarrow \tau\tau$ is the most challenging channel in suppressing BG because it has ~ 10 times more cross-section than that of the signal. Current analysis achieves 45% in BG level with 25% collection efficiency [78], however, which still leaves much to be desired. For example in reconstructing the mass $m_{\tau\tau}$, the collinear approximation is applied which blurs much the peak of $m_{\tau\tau}$ as shown in Fig. 5.18, as a result, the cut on $m_{\tau\tau}$ is not effective that allows much residual BG such as $ee \rightarrow ZZ \rightarrow \tau\tau q\bar{q}$ (pink dotted line) to sit under the peak. Most of them are "irreducible" BG channels that have the same final state topology as the signal channel, which can only be distinguished by $m_{\tau\tau}$. However, this is supposed to be drastically improved by implementing the kinematical fit as described in the bottom of section 2.4, instead of the collinear approximation. The peak of $m_{\tau\tau}$ will be sharpen with the width being about 3GeV, then the BG level will be accordingly reduced to around 15%, while the corresponding width is now about 10GeV with the collinear approximation.

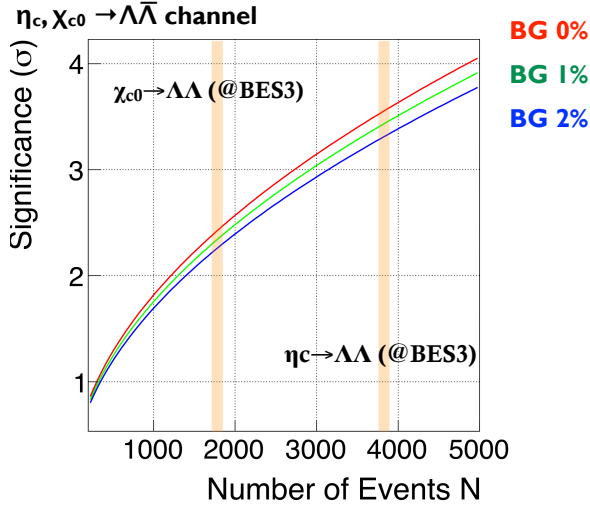


Figure 5.13: Expected significance with each BG level in the $\eta_c, \chi_{c0} \rightarrow \Lambda\bar{\Lambda}$ channel.

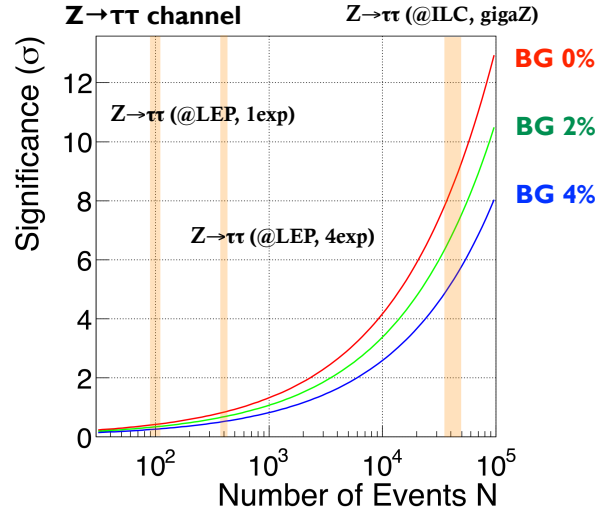


Figure 5.14: Expected significance with each BG level in the $Z \rightarrow \tau\tau$ channel.

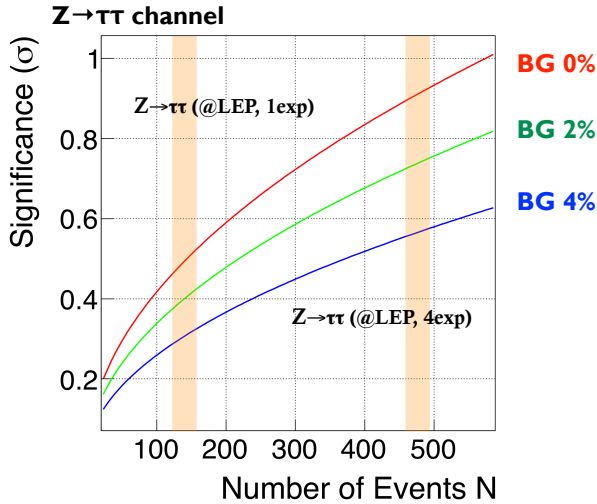


Figure 5.15: Expected significance with each BG level in the $Z \rightarrow \tau\tau$ channel in a wider scale of N

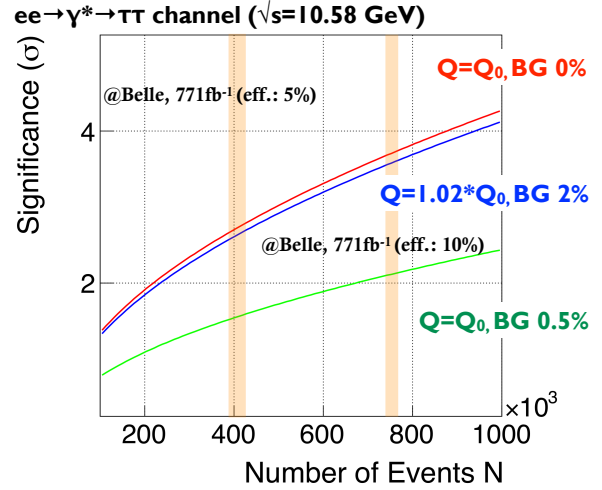


Figure 5.16: Expected significance with each BG level in the $ee \rightarrow \gamma^* \rightarrow \tau\tau$ channel. The effect of the contamination from the time-like events (evaluated in section 5.3) is included. Q_0 is the theoretical value $Q_{\max} = 1.037$ with tree-level calculation. The blue line indicates the case where the higher order corrections enhance Q_{\max} by 2%, with considering the BG level of 2%. The sensitivity highly depends on the uncertainty.

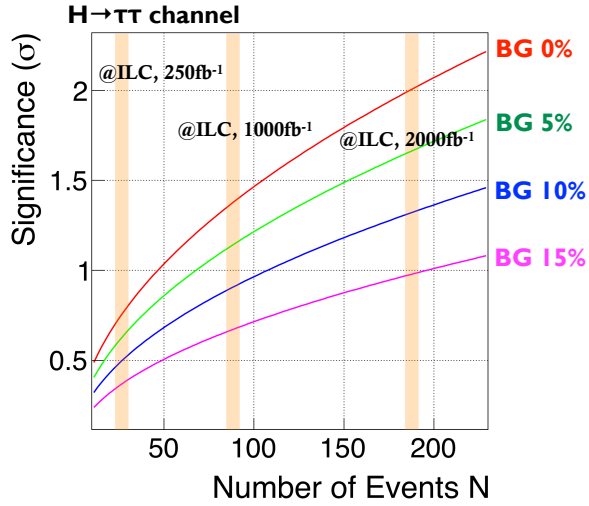


Figure 5.17: Expected significance with each BG level in the $H \rightarrow \tau\tau$ channel.

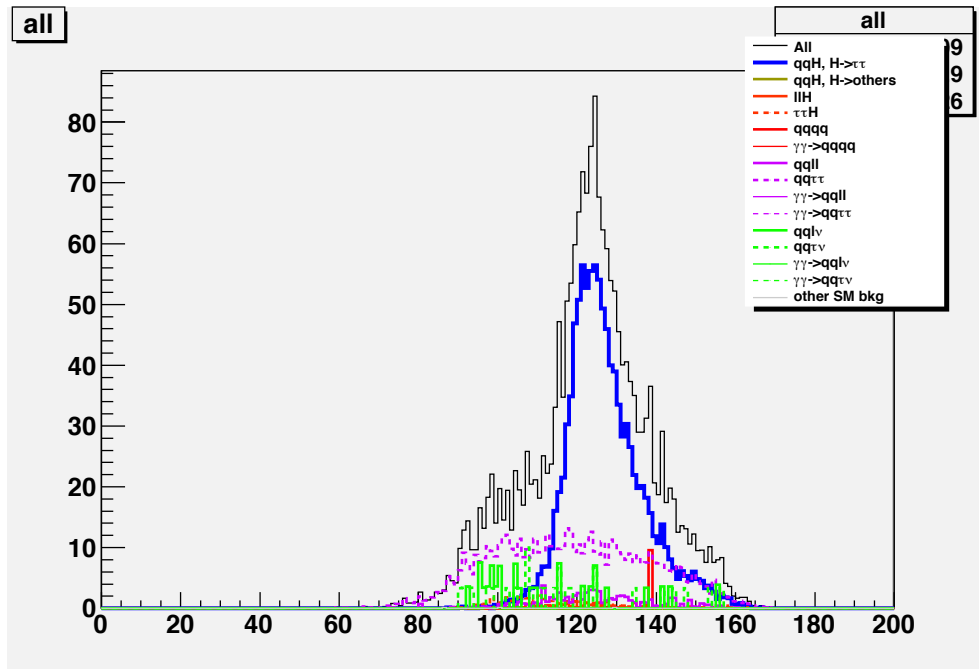


Figure 5.18: Simulation of the $H \rightarrow \tau\tau$; $Z \rightarrow q\bar{q}$ channel with ILD full simulation (with 120GeV Higgs mass). The horizontal axis indicates the reconstructed mass $om_{\tau\tau}$. Signal (blue line) peaks around the Higgs mass 120GeV, while the other BG is continually distributed. The collinear approximation is a rough method that broadens much the signal peak, allowing $ee \rightarrow ZZ \rightarrow \tau\tau q\bar{q}$ (pink dotted line) to overlap with.

- (ii) The classical limit of the inequality will be enforced to rise. Due to the contamination of BG, the achievable correlation Q_{\max} in LHVT is enhanced, which sounds contradictory to the statement above that BG generally smears out the correlation. The latter statement is true in reality, while the former is a theoretically introduced fact.

Recall that our Bell's inequality (3.12) relies upon the equation (3.11), however it results from the relation between the Λ or τ spin and the π direction (2.21) which is required as experimental results. This (3.11) holds true for the signal processes $\Lambda\bar{\Lambda} \rightarrow p\pi p\pi$ and $\tau\tau \rightarrow \pi\nu\pi\nu$ but in principle it has no reason to hold for the other channels.

Without (3.11), the restriction which can be generally imposed on the direction of two particles will be dramatically loosen as

$$|\langle n_a n'_b \rangle + \langle n_a n'_d \rangle + \langle n_c n'_b \rangle - \langle n_c n'_d \rangle| \leq 2. \quad (5.18)$$

This is no more than an algebraic inequality that 3 vectors generally follow. On the other hand, the inequality for the signals is

$$|\langle n_a n'_b \rangle + \langle n_a n'_d \rangle + \langle n_c n'_b \rangle - \langle n_c n'_d \rangle| \leq \frac{2\alpha^2}{9}, \quad (5.19)$$

therefore, the sample of admixture of signal and BG follows

$$|\langle n_a n'_b \rangle + \langle n_a n'_d \rangle + \langle n_c n'_b \rangle - \langle n_c n'_d \rangle| \leq (1-b) \times \frac{2\alpha^2}{9} + b \times 2. \quad (5.20)$$

where b is the BG level defined above. Since the upper limit for the BG inequality (5.18) is $9/2\alpha^2 = 9 \sim 20$ times greater than that of signal one (5.19), the impact of BG is huge.

In language of Q_{\max} ,

$$Q_{\max} \leq CL \quad (5.21)$$

$$CL = (1-b) \times 1 + b \times \frac{9}{\alpha^2} \quad (5.22)$$

$$= 1 + b \left(\frac{9}{\alpha^2} - 1 \right) \quad (5.23)$$

Considering the quantum limit of Q_{\max} is $\sqrt{2}$ at the most, the inequality (5.20) becomes extremely difficult to violate even with a tiny fraction of BG. Plugging $\alpha_\Lambda = 0.642 \pm 0.013$ and $\alpha_\tau = 0.998 \pm 0.005$ in (5.23), b has to be suppressed below 1.7% for the Λ series channels and 5.2% for the τ series channels otherwise Q_{\max} never overcomes the upper limit of (5.20).

By the way, how can the BG level b be estimated? MC simulation is the most common way, in which a particular model is assumed for example SM. We know that this is not ideal way here as long as the test of LHVT is considered because it is based on QM. However practically it is almost impossible to estimate BG without assuming any single model even though some experimental fact can be used (more precisely, there is even difficult to know if it is really impossible). This is another loophole arising in the phase of analysis.

In practice, a certain model has to be assumed for BG in an empirical way, such as the "uncorrelated BG" discussed in (i) above. In fact this not an absurd assumption at all, considering it almost never happens that the BG sample realize the maximum correlation 2 described as the BG inequality (5.18) such as when all π^- flies to the direction of \mathbf{a} and all π^+ to the \mathbf{b} . (5.18) is a theoretical rigorous inequality but compromise too much.

Thus eventually, with this "no correlation assumption" for BG, the inequality (3.12) is allowed to used again, and the impact of BG ends up in only the smearing effect illustrated in (i).

5.3 Effect from contamination of the time-like events

As pointed out in section 2.3, the τ series channels will experience the contamination of the time-like events in which the decays of τ^+ and τ^- are in the time-like configuration in space time, especially the $e^+e^- \rightarrow \tau\tau \rightarrow \pi\nu\pi\nu$ which ends up in having 6% of the events time-like.

Similar to the rhetoric adopted above, the inequality that the time-like sample does not follow (3.11), however the relation (2.21) and (2.22) should hold for both time-like and space-like events.

$$\begin{aligned} P(\mathbf{n}|\mathbf{s}) &= 1 + \alpha \mathbf{n} \cdot \mathbf{s} \\ P(\mathbf{n}'|\mathbf{s}') &= 1 - \alpha \mathbf{n}' \cdot \mathbf{s}'. \end{aligned}$$

Thus the eventual restriction imposed on the time-like events is

$$|\langle n_a n'_b \rangle + \langle n_a n'_d \rangle + \langle n_c n'_b \rangle - \langle n_c n'_d \rangle| \leq 2\sqrt{2}. \quad (5.24)$$

Therefore, the classical limit for the inequality that the sample with fraction t of the time-like events contaminated in becomes

$$1 \cdot (1 - t) + \sqrt{2} \cdot t, \quad (5.25)$$

which is 1.025 for $t = 0.06$ in the $e^+e^- \rightarrow \tau\tau \rightarrow \pi\nu\pi\nu$ channel.

This effect is included in calculating the sensitivity as in (5.16). Though the absolute effect is small, this consequence is severe in the case.

5.4 Effect from detector resolution

In this section, the effect due to the finite detector resolution is studied. Qualitatively it will definitely smear the correlation $\langle n_i n'_j \rangle$, however, the impact is almost negligible as mentioned in section 5.1.1.

This is because the $n_i n'_j$ distribution has a very large width which overwhelms the measurement error on \mathbf{n} and \mathbf{n}' unless the resolution is terrible. Fig. 5.19 display the $n_z n'_z$ distribution in the $\eta_c \rightarrow \Lambda\bar{\Lambda} \rightarrow p\pi p\pi$ channel. The red and blue lines show the case without and with measurement error respectively. δ stands for the resolution of n_z and n'_z . They are in perfect agreement up to $\delta n_z \leq 0.1$. However, the resolution for a typical measurement on charged particle momentum and the direction are $\sigma_{pT}/p_T \sim 1\%$ and $\sigma_\theta, \sigma_\phi \sim 10^{-3}(\text{rad})$ respectively, which is presumed safely below $\delta n_z \leq 0.1$.

Fig. 5.20 shows the Q_{\max} value dependence on δ , assuming a fixed number of sample size N . The points are the mean value and the error bars are the RMS (not the error of the mean). The effect of measurement error is tiny compared with the statistical fluctuation.

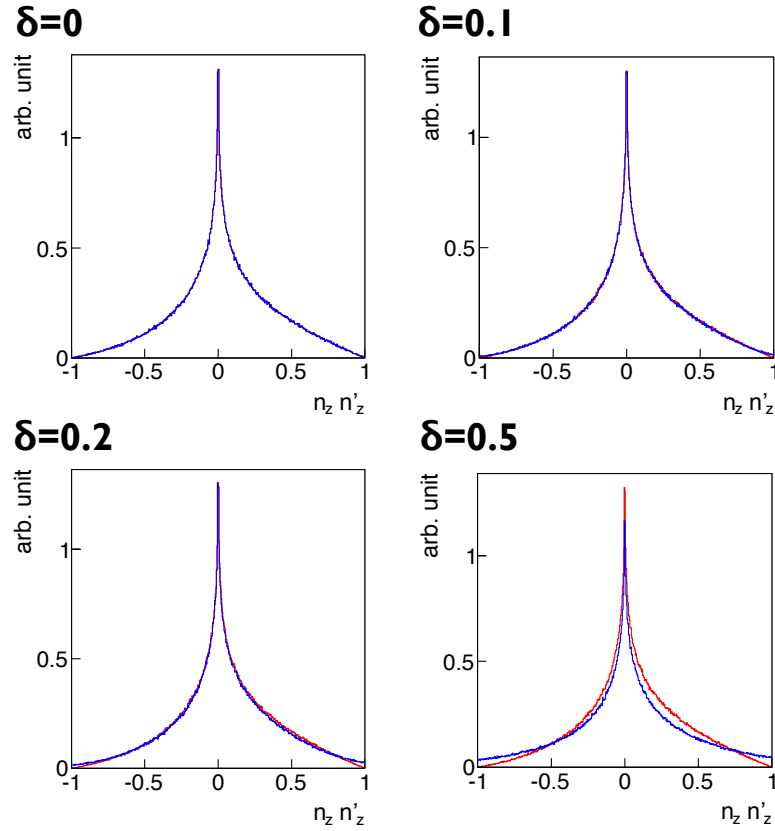


Figure 5.19: Simulated $n_z n'_z$ distribution in the $\eta_c \rightarrow \Lambda \bar{\Lambda}$ channel with (blue) and without (red) measurement error. The measurement error is implemented by randomly multiplying a coefficient to n_z and n'_z which follows according to a Gaussian distribution with the RMS of δ for each event ("smearing"). Cases with $\delta = 0, 0.1, 0.2, 0.5$ are displayed, which shows almost no impact until $\delta = 0.1$. The result is common to the other 4 channels as well.

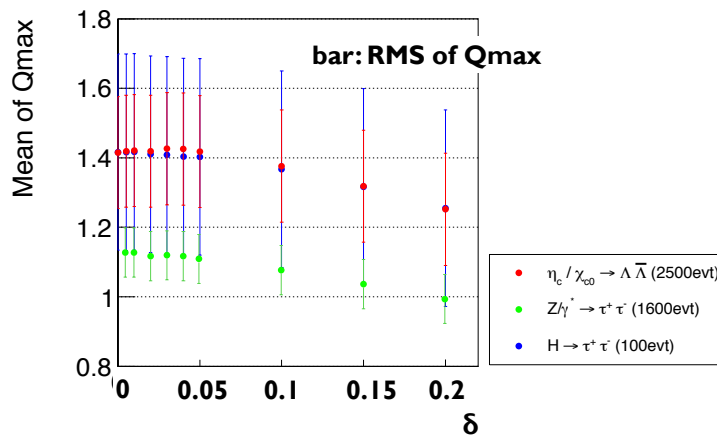


Figure 5.20: The dependence of Q_{\max} on the smearing δ with a fixed N . The points indicate the mean value and the error bars are the RMS. The realistic value of δ here is expected well below 0.1, thus the effect of mean drop is negligible compared with the statistical error, as far as this order of statistics is concerned.

5.5 Available sample size with current and future experiment and the feasibility

Last but not least, the realistic number of available sample size and the corresponding significance is estimated for each channel. The conclusion plots are Fig. 5.13~5.17. The colored band indicates the expected available sample size with respect to each scenario.

5.5.1 $\chi_{c0}, \eta_c \rightarrow \Lambda \bar{\Lambda}$

Experimentally, η_c and χ_{c0} are produced through the radiative deexcitation of J/ψ and ψ' respectively:

$$J/\psi \rightarrow \eta_c \rightarrow \gamma \qquad \psi' \rightarrow \chi_{c0} \rightarrow \gamma$$

The branching of each decay in the later cascade $\eta_c, \chi_{c0} \rightarrow \Lambda \bar{\Lambda} \rightarrow p\pi p\pi$ is displayed in Tab. 5.2.

Table 5.2: Branching ratio of each decay in $c\bar{c} \rightarrow \eta_c, \chi_{c0} \rightarrow \Lambda \bar{\Lambda} \rightarrow p\pi p\pi$

Channel	Branching fraction
$J/\psi \rightarrow \eta_c + \gamma$	$(1.7 \pm 0.4) \times 10^{-2}$
$\psi' \rightarrow \chi_{c0} + \gamma$	$(9.7 \pm 0.3) \times 10^{-2}$
$\eta_c \rightarrow \Lambda + \bar{\Lambda}$	$(1.41 \pm 0.17) \times 10^{-3}$
$\chi_{c0} \rightarrow \Lambda + \bar{\Lambda}$	$(3.3 \pm 0.4) \times 10^{-4}$
$\Lambda \rightarrow p + \pi^-$	$(6.39 \pm 0.05) \times 10^{-1}$
$\bar{\Lambda} \rightarrow \bar{p} + \pi^+$	$(6.39 \pm 0.05) \times 10^{-1}$
$J/\psi \rightarrow \gamma\eta_c; \eta_c \rightarrow \Lambda \bar{\Lambda} \rightarrow p\pi p\pi$	$(9.8 \pm 2.6) \times 10^{-6}$
$\psi' \rightarrow \gamma\chi_{c0}; \chi_{c0} \rightarrow \Lambda \bar{\Lambda} \rightarrow p\pi p\pi$	$(1.31 \pm 0.16) \times 10^{-5}$

Both the η_c and χ_{c0} mode maintain very tiny branching fraction with the order of 10^{-5} . Hence substantially large number of η_c or χ_{c0} sample is required. Only the charm factory experiments, for example BES3 or CLEO, can potentially meet the demand. Either of them is e^+e^- collision experiment and has been collecting enormous statistics at J/ψ and ψ' resonance.

As for BES3, about 1.2×10^9 of J/ψ and 3.0×10^8 of ψ' are produced by the end of 2013. The number of events of $J/\psi \rightarrow \eta_c\gamma; \eta_c \rightarrow \Lambda \bar{\Lambda} \rightarrow p\pi p\pi, \psi' \rightarrow \chi_{c0}\gamma; \chi_{c0} \rightarrow \Lambda \bar{\Lambda} \rightarrow p\pi p\pi$ are therefore 1.2×10^4 and 4×10^3 respectively.

Considering the efficiency for detection, selection and the fraction of events where the decays $\Lambda \rightarrow p\pi^-$ and $\bar{\Lambda} \rightarrow \bar{p}\pi^+$ is separated in space-like, the total efficiency is expected to 20 ~ 30%, assuming the detector of BES3. The efficiencies for each step throughout the event acquisition is listed in Tab. 5.3. The $\cos\theta_\Lambda$ cut is due to the limited angular acceptance of tracker. Tracking reconstruction efficiency is calculated as the probability to have more than 3 tracks out of $p\pi\bar{p}\pi$, based on the official number of tracking efficiency of single charged particle from BES3 publication [79]. The cut of reconstructed mass is for vetoing backgrounds since for signal events, the reconstructed mass $m_{p\pi}, m_{\bar{p}\pi}$ and $m_{p\pi\bar{p}\pi}$ should be around the mass shell of $\Lambda, \bar{\Lambda}$ and η_c (or χ_{c0}) respectively. Efficiency for the cuts is deducted from BES3 analysis of $\chi_{c0} \rightarrow \Lambda \bar{\Lambda}$ [80]. Fraction of the space-like events is calculated in 2.3.4 and the result is exhibited in Tab. 2.2.

Finally, the available sample size of η_c and χ_{c0} mode is found to be around 4000 and 1500 respectively, which corresponds to roughly 3.5σ and 2σ of significance.

Table 5.3: The efficiency flow of $\eta_c, \chi_{c0} \rightarrow \Lambda\bar{\Lambda} \rightarrow p\pi^-\bar{p}\pi^+$ events assuming BES3. The bracket number is assumed.

	$\eta_c \rightarrow \Lambda\bar{\Lambda}$	$\chi_{c0} \rightarrow \Lambda\bar{\Lambda}$
$ \cos\theta_\Lambda < 0.93$	0.86	0.86
Tracking reconstruction (3 & 4 prong)	0.95	0.98
Reconstructed mass cut	(0.6)	(0.6)
Space-like decays	0.66	0.76
Total	0.32	0.38

5.5.2 $Z \rightarrow \tau\tau$

From the viewpoint of statistics of Z , LHC sounds like an ideal experiment, however it is proton-proton collider thus the center of mass energy is unknown. Since one desires to measure \mathbf{n}, \mathbf{n}' here which is the $\pi^+\pi^-$ direction in $\tau^+\tau^-$ rest frame respectively, as pointed out in section 2.4, the 4 momentum of each tau has to be reconstructed where the missing 4 momentum is required to be precisely grasped. Therefore for the channels of τ series, e^+e^- collider experiment is the only possible option. LEP is the most promising candidate in its rich statistics of Z . It has 4 detectors along the ring (DELPHI; ALEPHE; L3; OPAL) and each collected about 10^6 of $e^+e^- \rightarrow Z$ events [81]. The list of branchings for respective decays in $Z \rightarrow \tau\tau \rightarrow \pi\nu\pi\nu$ is shown in Tab. 5.4. Thus about 400 $Z \rightarrow \tau\tau \rightarrow \pi\nu\pi\nu$ events are generated per experiment. The collection efficiency is typical $\sim 20\%$ [82], the number of available event sample is expected to be around 100 for one experiment, 400 for 4 experiments, which will give a low significance $\Delta = 0.4, 1.0$, corresponding to 75%CL, 85%CL respectively.

Table 5.4: Branching ratio of each decay in $Z \rightarrow \tau^-\tau^+ \rightarrow \pi^-\nu\pi^+\bar{\nu}_\tau$

Channel	Branching fraction
$Z \rightarrow \tau\tau$	$(3.37 \pm 0.0008)\%$
$\tau^- \rightarrow \pi^-\nu_\tau$	$(10.83 \pm 0.0006)\%$
$\tau^+ \rightarrow \pi^+\bar{\nu}_\tau$	$(10.83 \pm 0.0006)\%$
$Z \rightarrow \tau^-\tau^+ \rightarrow \pi^-\nu\pi^+\bar{\nu}_\tau$	$(3.95 \pm 0.04) \times 10^{-4}$

Other than LEP, ILC could be the potential candidate of experiment. Though of course the Higgs factory is the physics program of paramount importance in ILC, there is also a project called "gigaZ" is being planned [53]. This is a optional run depending on the result of the Higgs factory, aiming at ultra-fine measurement of electro-weak physics. It is plan to generate 10^9 of $e^+e^- \rightarrow Z$ events in ILC, which counts 10^3 times larger statistics than that in LEP. The corresponding significance reaches $4\sigma - 5\sigma$, realizing an observation with high sensitivity.

5.5.3 $e^+e^- \rightarrow \gamma^* \rightarrow \tau\tau$

According to the tree-level calculation, in order to have $\mu(Q_{\max}) > 1$ in this channel, $\sqrt{s} > 8.6\text{GeV}$ is at least needed and $\sqrt{s} = 10.58(\text{GeV})$ run of Belle experiment gives $\mu(Q_{\max}) = 1.03$ which barely violates the BL. Instead, this channel has by far abundant statistics. with the integrated luminosity $\mathcal{L} = 771\text{fb}^{-1}$ collected by 2010 run, 7×10^8 of $e^+e^- \rightarrow \tau\tau$, 8×10^6 of $e^+e^- \rightarrow \tau\tau \rightarrow \pi\nu\pi\nu$ are produced.

The drawback of this channel is that it is terribly vulnerable against theoretical uncertainty or experimental effects, (e.g. contamination of BG, detector resolution etc.) since the true value $\mu(Q_{\max})$ is just slightly above the CL, it will easily be close to or underneath CL when the correlation are smeared. The quantitative estimation of the sensitivity does not make any sense at the moment though, for reference, here the result of the case where the higher order corrections do not contribute to Q_{\max} is provided as Fig. 5.17.

The effect of the contamination from the time-like events (evaluated in section 5.3) is included. Considering the realistic BG level is $\sim 2\%$, there are almost no sensitivity. Fig. 5.17 also shows that it is sensitive to the deviation of theoretical Q_{\max} value (the blue line represent the case where the higher order corrections enhance Q_{\max} by 2%).

5.5.4 $H \rightarrow \tau\tau \rightarrow \pi\nu\pi\nu$

As $\tau\tau$ needs full reconstruction, ILC is the only candidate. For Higgs production, there is 2 main production mode; ZH associated production mode (Fig.5.21) and WW fusion mode (Fig. 5.22). In $\sqrt{s} = 250, 350\text{GeV}$ run, ZH channel is dominant while WW fusion are the main production process in high-energy runs ($\sqrt{s} > 500\text{GeV}$) (Fig. 5.23). Here only the ZH channel is available since the WW fusion process generates additional neutrinos which makes $\tau\tau$ reconstruction impossible.

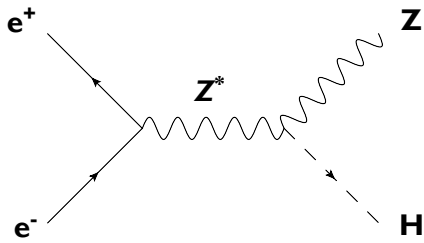


Figure 5.21: The ZH associated production. The dominant Higgs production channel at ILC low energy runs ($\sqrt{s} = 250, 350\text{GeV}$).

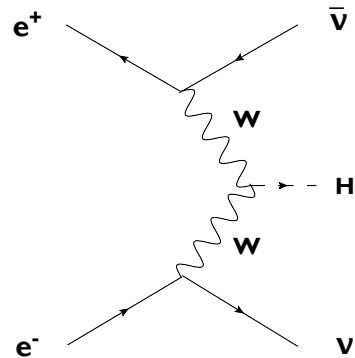


Figure 5.22: The WW fusion. The dominant Higgs production channel at ILC high-energy runs ($\sqrt{s} = 500, 1000\text{GeV}$).

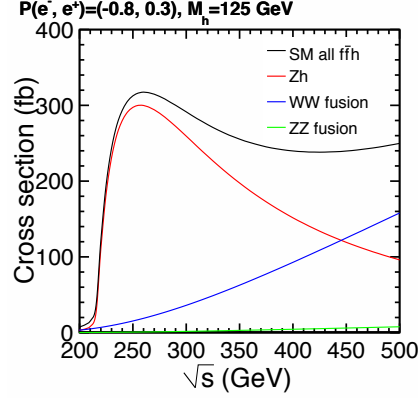


Figure 5.23: Cross-sections for each Higgs production channels in ILC.

Analysis of the ZH channel is still challenging in many aspects. First, reconstruction of $\tau\tau$ requires precise reconstruction of the missing 4 momentum. In the ZH case, this means that energy and momentum of the recoiled Z has also to be reconstructed in precision. Though it is easy when Z decays into lepton pairs as $Z \rightarrow ee, \mu\mu$ but those accounts for only 6% of the branchings. From statistical point of view, events of $Z \rightarrow q\bar{q}$ (branching: 70%) are inevitably counted on.

Fortunately, this is also the requirement from the original ILC physics program, dedicated detector systems [83] and reconstruction algorithms ("Particle Flow Algorithm" [84] etc.) have been developed, specialize for precise measurement of $q\bar{q}$ jets from Z or W bosons. The up-to-date ILD full simulation indicates typically $\sigma/E \sim 4\%$ of single jet energy resolution can be achieved. (Fig. 5.24). As for momentum, an approximate study is carried out using the sample of $Z \rightarrow q\bar{q}$ where the Z is at rest with respect to laboratory frame, to test if the 3 momentum can be reconstructed to 0. The result is shown in Fig. 5.25. Each component of the reconstructed 3 momentum peaks at the true value 0 but does have residual by 2GeV on average. Though the Z boson appearing in the ZH process is not at rest, from this result the momentum resolution of the recoiled Z can be inferred to the order of a few GeV, which is the precision of missing momentum as well. Rigid numerical estimation of the impact due to the imperfect precision of the missing 4 momentum on $\tau\tau$ reconstruction or Q_{\max} is still under study. However as discussed later in section 5.4, this order of measurement precision is sufficient that the effect is supposed to be negligible.

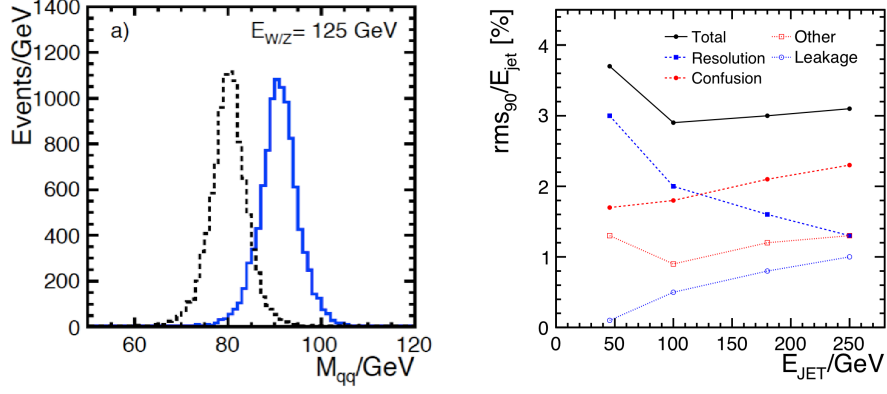


Figure 5.24: Distribution of reconstructed energy of 2 jets from $W \rightarrow q\bar{q}$ and $Z \rightarrow q\bar{q}$ events (left) and the single jet energy resolution in the function of jet energy (right).[84].

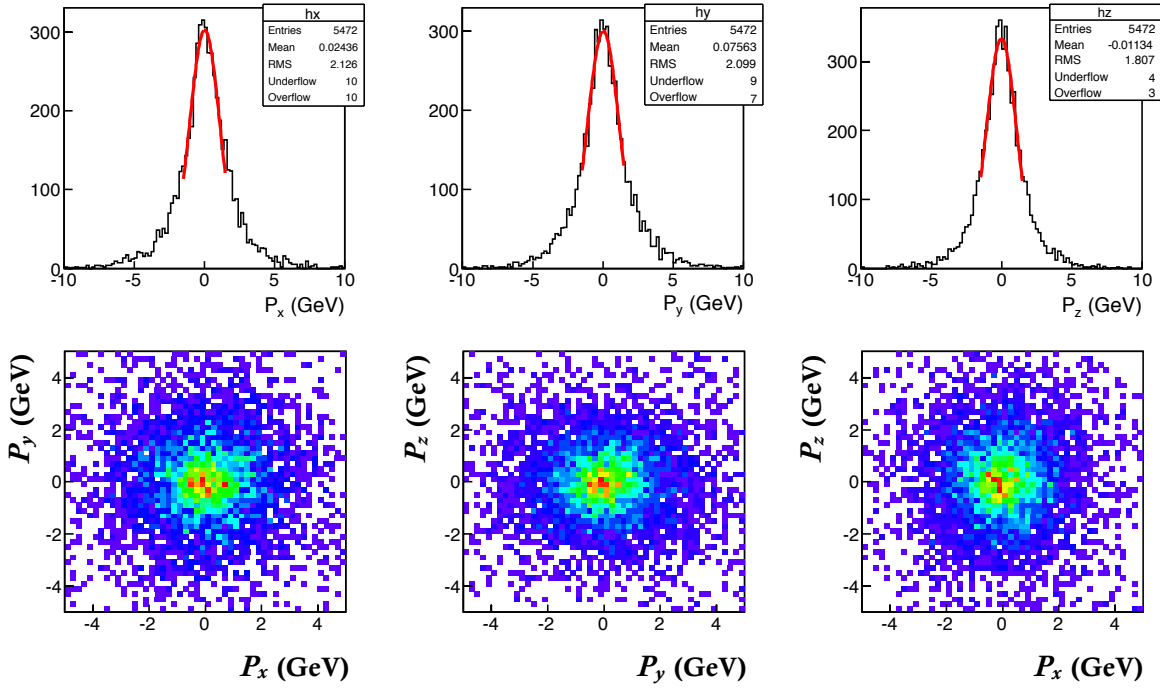


Figure 5.25: Reconstructed momentum of Z by summing the momenta of the particles in the final state of $Z \rightarrow q\bar{q}$ for x, y, z components (upper row). The distributions are settled at zero, with sharp Gaussian peaks (red line is the fit) and long tails. The RMS is typically 2 GeV for each component. The lower rows show absence of the correlation between them.

Finally, as done in the other channels above, the number of affordable event sample are estimated. The branching of each decay of $H \rightarrow \tau\tau \rightarrow \pi\nu\pi\nu$ is listed as Tab. 5.5). The total number of Higgs depends on run projections. Here 3 scenarios are assumed where the integrated luminosity is 250fb^{-1} ; 1000fb^{-1} ; 2000fb^{-1} respectively and the center of mass energies are all 250 GeV. The number of produced Higgs is 8×10^4 , 32×10^4 and 64×10^4 and the expected number of events for $H \rightarrow \tau\tau \rightarrow \pi\nu\pi\nu$ is around 45, 180, and 360 respectively. The collection efficiency in current analysis is 25% [78], however it still leaves much

Table 5.5: Branching ratio for each decay in $H \rightarrow \tau\tau \rightarrow \pi\nu\pi\nu$. The number for $H \rightarrow \tau\tau$ is calculated from SM with Higgs mass of 125 GeV assumed.

channel	branching fraction
$H \rightarrow \tau\tau$	$(6.32 \pm 0.36)\%$
$\tau^- \rightarrow \pi^- \nu_\tau$	$(10.83 \pm 0.0006)\%$
$\tau^+ \rightarrow \pi^+ \bar{\nu}_\tau$	$(10.83 \pm 0.0006)\%$
$Z \rightarrow q\bar{q}, e^+e^-, \mu^+\mu^-$	$(76.6 \pm 0.06)\%$
$e^+e^- \rightarrow Z^* \rightarrow ZH; H \rightarrow \tau^-\tau^+ \rightarrow \pi^-\nu\pi^+\bar{\nu}_\tau$	$(5.70 \pm 0.33) \times 10^{-4}$

to be improved and this number can be supposed to rise, at maximally optimistic expectation (including some anticipation), up to around 50% in future. With the assumption, the available sample size will be 20, 90, and 180, which lead to only poor sensitivity that the violation of the BI can be confirmed with 80%CL with 1000fb^{-1} , 95%CL with 2000fb^{-1} , if ignoring the contamination of BG. Here the impact of BG therefore a realistic number of significance should be something like 68%CL with 2000fb^{-1} , assuming 15% of BG level. Nevertheless the author thinks that this is a very interesting result in that this is the first attempt at application of Higgs boson.

Chapter 6

Conclusion

Bell inequality is an inequality that lets us learn whether the nature prefers classical physics or quantum ones, as well as signatures of quantum non-locality. While the violation has been extensively verified in photon experiments, tests with massive particles are still impotent which however have only few examples yet.

The particle decays in high energy collider experiments have been supposed to be new channels of the testing Bell inequality, using the spin entanglement from decays of particle, and the magical spin measurement scheme with weak decays provided by the nature, which enables the test with various types of systems and interactions as well.

On the basis of previous studies, this paper provided (i) a comprehensively review of the theoretical background, (ii) a formal establishment of the method which is free from the locality loophole for the first case in non-optical experiments, (iii) a formulation of a new Bell inequality, (iv) and a discussion on the feasibility of testing the Bell inequality by this method, with today's high specification collider machines, as a new proposition of the experiment.

In particular, the six decays below are examined:

- $\eta_c \rightarrow \Lambda \bar{\Lambda} \rightarrow p \pi^- \bar{p} \pi^+$
- $\chi_{c0} \rightarrow \Lambda \bar{\Lambda} \rightarrow p \pi^- \bar{p} \pi^+$
- $J/\psi \rightarrow \Lambda \bar{\Lambda} \rightarrow p \pi^- \bar{p} \pi^+$
- $e^+ e^- \rightarrow \gamma^* \rightarrow \tau^+ \tau^- \rightarrow \pi^- \nu_\tau \pi^+ \bar{\nu}_\tau$
- $Z \rightarrow \tau^+ \tau^- \rightarrow \pi^- \nu_\tau \pi^+ \bar{\nu}_\tau$
- $H \rightarrow \tau^+ \tau^- \rightarrow \pi^- \nu_\tau \pi^+ \bar{\nu}_\tau$

to violate the Bell inequality

$$Q_{\max} = \sqrt{\lambda_1 + \lambda_2}$$
$$Q_{\max} \leq 1$$

in the quantum mechanics.

The result of the analyses are

$$Q_{\max} = \begin{cases} \sqrt{2} & (\eta_c, \chi_{c0} \rightarrow \Lambda\bar{\Lambda} \rightarrow p\pi^-\bar{p}\pi^+, H \rightarrow \tau^+\tau^- \rightarrow \pi^-\nu_\tau\pi^+\bar{\nu}_\tau) \\ 0.976 \pm 0.048 & (J/\psi \rightarrow \Lambda\bar{\Lambda} \rightarrow p\pi^-\bar{p}\pi^+) \\ \sqrt{5}/2 & (Z \rightarrow \tau^+\tau^- \rightarrow \pi^-\nu_\tau\pi^+\bar{\nu}_\tau) \\ \frac{\sqrt{5-2\Gamma^2+2\Gamma^4}}{2+\Gamma^2}; \quad \Gamma^2 := \frac{4m_\tau^2}{s} & (e^+e^- \rightarrow \gamma^* \rightarrow \tau^+\tau^- \rightarrow \pi^-\nu_\tau\pi^+\bar{\nu}_\tau). \end{cases}$$

The conclusions are that **it is in principle possible to confirm the violation of the inequality for the all channels except $J/\psi \rightarrow \Lambda\bar{\Lambda} \rightarrow p\pi^-\bar{p}\pi^+$ and, with studies on experimental aspects, that current experiments can already afford the statistics to observe the violation in the channels $\eta_c, \chi_{c0} \rightarrow \Lambda\bar{\Lambda} \rightarrow p\pi^-\bar{p}\pi^+$, with the significance of 2σ and 3σ respectively.**

Maybe knowledge is as fundamental, or even more fundamental than reality.

Anton Zeilinger

Bibliography

- [1] J. von Neumann, "Mathematical foundations of quantum mechanics", Princeton Univ. Press, Princeton, N. J. , (1955).
- [2] M. Born, "Quantenmechanik der Stoßvorgänge." *Zeitschrift für Physik.* **38**, 803-827 (1926).
- [3] H. Everett, "Theory of the Universal Wave function", Thesis, Princeton University, (1956, 1973); H. Everett, "Relative State Formulation of Quantum Mechanics". *Reviews of Modern Physics* **29**, 454 (1957).
- [4] O. Stern, W. Gerlach, "Das magnetische Moment des Silberatoms". *Zeitschrift für Physik* **9**: 353 (1922).
- [5] J. J. Sakurai, 『現代の量子力学 (上)』, pp.3, 吉岡書店 (1989).
- [6] (Picture of Stern-Gerlach instrument): <http://www.upscale.utoronto.ca/GeneralInterest/Harrison/SternGerlach/Images/>
- [7] Bernard D'Espang, "Conceptual Foundations of Quantum Mechanics" 2nd edn., Reading, Mass. Benjamin (1976).
- [8] Colin Blues, 『量子力学の解釈問題』, 和田純夫 訳, 講談社 (2008).
- [9] Michael Redhead, "Incompleteness, Nonlocality, and Realism: A Prolegomenon to the Philosophy of Quantum Mechanics", Clarendon Press (1989). [レッドヘッド 『不完全性・局所性・実在主義-量子力学の哲学序説』 石垣壽郎訳, みすず書房, (1997)].
- [10] A. Einstein, B. Podolsky, and N. Rosen, "Can Quantum-Mechanical Description of Physical Reality Be Considered Complete?", *Phys. Rev.* **47**, 777 (1935).
- [11] D. Bohm, "A Suggested Interpretation of the Quantum Theory in Terms of "Hidden" Variables. I", *Phys. Rev.* **85**, 166 (1952); "A Suggested Interpretation of the Quantum Theory in Terms of "Hidden" Variables. II", *Phys. Rev.* **85**, 180 (1952).
- [12] J. S. Bell, "On The Einstein Podolsky Rosen Paradox", *Physics* **1**, 195 (1964).
- [13] J. F. Clauser, M. A. Horne, A. Shimony, and R. A. Holt, "Proposed Experiment to Test Local Hidden-Variable Theories", *Phys. Rev. Lett.* **23**, 880 (1969).
- [14] (Picture of the earth): <http://www.mt-planning.com/img2/eorc03.jpg>, JAXA.
- [15] 清水明 『現代の量子力学の基礎』, サイエンス社 (2003).
- [16] Y. B. Ding, J. Li, and C.F. Qiao, "Bell Inequalities in High Energy Physics", *High Ener. Phys. & Nucl. Phys.* **31**, 1086 (2007), arXiv:0702271.

- [17] 筒井泉, 「量子力学の基礎問題と近年の話題」 http://kincha.kek.jp/kincha020_tsutsui.pdf, 金茶会, KEK (2008).
- [18] J. F. Clauser, M.A. Horne, "Experimental consequences of objective local theories", *Phys. Rev. D* **10**, 526 (1974).
- [19] S. J. Freedman and J. F. Clauser, "Experimental Test of Local Hidden-Variable Theories", *Phys. Rev. Lett.* **28**, 938 (1972).
- [20] A. Aspect, P. Grangier, and G. Roger, "Experimental Tests of Realistic Local Theories via Bell's Theorem", *Phys. Rev. Lett.* **47** 460 (1981).
- [21] A. Aspect, P. Grangier, and G. Roger, "Experimental Realization of Einstein-Podolsky-Rosen-Bohm *Gedankenexperiment*: A New Violation of Bell's Inequalities", *Phys. Rev. Lett.* **49**, 91 (1982).
- [22] A. Aspect, P. Grangier, and G. Roger, "Experimental Test of Bell's Inequalities Using Time-Varying Analyzers", *Phys. Rev. Lett.* **49**, 1804 (1982).
- [23] Y. H. Shih and C. O. Alley, "New Type of Einstein-Podolsky-Rosen-Bohm Experiment Using Pairs of Light Quanta Produced by Optical Parametric Down Conversion", *Phys. Rev. Lett.* **61**, 2921 (1988).
- [24] A. Aspect "Bell's Theorem: The Naive View of an Experimentalist ", from R. A. Bertlmann and A. Zeilinger (eds.) "Quantum (Un)speakables - From Bell to Quantum information", Springer (2002) arXiv:0402001.
- [25] P. M. Pearle, "Hidden-Variable Example Based upon Data Rejection", *Phys. Rev. D* **2**, 1418 (1970).
- [26] E. Santos, "Critical analysis of the empirical tests of local hidden-variable theories", *Phys. Rev. A* **46**, 3646 (1992); "Unreliability of performed tests of Bell's inequality using parametric down-converted photons", *Phys. Lett. A* **212**, 10 (1996); "The Failure to Perform a Loophole-Free Test of Bell's Inequality Supports Local Realism", *Found. of Phys.*, **34**, 1643 (2004).
- [27] "Background level and counter efficiencies required for a loophole-free Einstein-Podolsky-Rosen experiment", P. H. Eberhard, *Phys. Rev. A* **47**, 747 (1993).
- [28] M. Giustina *et al.*, "Bell violation with entangled photons, free of the fair-sampling assumption", *Nature*, **497**, 227 (2013).
- [29] M. A. Rowe *et al.*, "Experimental violation of a Bell's inequality with efficient detection", *Nature (London)* **409**, 791 (2001).
- [30] G. Weihs *et al.*, "Violation of Bell's Inequality under Strict Einstein Locality Conditions", *Phys. Rev. Lett.* **81**, 5039 (1998).
- [31] W. Tittel *et al.*, "Violation of Bell Inequalities by Photons More Than 10 km Apart", *Phys. Rev. Lett.* **81**, 3563 (1998).
- [32] R. Ursin, *et al.*, "Entanglement-based quantum communication over 144km", *Nature Physics* **3**, 481 (2007).
- [33] J. Conway and S. Kochen, "The Free Will Theorem", *Found. of Phys.* **36**, 10 (2006).

- [34] M.M. Lamehi-Rachti and W. Mittig, "Quantum mechanics and hidden variables: A test of Bell's inequality by the measurement of the spin correlation in low-energy proton-proton scattering", *Phys. Rev. D* **14**, 2543 (1976).
- [35] H. Sakai *et al.*, "Spin Correlations of Strongly Interacting Massive Fermion Pairs as a Test of Bell's Inequality", *Phys. Rev. Lett.* **97**, 150405 (2006).
- [36] A. Apostolakis *et al.* (CPLEAR Collaboration), "An EPR experiment testing the non-separability of the $K^0\bar{K}^0$ wave function", *Phys. Lett. B* **422**, 339 (1998)
- [37] A. Go, "Observation of Bell inequality violation in B mesons", *Journal of Modern Optics* **51**, 991 (2004);
- [38] A. GO *et al.* (Belle Collaboration), "Measurement of Einstein-Podolsky-Rosen-Type Flavor Entanglement in $\Upsilon(4S) \rightarrow B^0\bar{B}^0$ Decays", *Phys. Rev. Lett.* **99**, 131802 (2007).
- [39] R.A. Bertlmann, A. Bramon, G. Garbarino, B.C. Hiesmayr, "Violation of a Bell inequality in particle physics experimentally verified?", *Phys. Lett. A* **332**, 355 (2004).
- [40] T. Ichikawa, S. Tamura, and I. Tsutsui, "Testing EPR locality using B-mesons", *Phys. Lett. A* **373**, 39 (2008).
- [41] A. Pompili and F. Selleri, "On a possible EPR experiment with $B_d^0\bar{B}_d^0$ pairs", *Eur. Phys. J. C* **14**, 469 (2000).
- [42] S. Kochen and E.P. Specker, "The problem of hidden variables in quantum mechanics", *Journal of Mathematics and Mechanics* **17**, 59 (1967).
- [43] A. J. Leggett, "Nonlocal Hidden-Variable Theories and Quantum Mechanics: An Incompatibility Theorem", *Found. of Phys.*, **33**, 1469 (2003).
- [44] S. Gröblacher *et al.*, "An experimental test of non-local realism", *Nature* **446**, 871 (2007)
- [45] Bohm and Y. Aharonov, "Discussion of Experimental Proof for the Paradox of Einstein, Rosen, and Podolsky", *Phys. Rev.* 108 1070 (1957).
- [46] N. A. Törnqvist, "Suggestion for Einstein-Podolsky-Rosen Experiments Using Reactions Like $e^+e^- \rightarrow \Lambda\bar{\Lambda} \rightarrow \pi^-p\pi^+\bar{p}$ ", *Found. Phys.* **11**, 171 (1981).
- [47] 山本祐靖 『高エネルギー物理学』, 培風館 (1973).
- [48] J. Beringer *et al.* (Particle Data Group), *Phys. Rev. D* **86**, 010001 (2012).
- [49] A. Stahl "Physcis with Tau Lepton", Springer (2000).
- [50] ATLAS Collaboration, "Evidence for Higgs Boson Decays to the $\tau^+\tau^-$ Final State with the ATLAS Detector", ATLAS-CONF-2013-108. <https://cds.cern.ch/record/1632191>; CMS Collaboration, Search for the Standard-Model Higgs boson decaying to tau pairs in proton-proton collisions at $\sqrt{s} = 7$ and 8 TeV, CMS-PAS-HIG-13-004. <https://cds.cern.ch/record/1528271>.
- [51] BESIII Experiment: <http://bes3.ihep.ac.cn>
- [52] CLEO Experiment: <http://w4.lns.cornell.edu/public/CLEO>

- [53] H. Baer *et al.* (eds.), "The International Linear Collider Technical Design Report - Volume 2: Physics", arXiv: 1306.6352.
- [54] LEP Experiment: <http://cern.web.cern.ch/CERN/Divisions/SL/lep2page.html>
- [55] Belle Wxperiment: <http://belle.kek.jp>
- [56] N. A. Törnqvist, "The Decay $J/\psi \rightarrow \Lambda\bar{\Lambda} \rightarrow \pi^- p \pi^+ \bar{p}$ as an Einstein-Podolsky-Rosen Experiment", Phys. Lett. A **117**, 1 (1986).
- [57] M. H. Tixier *et al.* (DM2 Collaboration), "Looking at CP invariance and quantum mechanics in $J/\psi \rightarrow \Lambda\bar{\Lambda}$ decay", Phys. Lett. B **212** 523 (1988).
- [58] X. Q. Hao *et al.*, "Testing the Bell Inequality at Experiments of High Energy Physics", Chin. Phys. C **34**, 311 (2010).
- [59] S. P. Baranov, "Bell's inequality in charmonium decays $\eta_c \rightarrow \Lambda\bar{\Lambda}$, $\chi_{c0} \rightarrow \Lambda\bar{\Lambda}$ and $J/\psi \rightarrow \Lambda\bar{\Lambda}$ ", J. Phys. G: Nucl. Part. Phys. **35** 075002 (2008).
- [60] J. Li and C. F. Qiao, "Testing Local Realism in $P \rightarrow VV$ Decays", Sci. China G **53**, 870 (2010).
- [61] X. Chen, S. G. Wang, and Y. Mao, "Understanding polarization correlation of entangled vector meson pairs", Phys. Rev. D **86**, 056003 (2012).
- [62] A. J. Weinstein, "CLEO Results on Tau Michel Parameters", Nucl. Phys. Proc. Suppl. **76**, 165 (1999).
- [63] P. Privitera, "Decay correlations in $e^+e^- \rightarrow \tau^+\tau^-$ as a test of quantum mechanics", Phys. Lett. B **275** 172 (1992).
- [64] S. A. Abel, M. Dittmar, and H. Dreiner, "Testing locality at colliders via Bell's inequality?", Phys. Lett. B **280**, 304 (1992).
- [65] H. Dreiner, "Bell's Inequality and τ -Physics at LEP", arXiv: 9211203.
- [66] G. C. Wick, A. S. Wightman, and E. P. Wigner, "The intrinsic parity of elementary particles," Phys. Rev. **88**, 101 (1952).
- [67] M. Peskin and D. Schröder, "An introduction to Quantum Field Theory", pp.46 (1995).
- [68] J. W. Cronin and O. E. Overseth, "Measurement of the Decay Parameters of the Λ^0 Particle", Phys. Rev. **129**, 1795 (1963).
- [69] O. E. Overseth and R. F. Roth, "Time Reversal Invariance in Λ^0 Decays", Phys. Rev. Lett. **19**, 391 (1967).
- [70] A. Afriat and F. Selleri, "The Einstein Podolsky and Rosen Paradox in atomic nuclear and particle physics", Plenum Press, New York, (1999).
- [71] T. Behnke *et al.* (eds.), "The International Linear Collider Technical Design Report - Volume 1: Exclusive summary", arXiv: 1306.6327.
- [72] S. Chen, Y. Nakaguchi and S. Komamiya, "Testing Bell's Inequality using Charmonium Decays", Prog. Theor. Exp. Phys. 063A01 (2013).

- [73] M. B. Voloshin, "Charmonium", pp. 14-21 "Charmonium Annihilation" (2008), arXiv: 0711.4556v3.
- [74] M. Peskin and D. Schröder, "An introduction to Quantum Field Theory", pp.68, equation (3.134) (1995).
- [75] A.Peres, "Separability Criterion for Density Matrices", Phys. Rev. Lett. **77** 1413 (1996); M.Horodecki, P.Horodecki, R.Horodecki, "Separability of mixed states: necessary and sufficient conditions", Phys. Lett. A **223** 1 (1996).
- [76] M. Ablikim *et al.* (BES Collaboration), "Study of the J/ψ decays to $\Lambda\bar{\Lambda}$ and $\Sigma^0\bar{\Sigma}^0$ ", Phys. Lett. B **632**, 181 (2006).
- [77] A. Djouadi *et al.*, "The couplings of the Higgs boson and its CP properties from fits of the signal strengths and their ratios at the 7 + 8 TeV LHC" (2013), arXiv: 1303.6591.
- [78] S. Kawada *et al.*, "Evaluation of measurement accuracy of $h \rightarrow \tau^+\tau^-$ branching ratio at the ILC with $\sqrt{s} = 250\text{GeV}$ and 500GeV ", arXiv:1308.5489.
- [79] J. B. Liu *et al.* "A beam test of a prototype of the BES III drift chamber in magnetic field", Nucl. Instrum. Meth. A, **557**, 436 (2006); L. K. Jia *et al.*, "Study of low momentum track reconstruction for the BESIII main drift chamber", Chin. Phys. C **34**, 1866 (2010).
- [80] M. Ablikim *et al.* (BES Collaboration), "Measurements of baryon pair decays of χ_{cJ} mesons", Phys. rev. D **87**, 032007 (2013).
- [81] J. Drees, "Review of Final LEP Results or A Tribute to LEP" (2001), arXiv: 0110077.
- [82] E. Etzion, "Analysis of the Tau Polarization and its Forward-Backward Asymmetry on the Z^0 " (PhD. thesis), Tel Aviv University (1996), arXiv: 9606011.
- [83] T. Benke *et al.* (eds.), "The International Linear Collider Technical Design Report - Volume 4: Detectors", arXiv: 1306.6329.
- [84] M. A. Thomson, "Particle Flow Calorimetry and the PandoraPFA Algorithm", Nucl. Instrum. Meth. A, **611**, 25 (2009).
- [85] H. Baer *et al.* (eds.), "The International Linear Collider Technical Design Report - Volume 2: Physics", arXiv: 1306.6352.